
Electronic Thesis and Dissertation Repository

12-5-2018 10:00 AM

Applications of CT Perfusion-Based Triaging and Prognostication in Acute Ischemic Stroke

Eric A. Wright
The University of Western Ontario

Supervisor
Lee, Ting Y
The University of Western Ontario

Graduate Program in Medical Biophysics
A thesis submitted in partial fulfillment of the requirements for the degree in Doctor of Philosophy
© Eric A. Wright 2018

Follow this and additional works at: <https://ir.lib.uwo.ca/etd>



Part of the [Medical Biophysics Commons](#)

Recommended Citation

Wright, Eric A., "Applications of CT Perfusion-Based Triaging and Prognostication in Acute Ischemic Stroke" (2018). *Electronic Thesis and Dissertation Repository*. 5888.
<https://ir.lib.uwo.ca/etd/5888>

This Dissertation/Thesis is brought to you for free and open access by Scholarship@Western. It has been accepted for inclusion in Electronic Thesis and Dissertation Repository by an authorized administrator of Scholarship@Western. For more information, please contact wlsadmin@uwo.ca.

Abstract

CT Perfusion (CTP) is a minimally invasive imaging technique that aids acute ischemic stroke (AIS) triage and prognostication by determining tissue viability based on hemodynamic parameters. The goals of this research are to determine: 1) CTP thresholds for estimation of infarct and penumbra volume, 2) how CTP scan duration impacts infarct and penumbra volume estimates, and 3) reliability of CTP for predicting functional outcomes following intra-arterial therapy (IAT).

Chapter 2 introduced an experimental study for determining ischemia-time dependent thresholds for brain infarction using multimodal imaging in a porcine stroke model that is easier to implement than previous large animal stroke models. CTP determined an absolute cerebral blood flow (CBF) threshold of $12.6 \pm 2.8 \text{ mL} \cdot \text{min}^{-1} \cdot 100 \text{ g}^{-1}$ for brain infarction after 3h of ischemia, which was close to that derived using hydrogen clearance in a previous study by Jones et al (*Journal of Neurosurgery*, 1981;54(6):773-782).

Chapter 3 retrospectively investigated the impact of CTP scan duration on cerebral blood volume (CBV), CBF, and time-to-maximum (T_{max}) and found optimal scan durations that minimized radiation dose while not under- or over-estimating infarct volumes measured using two previously derived CBF thresholds for infarction. We found that CBV and T_{max} decreased at shorter scan durations, whereas CBF was independent of scan duration, consequently, infarct volume estimated by both CBF thresholds was independent of scan duration.

Chapter 4 compared reperfusion seen on follow-up CTP to reperfusion predicted by post-IAT digital subtraction angiography (DSA) and the ability of the two modalities to predict good 90-day functional outcome in a retrospective study. We found that patients with ‘complete reperfusion’ grades on DSA often had ischemic tissue on follow-up CTP and that follow-up CTP had superior specificity and accuracy for predicting functional outcome compared to DSA.

In summary, this research has shown that CBF thresholds can reliably detect infarct in AIS and are independent of scan duration, allowing radiation dose to be minimized by limiting scans to 40s without compromising accuracy of infarct volume estimates. Finally, CTP is a more specific and accurate predictor of functional outcome than the commonly used post-procedural DSA, this could help select patients for neuroprotective therapy.

Keywords

Stroke, cerebral ischemia, computed tomography, computed tomography perfusion, functional imaging, cerebral blood flow, infarction, animal stroke model, mechanical thrombectomy.

Co-Authorship Statement

Chapter two was adapted from an original research manuscript entitled “Absolute cerebral blood flow infarction threshold for 3-hour ischemia time determined with CT Perfusion and ^{18}F -FFMZ-PET imaging in a porcine model of cerebral ischemia” published in *PLoS One* 11(6): e0158157, June 2016, by E.A. Wright, C.D. d’Esterre, L.B. Morrison, N. Cockburn, M. Kovacs, and T.Y. Lee. The study was designed by T.Y. Lee and myself with contributions from C.D. d’Esterre. I was responsible for performing the experiments with help from L.B. Morrison. For each experiment, N. Cockburn and M. Kovacs produced the ^{18}F -FFMZ required for PET imaging of tissue viability. I also collected and analyzed the data and wrote the manuscript under the supervision of T.Y. Lee. All authors reviewed and edited the manuscript.

Chapter three was adapted from an original research manuscript entitled “Impact of truncation artifacts on CT Perfusion-derived CBV, CBF, and time-to-maximum measurements in ischemic stroke patients” submitted to *American Journal of Neuroradiology* by E.A. Wright, C.D. d’Esterre, L. Hur, C. McDougall, M. Horn, M. Najm, M. Goyal, B.K. Menon, and T.Y. Lee. The study was designed by T.Y. Lee and myself with contributions from C. D. d’Esterre. The patient studies were provided by M. Goyal, and B.K. Menon. L. Hur, C. McDougall, M. Horn and M. Najm processed the patient studies to generate CT Perfusion maps using a pre-defined protocol. I verified that CT Perfusion maps were correct (visual assessment, verified that arterial input function and venous output function were measured appropriately, etc.) and performed post-processing to abstract data from the maps, performed all data analysis and wrote the manuscript under the supervision of T.Y. Lee. The manuscript was reviewed and edited by C.D. d’Esterre, M. Goyal, B.K. Menon, and T.Y. Lee.

Chapter four was adapted from an original research manuscript entitled “Reperfusion assessed by CT Perfusion is a more specific and accurate predictor of functional outcome than modified thrombolysis in cerebral infarction score in ischemic stroke patients treated with intra-arterial therapy” submitted to *Radiology* by E.A. Wright, E. Fainardi, A. Bernardoni, C.D. d’Esterre, M. Goyal, B.K. Menon, and T.Y. Lee. The study was designed by E. Fainardi and T.Y. Lee with contribution from myself. E. Fainardi and A. Bernardoni recruited patients and assessed admission CT angiography for all patients. I was responsible for computation of CT Perfusion maps, post-processing to abstract data from maps, analyzing all data, and writing the manuscript under the supervision of T.Y. Lee. All authors reviewed and revised the manuscript.

Acknowledgments

First and foremost, I would like to acknowledge my supervisor, Dr. Ting-Yim Lee. He allowed me to have a great deal of independence to forge my own path, but was also always available when I needed guidance, ready to help with his seemingly encyclopedic knowledge of CT Perfusion. I have learned an immense amount and grown as a person under his supervision, and I cannot thank him enough for his mentorship and support throughout my time in graduate school. I would also like to thank the members of my advisory committee, Dr. Keith St. Lawrence and Dr. Michael Kovacs.

I would like to thank Dr. Christopher d’Esterre from the University of Calgary, who was always available to offer valuable insight and encouragement, as well as Dr. Enrico Fainardi from the University of Florence for all his help with the study which comprises the 4th chapter of this thesis.

I would also like to express my deep gratitude to Laura Morrison. To say that my animal experiments would have been impossible without her would be an understatement. I will always be grateful for her hard work, and attention to detail, both of which were key to making those experiments a success. My thanks also go to Jennifer Hadway and Lise Desjardins, who were always available whenever I needed help or had questions in the lab.

My sincere appreciation must also be expressed to Anne Leaist. It would have been immeasurably harder to focus on my work without her help with conference expenses, stipend issues, and all other administrative matters. I also would like to thank all other current, and former members of the Lee Lab whose time in the lab overlapped with mine. All the interesting discussions and feedback whenever I had to present at journal club or practice conference

presentations was very much appreciated. Thank you all for creating a warm atmosphere that always made coming into the lab enjoyable.

I would also like to send out my heartfelt thanks to my parents Sandra and Bruce for their constant encouragement, and frequent weekend trips to London to visit. Finally, thank you to my long-time girlfriend Joanna, for her love, support, and patience, and for always keeping me grounded through all the highs and lows that have come over the last five years. I could never have done this without her.

Table of Contents

Abstract.....	i
Co-Authorship Statement.....	iii
Acknowledgments.....	v
Table of Contents.....	vii
List of Tables.....	xi
List of Figures.....	xii
List of Appendices.....	xiv
List of Abbreviations.....	xv
Chapter 1.....	1
1 Introduction.....	1
1.1 Stroke Pathophysiology.....	2
1.1.1 Cerebral Ischemia.....	2
1.1.2 Tissue Subtypes in Ischemic Stroke.....	6
1.2 Treatment of Ischemic Stroke.....	8
1.2.1 Thrombolytic Therapy.....	9
1.2.2 Mechanical Thrombectomy.....	12
1.3 Medical Imaging in Ischemic Stroke.....	17
1.3.1 Positron Emission Tomography.....	17
1.3.2 Magnetic Resonance Imaging.....	20
1.3.3 Computed Tomography.....	24
1.4 Animal Models of Ischemic Stroke.....	40
1.5 Future Diagnosis and Treatment of Stroke.....	42
1.6 Research Objectives.....	44
1.7 References.....	44

Chapter 2.....	86
2 Absolute Cerebral Blood Flow Infarction Threshold for 3-hour Ischemia Time Determined with CT Perfusion and ¹⁸ F-FFMZ-PET Imaging in a Porcine Model of Cerebral Ischemia.....	86
2.1 Introduction.....	86
2.2 Methods.....	88
2.2.1 Acute Cerebral Ischemia Model	88
2.2.2 On-line CBF Monitoring with CT Perfusion	89
2.2.3 ¹⁸ F-FFMZ-PET Imaging for Detecting Cerebral Infarction	90
2.2.4 Data Analysis	91
2.3 Results.....	94
2.4 Discussion	101
2.5 Conclusion	104
2.6 References.....	105
Chapter 3.....	110
3 Impact of Truncation Artifacts on CT Perfusion-derived CBV, CBF, and Time-to- Maximum Measurements in Ischemic Stroke Patients	110
3.1 Introduction.....	110
3.2 Methods.....	113
3.2.1 Patients.....	113
3.2.2 Image Acquisition.....	114
3.2.3 CTP Postprocessing	114
3.2.4 Image Analysis.....	115
3.2.5 Statistical Analysis.....	116
3.3 Results.....	117
3.3.1 Patients.....	117
3.3.2 Median Parameter Values.....	117

3.3.3	Threshold-derived Infarct Volumes	120
3.4	Discussion	123
3.5	Conclusion	127
3.6	References.....	127
Chapter 4.....		132
4	Reperfusion Assessed by CT Perfusion is a More Specific and Accurate Predictor of Functional Outcome than Modified Thrombolysis in Cerebral Infarction Score in Ischemic Stroke Patients Treated with Intra-Arterial Therapy	132
4.1	Introduction.....	132
4.2	Methods.....	133
4.2.1	Patient Selection.....	133
4.2.2	Imaging Protocol.....	135
4.2.3	Image Analysis.....	136
4.2.4	Statistical Analysis.....	138
4.3	Results.....	139
4.3.1	Comparison of mTICI Scores to S_{CTP}	139
4.3.2	Comparison of mTICI Scores to S_{CTP} for Predicting Functional Outcome	143
4.4	Discussion.....	152
4.5	References.....	155
Chapter 5.....		161
5	Conclusions and Future Work.....	161
5.1	Summary	161
5.1.1	Development of Porcine AIS Model and Derivation of 3h CBF Threshold for Infarction	161
5.1.2	Assessment of Scan Duration Effect on Quantitative CTP Results.....	162
5.1.3	Follow-up CTP as a Prognosticator of Functional Outcome in IAT-Treated Patients	164

5.2 Experimental and Clinical Impact	165
5.3 Future Work	166
5.3.1 Deriving CBF Thresholds for a Greater Range of Ischemia Durations..	166
5.3.2 Using PS to Identify Patients at Increased Risk of Hemorrhagic Transformation.....	169
5.3.3 Assessment of Post-IAT Reperfusion using ‘DSA Perfusion’ Maps	171
5.4 Conclusion	173
5.5 References.....	173
Appendices.....	176
Curriculum Vitae	187

List of Tables

Table 2.1: ROC parameters for each animal.....	100
Table 3.1: Average \pm S.E. tissue volumes specified by CBF thresholds.....	122
Table 4.1: Demographic, clinical and imaging characteristics of the 96 patients included in the study.....	144
Table 4.2: Logistic regression for predicting 90-day functional outcome based on S_{CTP} and admission NIHSS.....	147

List of Figures

Figure 1.1: The concept of deconvolution applied to CT Perfusion.....	31
Figure 1.2: Graphical representation of CTP deconvolution equation	33
Figure 1.3: Sample IRF.....	35
Figure 2.1: Image analysis method	93
Figure 2.2: Average relative CBF of infarct ROIs.....	95
Figure 2.3: Predicted probability of infarction versus CBF.....	97
Figure 2.4: ROC curves for each animal	99
Figure 3.1: Truncation of ischemic tissue TDCs	112
Figure 3.2: Median CBV, CBF, and T_{max} versus scan duration in infarct, ipsilateral non- infarct, and contralateral ROIs	119
Figure 3.3: Confidence intervals and range of volume differences relative to 150s scan for $CBF < 7 \text{ mL} \cdot \text{min}^{-1} \cdot 100\text{g}^{-1}$ and $7 < CBF < 13 \text{ mL} \cdot \text{min}^{-1} \cdot 100\text{g}^{-1}$	121
Figure 4.1: Patient exclusion flow chart	134
Figure 4.2: Mean S_{CTP} at each level of post-procedural mTICI score	140
Figure 4.3: Ischemic lesion on 24h follow-up T_{max} map for patient with post-procedural mTICI score of 3.....	142
Figure 4.4: ROC curves for predicting good functional outcome based on S_{CTP} and post- procedural mTICI score	149
Figure 4.5: Sensitivity, specificity, accuracy, PPV, and NPV for regression model, $S_{CTP} >$ 81.5% and mTICI 2b/3 for predicting functional outcome.....	151
Figure 5.1: Localization of MCA in porcine AIS model with dynamic images from CTP..	168

Figure 5.2: Elevated PS in patient with hemorrhagic transformation after IAT..... 170

Figure 5.3: Blood flow maps derived from DSA (anterior-posterior view) 172

List of Appendices

Appendix A: Supplementary Figures for Chapter 2	176
Appendix B: Animal Ethics Approval for the work contained in Chapter 2.....	183
Appendix C: Ethics Approval for the work contained in Chapter 3.....	184
Appendix D: Copyright Agreement.....	186

List of Abbreviations

ACA	Anterior cerebral artery
AIF	Arterial input function
AIS	Acute ischemic stroke
ASPECTS	Alberta Stroke Program Early CT Score
ATP	Adenosine triphosphate
BBB	Blood-brain barrier
BV	Blood volume
$C_a(t)$	Arterial contrast concentration versus time curve
CBF	Cerebral Blood Flow
CT	Computed tomography
CTA	Computed tomography angiography
CTP	Computed tomography perfusion
DCE-MRI	Dynamic contrast-enhanced magnetic resonance imaging
DSC-MRI	Dynamic susceptibility contrast magnetic resonance imaging
DSA	Digital subtraction angiography
DWI	Diffusion weighted imaging
ECASS	European Cooperative Acute Stroke Study
ET-1	Endothelin-1
F	Flow

FDA	Food and Drug Administration
FFMZ	Fluoroethylflumazenil
FLAIR	Fluid-attenuated inversion recovery
FMZ	Flumazenil
GRE	Gradient recalled echo
HU	Hounsfield Unit
IA	Intra-arterial
IAT	Intra-arterial therapy
ICA	Internal carotid artery
ICH	Intracerebral hemorrhage
IQR	Interquartile range
IRF	Impulse residue function
IV	Intra-venous
LVO	Large vessel occlusion
MCA	Middle cerebral artery
MERCI	Mechanical Embolus Removal in Cerebral Ischemia
MRA	Magnetic resonance angiography
MRI	Magnetic resonance imaging
mRS	Modified Rankin scale
mTICI	Modified thrombolysis in cerebral infarction

MTT	Mean transit time
NCCT	Non-contrast CT
NIHSS	National Institutes of Health Stroke Scale
NINDS	National Institute of Neurological Disorder and Stroke
PET	Positron emission tomography
PS	Permeability-surface area product
PWI	Perfusion-weighted imaging
Q(t)	Tissue contrast concentration versus time curve
RAPID	RApid processing of PerfusIon and Diffusion
$R_F(t)$	Flow-scaled impulse residue function
rLMC	Regional leptomenigeal collateral
ROI	Region of interest
R(t)	Impulse residue function
S_{CTP}	Reperfusion score
SWI	Susceptibility-weighted imaging
T_0	Arrival time
TDC	Time-density curve
T_{max}	Time-to-maximum
TNK	Tenecteplase
TOAST	Trial of Org 10172 in Acute Stroke Treatment

t-PA	Tissue plasminogen activator
u-PA	Urokinase
VOF	Venous output function

Chapter 1

1 Introduction

Stroke is the second leading cause of death, and third leading cause of disability worldwide¹ according to the World Health Organization. Overall, stroke mortality rates have declined over the last 30 years in the United States², and Canada³, but incidence rates remain higher in certain racial⁴, and gender cohorts⁵, and in certain geographical areas⁶. The decline in overall stroke mortality rate is due to a decrease in the number of fatal strokes⁷, rather than a decrease in stroke incidence, which is projected to more than double over the next 30 years, with most of the increase coming from people aged 75 years or older⁸. Approximately half the survivors of stroke are institutionalized or disabled within 5 years⁹, and due to the aging population, the number of individuals living with disability resulting from stroke is projected to almost double in the next 2 decades¹⁰. Long term care for these patients will further increase the socioeconomic burden of cerebrovascular disease¹¹. CT Perfusion (CTP) is a minimally invasive imaging technique that produces quantitative maps of hemodynamic parameters which can be used to assess tissue viability. CTP could improve outcomes after stroke by allowing triaging based on each patients' brain tissue viability, allowing the optimal treatment to be selected on an individualized basis. Post treatment CTP is not commonly performed but could also be used to improve prognostication by quantitatively assessing reperfusion of ischemic tissue. The goals of this research are to determine: 1) CTP thresholds for estimation of infarct and penumbra volume, 2) how CTP scan duration impacts infarct and penumbra volume estimates, and 3) the prognostic utility of CTP for predicting functional outcomes following intra-arterial therapy (IAT). To lessen the

future socioeconomic burden of cerebrovascular disease, CTP-based acute treatment and patient-specific triaging and management must be improved to reduce the proportion of stroke patients living with severe disability following their stroke.

1.1 Stroke Pathophysiology

Stroke is caused by a reduction in blood flow to the brain and can be divided into two broad categories. Hemorrhagic strokes are caused by leakage from damaged cerebral blood vessels, and ischemic strokes are caused by blockage of an artery supplying the brain tissue. This thesis deals only with ischemic stroke and not hemorrhagic stroke. Studies suggest that the overall annual incidence of first-ever stroke in North America is 189 per 100,000 people, with ischemic strokes accounting for ~85% of the total incidence¹². Approximately 30% of ischemic stroke patients die within 3 months of the stroke¹³, and ~45% of survivors will not be able to live independently¹⁴.

1.1.1 Cerebral Ischemia

Cerebral ischemia is a condition where restricted cerebral blood flow (CBF) leads to insufficient supply of oxygen and glucose to meet the metabolic demands of brain tissue. Cerebral ischemia can be global, such as when cardiac arrest or open-heart surgery results in complete cessation of systemic blood flow, or focal, where CBF is reduced in one region of the brain¹⁵. There are multiple arterial etiologies of focal cerebral ischemia. The most common are thrombosis in situ, clot formation in a cerebral artery due to endothelial injury triggering the coagulation cascade; and thromboembolism, where emboli travel to cerebral vessels through the blood after rupture of a thrombus or atherosclerotic plaque elsewhere in the body¹⁶. Cerebral emboli are also formed in the heart due to blood becoming static

during atrial fibrillation, or from coagulation following open heart surgery. Sustained hypertension can lead to fibrinoid deposits within cerebral arterioles, which is often associated with lacunar infarction¹⁶. Ischemia in tissue supplied by the distal part of the cerebral vascular tree is referred to as watershed stroke. Watershed stroke is usually caused by decreased mean arterial pressure in the internal carotid arteries (ICA) due to myocardial dysfunction, systemic hypotension, or ICA stenosis¹⁷.

The trial of Org 10172 in acute stroke treatment (TOAST)¹⁸ established a classification system which denoted five subtypes of ischemic stroke: large-artery atherosclerosis, cardioembolism, small-vessel occlusion, stroke of other determined etiology, and stroke of undetermined etiology¹⁹. Strokes of different subtypes (as identified by TOAST criteria) can have varying clot composition, size, and density, which can impact stroke severity and response to acute treatment^{20,21}. Regardless of vascular etiology, reduced delivery of oxygen and glucose due to reduced CBF results in inadequate production of adenosine triphosphate (ATP) by cellular respiration. Neuronal cells require ATP for active, facilitated transport of Na⁺, K⁺ and other ions to maintain their resting membrane potential, and for action potential propagation. Intracellular ATP stores are exhausted within minutes post ictus, leading to loss of ionic homeostasis²², this is the first step in a complex 'ischemic cascade' which ultimately leads to cell death caused mainly by excitotoxicity, Ca²⁺ dysregulation, and oxidative/nitrative stress.

Anoxic depolarization due to influx of Na⁺, and failure of normal reuptake mechanisms causes excessive accumulation of the excitotoxic neurotransmitter, glutamate, in the extracellular space²³. This leads to overstimulation of ionotropic glutamate receptors, resulting in a large influx of Ca²⁺, Na⁺, and water into neurons. Accumulation

of intracellular Ca^{2+} is further exacerbated by other anion channels activated during ischemia²⁴⁻²⁶, and failure of normal Ca^{2+} efflux mechanisms, such as the $\text{Na}^+/\text{Ca}^{2+}$ exchanger²⁷. Influx of Ca^{2+} activates proteases, lipases, and nucleases²⁸, and also leads to increased production of reactive oxygen species²⁹. These factors can trigger release of Ca^{2+} from the endoplasmic reticulum, as well as reactive oxygen species and enzymes from the mitochondria³⁰, further accelerating the death spiral. Continued build-up of metabolic, oxidative, and nitrate stressors eventually lead to cell death by necrosis or apoptosis. Glutamate excitotoxicity also expands the ischemic injury at a macroscopic level by causing cortical spreading depolarization, where elevated extracellular glutamate and K^+ cause slowly propagating depolarization of surrounding neurons and astrocytes, and disruption of ionic gradients³¹. Disruption of ionic gradients, and mismatch between reduced CBF and high metabolic demand to support membrane repolarization lead to expansion of the initial ischemic injury³².

Cerebral blood vessels are separated from brain tissue by a selectively permeable barrier called the blood-brain barrier (BBB) which tightly regulates the passage of molecules between the blood and brain tissue. The BBB consists of endothelial cells, astrocytic end-feet, pericytes and a basement membrane. Tight junctions between adjacent endothelial cells and astrocytic end-feet form a physical barrier, allowing lipophilic molecules and metabolic products to cross by passive diffusion, and preventing diffusion of hydrophilic molecules, and potential neurotoxins³³. Pericytes embedded in the basement membrane envelope the endothelial cells interact closely with them and play a role in maintaining and regulating BBB function³⁴. Prolonged ischemia triggers several responses which compromise the integrity of the BBB. In the acute phase of stroke, ischemia causes

pericytes to detach from endothelial cells, disrupting intercellular signalling interactions which results in blood-borne substances entering the brain via increased endothelial transcytosis³⁵. Ischemia also degrades tight junctions between endothelial cells, allowing molecules to travel out of the blood via paracellular diffusion³⁶, and causes astrocytes to retract their end-feet and release pro-inflammatory cytokines³⁷. The longer the duration of ischemia, the more severe the BBB breakdown and inflammatory response. This in turn increases the likelihood of blood extravasation if the ischemic tissue is eventually reperfused, a process known as hemorrhagic transformation of cerebral infarction. Furthermore, hyperglycemia caused by diabetes mellitus is known to worsen BBB breakdown, in addition to enhancing atherosclerosis, arterial stiffness, oxidative stress, and systemic inflammation³⁸. As a result, patients with diabetes mellitus are more likely to have ischemic strokes, and also have higher rates of hemorrhagic transformation³⁹ and mortality 90 days post stroke⁴⁰.

Tissue fate in ischemic stroke is time dependent (this will be detailed in the next subsection); tissue remains viable after symptom onset, but ~1.9 million neurons become irreversibly damaged every minute that stroke symptoms persist⁴¹. Treatment for acute ischemic stroke (AIS) revolves around salvaging viable ischemic tissue by restoring normal perfusion to the affected region as quickly as possible. However, restoring CBF to ischemic tissue regions with a potentially compromised BBB can lead to hemorrhagic transformation. For this reason, decisions surrounding the treatment of AIS are often determined by weighing the potential benefits of reperfusion, which declines over time^{42,43}, against the risks of hemorrhagic transformation or other complications.

1.1.2 Tissue Subtypes in Ischemic Stroke

In neuronal cells, the energy requirements, and by extension the CBF requirements, for signal transduction (action potential propagation and neurotransmission) and maintaining morphological integrity are different⁴⁴. Consequently, tissue affected by focal ischemia in the acute phase of ischemic stroke can be classified into distinct categories based on blood flow thresholds. Studies show there are two critical thresholds of decreased CBF: a threshold for reversible functional failure, and a lower threshold for irreversible morphological damage⁴⁵.

Tissue in the central, most hypoperfused region, with CBF below the threshold for irreversible damage, is termed the infarct core. The definition of infarct core was originally based on substantial increases in extracellular K^+ concentration seen in baboons when CBF was reduced by occlusion of the middle cerebral artery (MCA)^{45,46}. Increased extracellular K^+ is a marker of anoxic depolarization, one of the early steps in the ischemic cascade which ultimately leads to necrosis or apoptosis, therefore the infarct core is irreversibly damaged and no longer viable, even with reperfusion. In cases where cerebral circulation is completely arrested (e.g. cardiac arrest) brain infarction can occur within minutes, but when cessation of blood flow is not complete the time it takes for infarction to occur depends on the level of residual CBF. Experiments in animal models established that for 1 to 2 hours of ischemia, tissue with CBF less than $8-10 \text{ mL}\cdot\text{min}^{-1}\cdot 100\text{g}^{-1}$ will become infarcted^{47,48}.

The tissue surrounding the infarct core, with CBF below the threshold for functional failure, but above the threshold to induce acute infarction, is termed the penumbra. The concept of penumbra was based on observations that electroencephalography activity was

affected at a higher CBF level than the threshold for increased extracellular K^+ in a baboon model of focal ischemia^{45,46}. Clinical⁴⁹ and animal studies^{50,51} show that the CBF threshold for functional impairment ranges from 15-20 $\text{mL}\cdot\text{min}^{-1}\cdot 100\text{g}^{-1}$, depending on the species and measurement method used. Tissue with CBF between the thresholds for functional impairment and acute infarction will remain salvageable if normal blood flow is restored promptly. As mentioned previously, the window for tissue viability before infarction becomes inevitable depends on the level of residual blood flow and the duration of ischemia⁵². The threshold for infarction after 1 hour of ischemia is $\sim 8 \text{ mL}\cdot\text{min}^{-1}\cdot 100\text{g}^{-1}$, if ischemia persists for 3 hours the infarction threshold rises to $\sim 12 \text{ mL}\cdot\text{min}^{-1}\cdot 100\text{g}^{-1}$ ^{47,48}, if normal CBF is not restored and ischemia persists indefinitely, then all penumbral tissue will eventually progress to infarction⁴⁸.

Lastly, tissue with CBF that is lower than normal levels but still above the threshold for functional impairment is termed benign oligemia⁴⁵. Despite hypoperfusion, this tissue does not progress to infarction, regardless of the duration of ischemia, and is therefore not as clinically important as infarct or penumbra.

The human brain is composed of two distinct types of tissue, gray and white matter. Gray matter mainly consists of neuronal cell bodies, unmyelinated axons, glial cells and synapses and is found in the cerebral cortex, thalamus, hypothalamus, and basal ganglia. White matter consists of myelinated axons, and glial cells and connects various gray matter regions together, allowing neuronal signals to be conducted through the brain quickly⁵³. Resting CBF is lower in white matter (20-25 $\text{mL}\cdot\text{min}^{-1}\cdot 100\text{g}^{-1}$) than gray matter (50-60 $\text{mL}\cdot\text{min}^{-1}\cdot 100\text{g}^{-1}$)⁵⁴ because white matter consumes only about one third of the energy consumed by gray matter due to greater efficiency conducting action potentials and the

absence of synapses⁵⁵. Since white matter has a lower energy demand and perfusion level, it follows that CBF thresholds for infarction and electrical silence are also lower than in gray matter for a given ischemia duration. Clinical studies have confirmed that the CBF threshold for infarction in gray matter is significantly higher than in white matter for similar ischemia durations⁵⁶. Therefore, using the same infarction thresholds for both white and gray matter may overestimate the volume of infarcted white matter⁵⁶.

1.2 Treatment of Ischemic Stroke

Treatment of AIS was limited to medical management and basic life support until the introduction of thrombolytic therapy in 1996⁵⁷. Current treatment of AIS is based on recanalization of the occluded artery to restore CBF to ischemic tissue. There are two approved treatment options: thrombolytic therapy – which works by dissolving the clot via fibrinolysis, and mechanical thrombectomy – an interventional procedure where the clot is mechanically removed using a specialized catheter⁵⁸. Regardless of what treatment is used, initiating therapy as soon as AIS is diagnosed by imaging is crucial for maximizing penumbral salvage and lessening the risk of hemorrhagic transformation or other complications^{42,43}. Current clinical guidelines suggest implementing protocols such as pre-arrival hospital notification of incoming patients with possible AIS⁵⁹, or using telemedicine to accelerate image interpretation for rural centers without a neuroradiologist on site⁶⁰, to minimize the delay between hospital admission and initiation of treatment (referred to as ‘door-to-needle time’). The goal of implementing such protocols is to perform CT within 20 minutes of admission and keep door-to-needle times less than 60 minutes in at least 50% of patients⁶¹.

1.2.1 Thrombolytic Therapy

Thrombus formation (thrombosis) and dissolution (thrombolysis) are complex interconnected processes. Thrombosis starts when platelets are activated by contact with sub-endothelial proteins⁶². Activated platelets trigger a series of protease-mediated cleavages which ultimately ends with the serine protease thrombin cleaving soluble fibrinogen into insoluble fibrin⁶³. Fibrin polymerizes to form the bulk of the blood clot along with activated platelets, red blood cells, and white blood cells⁶⁴. This clotting cascade prevents excessive blood loss from damaged blood vessels but can also lead to thromboembolic stroke when clots form in cerebral arteries, or travel to cerebral arteries from elsewhere in the body. Clot dissolution is mediated by endogenous fibrinolysis, which relies on the formation of plasmin, a fibrinolytic enzyme, from its precursor plasminogen. This conversion is catalyzed by a group of enzymes called plasminogen activators⁶⁵. Thrombolytic therapy involves administering drugs that are either recombinant versions of endogenous plasminogen activators (e.g. tissue plasminogen activator (t-PA) or urokinase-plasminogen activator (u-PA)), or exogenous plasminogen activating agents (e.g. streptokinase), that enhance plasmin-mediated fibrinolysis⁶⁵. The likelihood of early recanalization and good outcome after IV thrombolysis is dependent on the clot fibrin content⁶⁶, and its length and density on CT^{67,68}. Early vessel recanalization and good functional outcome are also more likely in cardioembolic strokes compared to other stroke subtypes^{69,70}. A significant drawback to thrombolysis is that degradation of fibrin and fibrinogen inhibits the coagulation cascade⁷¹, and therefore increases the risk of intracerebral hemorrhage (ICH)⁷². Additionally, in patients with compromised BBB due to prolonged ischemia, t-PA can cross into the interstitial space, where it has neurotoxic

effects that can enhance excitotoxicity and further damage the BBB⁷³. For this reason, primary ICH must be ruled out by computed tomography (CT) or magnetic resonance imaging (MRI) before initiating thrombolysis⁷⁴.

The first clinical trial to show a significant benefit of thrombolytic therapy was the National Institute of Neurological Disorders and Stroke (NINDS) trial in 1995. Alteplase, a recombinant version of t-PA was administered intravenously within 3 hours of symptom onset, in patients with no evidence of ICH on CT. The percentage of patients with excellent outcome (assessed as a score of 0 or 1 on the modified Rankin Scale (mRS)) in the t-PA group was 43% compared to only 26% in the control group, and 90 day mortality was also lower in the t-PA group, despite increased risk of ICH (6.4% vs 0.6%)⁵⁷. Based on these results, the United States Food and Drug Administration (FDA) approved IV t-PA for the treatment of AIS within 3 hours post symptom onset. Phase IV trials in Canada⁷⁵ and Europe⁷⁶ would later confirm the efficacy of IV t-PA in routine care settings, showing that rates of excellent outcome (mRS \leq 1) (~38%), mortality within 90 days (11% to 22%), and symptomatic ICH (~6%) were all similar to pooled results from randomized controlled trials.

In the decade after FDA approval, administration rates of IV t-PA remained as low as 0.9% to 2.4%^{77,78}, with the 3 hour time window posing a significant barrier to treatment⁷⁹. Multiple trials comparing placebo to IV t-PA given within the first 6 hours post onset^{80,81}, or in the 3 to 5 hour time window⁸², failed to show a significant improvement in functional outcome, and had higher rates of symptomatic ICH in the treatment group. Meta-analysis of pooled data from six randomized controlled trials of IV t-PA found decreased odds of an excellent outcome (mRS \leq 1) as onset-to-treatment times

increased, but there was still a significant benefit in the 3 to 4.5 hour time window⁸³. Efficacy of IV t-PA given within 3 to 4.5 hours post onset was confirmed in the European Cooperative Acute Stroke Study (ECASS) III trial, which found significantly higher rates of excellent functional outcomes (52 vs 45% in the control group) in the IV t-PA group, and similar mortality rates despite increased risk symptomatic ICH⁸⁴. Administration of IV t-PA remains a frontline therapy for AIS patients, but the time window still presents a major barrier to treatment; studies suggest up to 67% of patients not receiving thrombolysis are deemed ineligible because of the time window⁸⁵.

Current clinical guidelines suggest administering IV t-PA within 4.5 hours of symptom onset, at a dosage of 0.9 mg/kg, with the first 10% of the dose given as a bolus⁵⁸, although a dosage of 0.6 mg/kg may result in similar improvement in functional outcome with lower rates of symptomatic ICH⁸⁶. Patients can be treated regardless of age, or admission stroke severity (assessed by the National Institute of Health Stroke Scale or NIHSS), provided admission non-contrast CT (NCCT) rules out primary ICH⁷⁴. IV t-PA within 4.5 hours is currently indicated for both genders, but the treatment effect may be more beneficial in women than in men⁸⁷. Patients who are at risk of a serious bleeding complication due to recent stroke, head trauma, brain surgery, or administration of low molecular weight heparin within 24 hours preceding the stroke should not be treated with thrombolysis⁵⁸. Blood glucose must be measured before initiating thrombolytic therapy because hypoglycemia can be incorrectly diagnosed as AIS⁸⁸, and severe hyperglycemia (blood glucose > 400mg/dL) is associated with lower recanalization rates⁸⁹ and increased the risk of ICH and poor outcome⁹⁰. Consequently, diabetes mellitus is also associated with higher rates of hemorrhagic transformation⁹¹ and in-hospital mortality⁹² in AIS

patients treated with thrombolysis, though studies suggest diabetic AIS patients still benefit from IV t-PA⁹³. Hypertension is also associated with increased risk of hemorrhagic transformation following thrombolytic therapy, increased mortality, and decreased probability of good functional outcome⁹⁴. Hypertensive patients can only receive IV t-PA if systolic and diastolic blood pressure can be safely lowered to less than 185, and 110mmHg respectively, and should be maintained at less than 180 and 105mmHg respectively for twenty-four hours after initiating thrombolytic therapy⁵⁸.

1.2.2 Mechanical Thrombectomy

Successful trials of IV thrombolysis were a breakthrough in treatment of AIS, but the time window still posed a major impediment to treatment⁸⁵, and recanalization rates were poor for large vessel occlusions (LVO)⁹⁵. LVO refers to occlusions of large proximal cerebral arteries, such as the M1 segment of the MCA, anterior cerebral artery (ACA), distal ICA, or the basilar artery. Although only ~40% of ischemic strokes are caused by LVO they account for ~60% of post-stroke dependence and ~95% of post-stroke mortality⁹⁶. Poor recanalization rates for LVO and the relatively short time window for administering IV t-PA were major drivers for development of IAT for AIS.

Early attempts at IAT involved administering thrombolytic drugs directly to the thrombus by guiding an endovascular microcatheter delivery system to the occlusion site, allowing a high concentration of thrombolytic agent to be delivered to the thrombus while also minimizing systemic exposure, theoretically minimizing the risk of hemorrhage. The earliest clinical use of IAT in the literature used intra-arterial (IA) delivery of streptokinase to treat patients with basilar artery thrombosis and reported excellent outcomes in 3 of 5 patients⁹⁷. Later studies found that IA recombinant u-PA within 6 hours of onset was

associated with improved functional outcome^{98,99}, but also high rates of ICH, and symptomatic ICH^{98,99}. Several studies also combined IV t-PA initiated as soon as possible, followed by IA delivery of t-PA directly to the thrombus for patients who still had clot visible on angiography. These studies found similar rates of ICH and a nonsignificant improvement in outcome compared to IV t-PA alone¹⁰⁰⁻¹⁰². Although IA thrombolysis was shown to improve recanalization rates compared to IV thrombolysis⁹⁸⁻¹⁰³, there is no level 1 evidence that IA thrombolysis alone improves functional outcome compared to IV thrombolysis alone.

Catheter devices for mechanically removing thrombus were developed as an alternative to IA delivery of thrombolytic agents. Mechanical removal of the thrombus is advantageous because of high recanalization rates for LVO¹⁰⁴, faster recanalization relative to IA thrombolysis which requires prolonged infusion of thrombolytic agents for up to 2 hours¹⁰², and reduced hemorrhage risk by avoiding the use of thrombolytic drugs¹⁰⁵. In a mechanical thrombectomy procedure: a microcatheter is advanced to the occlusion site and passed through the thrombus, the device is deployed distal to the thrombus and retracted to ensnare the thrombus and pull it to a proximally placed guide catheter for aspiration¹⁰⁶. The first endovascular device approved for AIS treatment used a flexible corkscrew design and was called the Mechanical Embolus Removal in Cerebral Ischemia (MERCi) retriever¹⁰⁶. Trials of the MERCi device showed that LVOs could be recanalized in 46% to 57% of patients treated within 8 hours, but design limitations meant up to 6 passes had to be made to remove the entire clot^{106,107}. Second generation devices using a flexible, retrievable wire stent were shown to be superior to the MERCi device^{108,109}.

Early randomized controlled trials of mechanical thrombectomy all failed to show a significant improvement in functional outcome compared to IV t-PA¹¹⁰⁻¹¹², but these trials had several important limitations. Only ~20% of patients in the IAT arm of each trial were treated with second generation devices¹¹⁰⁻¹¹², and in 2 trials 50% to 66% of patients were treated with IA thrombolysis instead of thrombectomy^{110,111}. IV t-PA was not administered to patients randomized into the IAT arm of 1 trial. As a result, treatment was initiated an average of 1h later in patients receiving IAT compared to patients treated with IV t-PA¹¹¹. CT angiography (CTA) was not used to confirm the presence of a LVO for all patients in 2 of the trials, resulting in many patients randomized into the IAT arm not having an occlusion that was suitable for treatment with IAT^{110,111}. Lessons learned from these trials informed the design of subsequent randomized, controlled trials of IAT.

In 2015, 5 trials comparing patients treated with IV t-PA plus IAT to patients treated with IV t-PA alone were stopped early after demonstrating significant benefit of IAT. All 5 trials used NCCT or MRI to rule out ICH, angiography to confirm the presence of LVO, and initiated IAT within 6¹¹³⁻¹¹⁶ to 8¹¹⁷ hours of symptom onset. In addition to demonstrating the efficacy of IAT for treating patients with LVO, these trials also provided early evidence that advanced neuroimaging, such as multi-phase CTA or CTP could be used to identify patients with a small infarct core and large penumbra, who would be most likely to benefit from revascularization. The ESCAPE trial, performed in Canada, used a semi-quantitative scale called the Alberta Stroke Program Early CT Score (ASPECTS) to assess NCCT for signs of early ischemic damage indicative of a large infarct core¹¹⁸, and a novel CTA imaging technique (multiphase CTA) to evaluate the degree of collateral circulation, which reflects the amount of residual CBF in the ischemic tissue¹¹⁹. The

SWIFT-PRIME and EXTEND-IA trials, performed in the United States and Australia/New Zealand respectively, used thresholds applied to parameter maps from CTP to estimate the volume of infarct and penumbra; patients with large infarct volumes and/or small penumbra volumes were excluded^{113,115}. These trials, which included imaging to evaluate the extent of irreversibly damaged infarct and salvageable penumbra, had higher rates of good functional outcome in the IAT group (53% to 71%), than the MRCLEAN and REVASCAT trials, conducted in the Netherlands and Spain respectively, which did not use advanced neuroimaging (33% to 44%)^{116,117}.

Several retrospective studies noted that there was no significant difference in the rate of good functional outcome, symptomatic ICH or mortality when patients were triaged based on admission CTP or MRI^{120,121}, providing more support for image-based triaging rather than strictly time-based triaging. The efficacy of image-based triaging for IAT was confirmed recently in the DEFUSE 3 and DAWN trials – two randomized, controlled trials comparing standard medical therapy alone to standard medical therapy plus IAT in patients arriving up to 16 hours¹²² to 24 hours¹²³ post symptom onset, or those with unknown onset times. Patients were eligible if they had LVO confirmed on CTA, no evidence of hemorrhage on NCCT, and mismatch between infarct volume and either penumbra volume¹²² or clinical deficit¹²³. The treatment effect of IAT (difference in rate of functional independence between IAT and control groups) seen in these trials (28% to 36%)^{122,123} was paradoxically larger than what was seen in a meta-analysis of the trials where IAT was initiated within 6 hours of symptom onset (19.5%)¹⁰⁴. This was mainly because patients in the control group were not eligible for IV t-PA since these trials only enrolled patients where time from symptom onset was 6 hours or more (87% of patients in the control groups

in earlier trials received IV t-PA)¹⁰⁴. Nevertheless, the rate of IAT-treated patients with good functional outcomes (45% to 49%)^{122,123} was similar to when IAT was initiated within 6 hours of symptom onset (46%)¹⁰⁴, showing that IAT could still be effective in certain patients up to 24 hours post symptom onset.

Current clinical guidelines recommend performing mechanical thrombectomy with a stent retriever within 6 hours of symptom onset in patients aged 18 years or older, no sign of extensive early ischemic damage on NCCT (ASPECTS ≥ 6), and occlusion of the intracranial portion of the ICA or M1 segment of the MCA confirmed on CTA⁵⁸. Mechanical thrombectomy is also recommended up to 24 hours post symptom onset in patients aged 18 years or older, with CTA-confirmed occlusion of ICA or M1 segment of the MCA, and either an infarct/penumbra mismatch, defined by the DEFUSE 3 trial criteria, or a clinical/imaging mismatch, defined by the DAWN trial criteria. Both trials used thresholds applied to CTP-CBF maps or diffusion-weighted MRI (diffusion-weighted imaging or DWI) to estimate the volume of infarct core. The DEFUSE 3 trial used thresholds applied to time-to-maximum (T_{\max}) maps from CTP or perfusion-weighted MRI (perfusion-weighted imaging or PWI) to estimate the penumbra volume; patients were eligible for treatment if penumbra volume was 1.8 times larger than the infarct, infarct volume was $< 70\text{mL}$, and penumbra volume was $> 15\text{mL}$ ¹²². The DAWN trial inferred the volume of penumbra from clinical assessment with the NIHSS. Clinical deficit defined by NIHSS reflects the total volume of ischemic tissue since both infarct and penumbral tissue are functionally silent, therefore a large penumbra volume is implied in patients with severe clinical deficits but only a small infarct core volume. Patients younger than 80 years were eligible if infarct volume $< 31\text{mL}$ and NIHSS ≥ 10 , or if $31\text{mL} \leq \text{infarct volume} < 51\text{mL}$

and NIHSS ≥ 20 ; patients 80 years or older were eligible if infarct volume $< 21\text{mL}$ and NIHSS ≥ 10 ¹²³.

1.3 Medical Imaging in Ischemic Stroke

Medical imaging has become an important part of routine clinical care for AIS. Structural and functional information from admission neuroimaging is used to inform three key factors for triaging and management of patients with AIS symptoms: 1) is the stroke ischemic or hemorrhagic? 2) is there an intravascular occlusion? 3) is there viable penumbra tissue? NCCT or MRI must be performed at admission to determine if the stroke is ischemic or hemorrhagic before initiating treatment, since treatment options for AIS can be detrimental to patients with primary ICH¹²⁴. CTA or magnetic resonance angiography (MRA) is also required to define the presence and location of LVO and to assess ease of access in patients being considered for IAT, and many centers now also routinely use CTP or PWI to guide treatment decisions. In addition to improving acute diagnosis and providing personalized triaging based on tissue status instead of time from onset, physiological information from functional CT, MRI, and positron emission tomography (PET) has shaped AIS treatment strategies by advanced our understanding of stroke pathophysiology and tissue viability.

1.3.1 Positron Emission Tomography

PET imaging relies on detection of coincident gamma rays produced in positron annihilation events to measure the spatial distribution of biological molecules radioactively labelled with positron emitting nuclides, known as radiotracers. PET is a highly sensitive imaging modality, capable of detecting nanomolar concentrations of radiotracer, which can

assess a wide range of hemodynamic, functional, and metabolic parameters depending on properties of the radiotracer used. A static PET scan performed sometime after radiotracer administration can measure the spatial distribution of radioactivity in the body relative to the total injected amount and body weight. On the other hand, dynamic scanning used in conjunction with arterial blood sampling to quantify arterial delivery (arterial input function or AIF) of the radiotracer can allow more detailed pharmacokinetic modelling to be performed¹²⁵.

PET imaging with ¹⁵O-labelled water and oxygen gas allows quantification of CBF, cerebral metabolic rate of oxygen (CMRO₂), and oxygen extraction fraction (OEF) (fraction of oxygen extracted from the blood). Contemporaneous assessment of blood flow and oxygen metabolism with PET imaging greatly advanced the understanding of the time-dependence of tissue viability in ischemic stroke patients^{126,127}. Tissue with decreased CBF (CBF < 12 mL·min⁻¹·100g⁻¹) and CMRO₂ usually progressed to infarction, while penumbral tissue had CBF between 12-22 mL·min⁻¹·100g⁻¹, elevated OEF, and preserved CMRO₂ in the acute phase¹²⁸. The coupled decrease in CBF and increase in OEF (termed ‘misery perfusion’)¹²⁹ was representative of still-viable tissue, that would eventually progress to infarction without reperfusion due to mismatch between metabolic demand and decreased oxygen delivery from CBF. Animal studies of reversible focal cerebral ischemia showed that brain tissue with acutely elevated OEF progressed to infarction in animals with permanent MCA occlusion, but not in animals where the occlusion was reversed after 6 hours, establishing the time-dependence of penumbral viability^{130,131}. Although tissue compartments in AIS are well defined by CBF, CMRO₂, and OEF, there are drawbacks to using these parameters: a PET scanner and on-site cyclotron are required since the half-life

of ^{15}O is only ~2 minutes¹³², and the rapid arterial blood sampling required for quantification is invasive.

More recently, tracers labelled with ^{11}C or ^{18}F which bind to neuronal cell surface receptors have been developed. The half-lives of ^{11}C and ^{18}F are ~20 minutes and 110 minutes respectively¹³², making them easier to use than ^{15}O logistically. One example is ^{11}C -labelled flumazenil (FMZ), which is a selective, high-affinity ligand for the central benzodiazepine receptor of the GABA receptor complex¹³³. GABA receptor activity can be used as a marker of neuronal integrity since GABA receptors are sensitive to ischemic damage¹³⁴. Clinical studies have shown that neocortex with decreased uptake of ^{11}C -FMZ in the acute phase of stroke is infarcted¹³⁴⁻¹³⁶. Fluoroethylflumazenil (FFMZ), a fluorinated analog of FMZ, works similarly for mapping GABA receptor activity¹³⁷, and can be labelled with ^{18}F , which is advantageous because the half-life is longer than ^{11}C ¹³⁸. The density of GABA receptors is low in the basal ganglia and negligible in white matter¹³⁹, meaning FMZ, FFMZ and other benzodiazepine receptor ligands are not suitable for detecting infarction outside of cortical grey matter¹³³. Fluoromisonidazole (FMISO) radiolabelled with ^{18}F is a hypoxia tracer which has been proposed as a marker of penumbral tissue. FMISO accumulates in ischemic tissue by binding to macromolecules after being reduced by nitroreductases¹⁴⁰. Studies in a rat MCA occlusion model of AIS showed a pattern of FMISO uptake throughout the entire MCA territory at early time points 30 to 60 minutes post occlusion, that evolved into a small rim of uptake surrounding the infarct core, and by 24 to 48 hours post occlusion there was minimal uptake in the final infarct^{141,142}. A similar time-dependent uptake pattern was also observed in human patients with AIS due to MCA occlusion¹⁴³. However, more recent studies using the same rat model

of AIS found that FMISO was retained in ischemic tissue for up to 6 hours post occlusion, consequently penumbral tissue which had already progressed to infarction within 6 hours still had elevated FMISO uptakes¹⁴⁴. Subsequent study showed strong FMISO uptake throughout the MCA territory even when administered up to 6 hours post occlusion, when most ischemic tissue had likely progressed to infarction. Approximately 50% of the FMISO-retaining lesion was infarcted on histology, and most of the salvaged tissue in the lesion had signs of neuronal damage¹⁴⁵. These findings suggest increased FMISO uptake may not be a specific marker of penumbral tissue, further study is required to determine the applications of this radiotracer in AIS research.

Although the clinical utility of PET in AIS is limited due to cost and logistical complexity, it is still an invaluable tool for studying pathophysiological processes of AIS and serves as a gold standard for validating other imaging techniques used in AIS.

1.3.2 Magnetic Resonance Imaging

MRI is a versatile imaging technique used for AIS diagnosis and prognosis, that can provide both structural and functional information depending on the pulse sequence used to create the image. Acute ICH can be seen on MRI with gradient recalled echo (GRE) pulse sequences as a core of heterogenous signal intensity surrounded by a rim of hypointensity. Studies have shown that NCCT and MRI with GRE pulse sequences are equivalent for ruling out ICH in patients being considered for IV t-PA¹²⁴. Thrombus location and length can also be assessed on susceptibility-weighted imaging (SWI) with GRE sequences, where the thrombus appears as a hypointense blooming artifact due to paramagnetic properties of deoxyhemoglobin contained in the clot¹⁴⁶. SWI has a high sensitivity (81% to 86%) and specificity (90%) for detecting clots in the anterior cerebral

circulation^{146,147}, can reliably measure the length of clots longer than 6mm¹⁴⁷, and clot composition can even be inferred since SWI is related to the red blood cell content of the clot¹⁴⁸.

MRA can be performed either by injecting gadolinium-based contrast agent, or with non-contrast methods like the time-of-flight (TOF) technique, where flowing blood has hyperintense signal relative to surrounding static tissue. Both contrast-enhanced and non-contrast enhanced MRA can assess vessel patency in AIS¹⁴⁹ and both methods have advantages and disadvantages. TOF-MRA can be performed when contrast administration is not possible, but compared to contrast-enhanced MRA, the acquisition time is longer, making patient motion problematic, and the field of view (FOV) is smaller, so extracranial arteries cannot be imaged¹⁴⁹.

DWI and associated apparent diffusion coefficient (ADC) maps are the clinical gold standard for detecting early ischemic damage. One of the final steps towards irreversible tissue damage is cytotoxic edema, where water shifts to the intracellular space due to the increase in intracellular sodium and calcium after membrane ion pump failure. DWI is sensitive to Brownian motion of water molecules and detects cytotoxic edema as a hyperintense lesion due to restricted diffusion of water molecules in the intracellular space¹⁵⁰. Contrast in DWI is due to differences in ADC as well as T2-weighted contrast, commonly referred to as 'T2 shine-through'¹⁵¹. To remove the effects of T2 shine-through, ADC maps are generated where cytotoxic edema is seen as a hypointense lesion with decreased ADC values¹⁵¹. Acute DWI lesions are highly sensitive and specific markers of AIS¹⁵² and provide reliable estimates of the size and location of the final infarct core measured on follow-up imaging^{136,153}. Lesion reversal may occur in ~10% of patients,

where a small part of the acute lesion may appear normal on follow-up imaging,¹⁵³ however the reversal is often transient and unlikely to represent salvaged tissue¹⁵⁴.

Imaging of the infarct core with DWI can be complemented with PWI performed using IV administration of exogenous gadolinium-based contrast agent. PWI with exogenous contrast agents can be broadly divided into dynamic contrast-enhanced (DCE)-MRI, which relies on the T1 effects of gadolinium, or dynamic susceptibility contrast (DSC)-MRI, which relies on the susceptibility effect of gadolinium. Signal enhancement versus time curves are measured by T1-weighted or T2/T2*-weighted echo-planar imaging and summary parameters like time-to-peak (TTP) and area-under curve (AUC) can be determined in a model-free approach¹⁵⁵. Or quantitative maps of CBF, T_{max} , and other parameters can be computed with pharmacokinetic modelling if the measured signal enhancement curves are converted to contrast concentration versus time curves, and an AIF is available. Measured signal enhancement is not linearly related to contrast concentration in PWI, making absolute quantitation of hemodynamic parameters more difficult. Contrast concentration can be calculated from signal enhancement using pulse sequence-dependent equations¹⁵⁵, DCE-MRI requires pre-contrast T1 mapping in addition to pulse sequence-dependent equations to calculate the contrast concentration versus time from the measured signal¹⁵⁶. Accurately measuring the AIF can also be problematic because of in-flow/out-flow effects (blood flowing into or out of the imaging volume causing signal increases and decreases respectively), limited temporal resolution and other factors¹⁵⁶. When an AIF of sufficient quality cannot be derived from the PWI scan, alternatives such as population-averaged AIFs may be used instead¹⁵⁶, but this can lead to errors in parameter calculation if the chosen population-averaged AIF is not representative of the individual patient.

Studies have shown that the deconvolution-based T_{\max} parameter is optimal for identifying penumbra ($T_{\max} > 6s$) on admission DSC-MRI^{157,158}. Model-free summary parameters do not account for arterial delivery and are therefore affected by factors like bolus dispersion and cardiac output¹⁵⁹, but studies show TTP is highly correlated with T_{\max} and performs similarly for predicting penumbra volume^{160,161}. DWI/PWI mismatch is a widely used neuroimaging paradigm for managing AIS patients based on infarct and penumbra volumes measured from admission DWI and PWI using fully automated post-processing software (RApid processing of PerfusIon and Diffusion, or RAPID)¹⁶². DEFUSE 3 recently used RAPID to show that patients with LVO and mismatch on admission DWI/PWI or CTP (infarct volume $< 70\text{mL}$, infarct/penumbra ratio > 1.8 , and penumbra volume $> 15\text{mL}$) can still benefit from IAT up to 16 hours post symptom onset¹²². PWI can also be performed with endogenous contrast using arterial spin labelling (ASL), where magnetically-labelled, arterial blood acts as an endogenous tracer rather than administering exogenous gadolinium-based contrast. However, ASL is not commonly used for AIS because relaxation of the magnetic label during prolonged transit times caused by ischemia can lead to poor signal-to-noise ratio and underestimated CBF¹⁶³.

Another MRI-based paradigm for AIS patient management is mismatch between admission fluid-attenuated inversion recovery (FLAIR) and DWI. Hyperintense lesions on FLAIR are highly sensitive markers of infarct core¹⁶⁴ but are generally not visible in the first 3 hours post onset, whereas DWI lesions are visible 1 hour or less post onset¹⁶⁵. Studies have shown that FLAIR-DWI mismatch (hyperintense DWI lesion with no FLAIR lesion) is a surrogate marker of ischemia duration¹⁶⁶ that can identify patients with time from symptom onset < 4.5 hours with high specificity¹⁶⁷. A recent randomized, placebo-

controlled trial found that treating patients with FLAIR-DWI mismatch and unknown stroke onset time with IV t-PA improved functional outcome despite increased risk of symptomatic ICH¹⁶⁸. FLAIR-DWI mismatch could potentially be used in patients with unknown onset times (approximately 14 to 25% of all AIS patients)^{169,170} to identify those with ischemia duration < 4.5 hours, who are more likely to benefit from thrombolysis.

In addition to providing anatomical and functional information about vessel patency, tissue viability, ischemia duration and other factors, MRI is more readily available in the AIS setting than PET and does not require ionizing radiation. However, MR scanners have limited availability compared to CT outside of large city hospitals or academic centers, and patients with MRI contraindications (e.g. claustrophobia, ferromagnetic implants, pacemakers) must be excluded from imaging; screening for contraindications also results in longer door-to-needle times compared to CT¹⁷¹. Despite these limitations, MRI is an important modality for triaging and management of AIS patients.

1.3.3 Computed Tomography

CT is the most commonly used modality for assessing AIS patients because it is more widely available¹⁷², less expensive, and faster compared to MRI, and CT can be performed without first screening the patient for common MRI contraindications. Patients with AIS symptoms are often assessed with NCCT, CTA or multiphase CTA, and CTP.

1.3.3.1 Non-Contrast Computed Tomography

Admission NCCT is required for any patient with stroke symptoms to rule out non-vascular stroke mimics and primary ICH. The intensity in each voxel of CT images, expressed in Hounsfield Units (HU), is linearly proportional to the x-ray linear attenuation

coefficient. NCCT has good sensitivity for detecting acute phase ICH which appears as a hyperintense lesion¹²⁴, and is more cost-effective as a screening tool than MRI⁷⁴. In addition to ruling out ICH, careful examination of NCCT can also yield information about early ischemic damage and clot characteristics. ASPECTS is a standardized CT reading method based on assessment of 10 regions of interest (ROI) located in the MCA territory visible in two 5mm thick CT slices, one at the level of the thalamus and basal ganglia, and one just rostral to ganglionic structures. One point is subtracted from 10 for each ROI with evidence of early ischemic damage¹¹⁸. Signs of early ischemic damage visible on NCCT include hypoattenuation, sulcal effacement due to mass effect from edema, and loss of gray-white matter differentiation, including loss of the insular ribbon and obscuration of the lentiform nucleus¹⁷³. ASPECTS ≤ 7 has been associated with increased risk of poor functional outcome and symptomatic ICH in patients treated with IV t-PA¹¹⁸. Retrospective studies of patients in the NINDS and ECASS II trials found no significant effect of baseline ASPECTS on IV t-PA treatment effect^{174,175}, however ASPECTS ≤ 7 was associated with significantly increased risk of symptomatic ICH in the ECASS II patients¹⁷⁵, and there was a trend toward decreased treatment benefit and increased mortality in the NINDS patients¹⁷⁴. Low ASPECTS was also associated with increased risk of poor functional outcome, mortality, and symptomatic ICH in patients treated with IAT¹⁷⁶ and was part of the exclusion criteria for three of the seminal trials demonstrating the efficacy of IAT^{113,114,117}. Current clinical guidelines suggest IAT should only be performed in patients with ASPECTS ≥ 6 ⁵⁸, but there is some evidence that patients with ASPECTS ≤ 5 still benefit from IAT^{177,178}.

Intraluminal thrombus in the distal ICA, M1, and M2 segments of the MCA can also be visualized in patients as hyperintensity on NCCT, this has been proposed as a method of confirming the presence of LVO without performing CTA in patients being considered for IAT. The hyperdense artery sign can detect LVO (as assessed with gold standard CTA) with high specificity (95-100%) and moderate sensitivity (30-55%) when NCCT is reconstructed with standard 5mm thick slices^{179,180}, studies have shown that sensitivity can be improved to 70-100% by using thinner (0.625-1.5mm) slices¹⁸⁰⁻¹⁸². Thrombus length measured on NCCT also agrees with length measured on CTA within $\pm 1\text{mm}$ when slice thickness is $\leq 2.5\text{mm}$ ¹⁸³. Studies have shown that IV t-PA is less effective for thrombi longer than 10mm on NCCT¹⁸⁴, and that clot length and location are associated with outcome in IAT-treated patients¹⁸⁵.

1.3.3.2 Computed Tomography Angiography

CTA requires IV administration of iodinated contrast agent and rapid scanning after a short delay to capture peak intravascular enhancement. Iodinated k-edge falls within the energy range of diagnostic x-rays, causing iodinated contrast agents to produce a measurable increase in x-ray attenuation ($\sim 30\text{HU}$ per 1mg/mL of iodine), and therefore signal intensity measured on CT. CTA source images can be viewed directly, or as maximum intensity projections or 3D reconstructions with postprocessing; blood vessels perfused with contrast agent as the image is acquired will appear hyperdense. Evaluation of flow dynamics is also possible with 4D-CTA or multiphase CTA, where images are acquired either continuously (4D-CTA), or at multiple discrete time points (multiphase CTA) as contrast travels through cerebral vasculature, rather than conventional CTA where imaging at a single time point is performed. CTA has better spatial resolution ($\sim 0.5\text{mm}$

isotropic resolution)¹⁸⁶ than MRA and is less invasive and faster than digital subtraction angiography (DSA), the gold standard for cerebral angiography, while also providing near equivalent evaluation of the presence and location of occlusions^{187,188}.

The presence, and location of occlusions on angiography are important prognostic factors that have implications for patient triaging and management. Current clinical guidelines require LVO to be confirmed on angiography before initiating IAT⁵⁸. Failure to perform admission CTA was one major limitation of earlier IAT trials, resulting in many enrolled patients having no evidence of occlusion, or occlusions not accessible by IAT upon arrival to the angiography suite^{110,111}. All trials showing benefit of IAT to date have used CTA or MRA to confirm the presence and location of LVO. Presence, length and location of the clot on CTA is also a predictor of recanalization in IV t-PA treated patients. The benefit of IV t-PA may be diminished in up to ~25% of AIS patients who have no visible occlusion on CTA¹⁸⁹; in patients with visible occlusions, lower recanalization rates are observed for proximal occlusions^{95,190}, and clots longer than 15mm¹⁹¹. These and other clot characteristics evaluated on CTA, such as absence of residual flow through the clot¹⁹², can help identify patients who are more likely to benefit from IAT rather than IV t-PA. The overall extent of anterior circulation clots can also be assessed on CTA using a semi-quantitative scale called the clot burden score. Points are subtracted from 10 for absence of contrast opacification across the full cross-section of any parts of the intracranial ICA, proximal, or distal M1 segment of the MCA (2 points each), M2 segments of the MCA, A1 segment of the ACA, and extracranial ICA (1 point each)¹⁹³. High clot burden scores have reasonable sensitivity and specificity (73% and 65% respectively) for predicting good

functional outcome in patients treated with IV t-PA¹⁹⁴ and have been associated with smaller final infarct volume and improved functional outcome in IAT-treated patients¹⁹⁵.

Another important aspect of CTA is evaluation of collateral circulation, which provides alternative routes for blood to reach tissue when a proximal cerebral artery is occluded. Cerebral collateral circulation consists of the Circle of Willis, which links the anterior and posterior circulation, connections between external carotid artery branches and branches of the ICA, and leptomeningeal collaterals which connect territories of the MCA, ACA, and posterior cerebral artery¹⁹⁶. More extensive collateral circulation implies more preserved CBF in the affected vascular territory, and therefore slower progression of ischemic penumbra to infarction. Studies have confirmed that more extensive collateral circulation observed on angiography were associated with smaller final infarct volumes and better functional outcomes in AIS patients^{197,198}. There are numerous semi-quantitative 3- or 5-point scales for grading collateral circulation on CTA by assessing the degree of collateral vessel opacification in the affected vascular territory relative to the contralateral side¹⁹⁹⁻²⁰². The regional leptomeningeal collateral (rLMC) score differs by scoring the collateral circulation relative to the contralateral side in the predefined regions used in ASPECTS²⁰³. Since conventional CTA represents only a single time point, delayed collateral vessel opacification can be missed depending on bolus characteristics and the timing of the scan. Dynamic CTA techniques, such as 4D-CTA or multiphase CTA, provide time resolved data which is less dependent on scan timing or bolus characteristics. Collateral scoring on dynamic CTA assesses the extent and prominence of collateral vessel, as well as the time delay for retrograde contrast filling relative to the contralateral side²⁰⁴. Multiple studies have found collateral evaluation on dynamic CTA to better predict

functional outcome compared to conventional single-phase CTA^{119,205,206}, likely due to less instances of underestimated collateral score due to delayed enhancement missed on single-phase CTA²⁰⁷. Collateral scores from multiphase CTA were used to select patients for IAT within 6 hours of symptom onset in the ESCAPE trial¹¹⁴.

1.3.3.3 Computed Tomography Perfusion

In the last decade CTP has become more common upon admission of patients with AIS symptoms. Similar to perfusion-weighted MRI, CTP involves repeated CT scanning of the brain as an IV bolus injection of iodinated contrast agent is administered and transient changes in signal intensity versus time (time-density curves or TDC) are measured in each tissue voxel as contrast passes through brain vasculature. Signal enhancement measured in each voxel by CTP is linearly proportional to the concentration of iodinated contrast agent in the tissue, so difficulties converting measured signal enhancement to tissue and arterial contrast concentration versus time curves ($Q(t)$ and $C_a(t)$ respectively) encountered in perfusion-weighted MRI due to contrast non-linearity are avoided²⁰⁸. CTP also has faster sampling rates and is not affected by in-flow/out-flow effects seen in perfusion-weighted MRI, allowing the AIF to be measured from the CTP acquisition rather than relying on population-averaged AIFs and other alternatives used in PWI.

1.3.3.3.1 Calculation of Hemodynamic Parameters

Hemodynamic parameters can be calculated using deconvolution or non-deconvolution models. Generally, non-deconvolution models are faster but rely on simplifying assumptions about brain hemodynamics which do not always hold true, whereas deconvolution models are more physiologically appropriate but require advanced

algorithms that extend computation time²⁰⁸. The work in this thesis only uses deconvolution models. The tissue TDC measured in each voxel during the CTP acquisition is dependent on the arterial TDC ($C_a(t)$), and the inherent hemodynamic properties of the tissue²⁰⁸. Under ideal injection conditions, where a unit bolus of contrast is deposited in a feeding artery immediately upstream from the tissue of interest (i.e. $C_a(t)$ is a delta function of unit height), $Q(t)$ in each voxel would depend only on the hemodynamic properties of the tissue. The theoretical $Q(t)$ corresponding to an ‘impulse’ arterial input is called the impulse residue function (IRF or $R(t)$) and can be thought of as the fraction of contrast remaining in the tissue over time following a unit bolus of contrast. Clinical replication of these injection conditions is not practical, so the AIF is measured from a proximal cerebral artery and assumed to represent the arterial input to all of the tissue of interest²⁰⁸. Since the amount of contrast delivered to the tissue at any instant is $F \cdot C_a(t)$, any general $Q(t)$ can be represented as the sum of time-shifted IRFs scaled by $F \cdot C_a(t)$ at each time point²⁰⁹ (Figure 1.1):

$$Q(t) = F \cdot \int_0^t C_a(t') \cdot R(t - t') \cdot dt'$$

Where t is the total scan time. The integral term is the convolution of the arterial TDC and the IRF. This can be rewritten as the following by multiplying F into $R(t)$ (flow-scaled IRF or $R_F(t)$)²¹⁰:

$$Q(t) = F \cdot C_a(t) \otimes R(t) = C_a(t) \otimes R_F(t)$$

Where \otimes is the convolution operator (Figure 1.2).

Figure 1.1: The concept of deconvolution applied to CT Perfusion

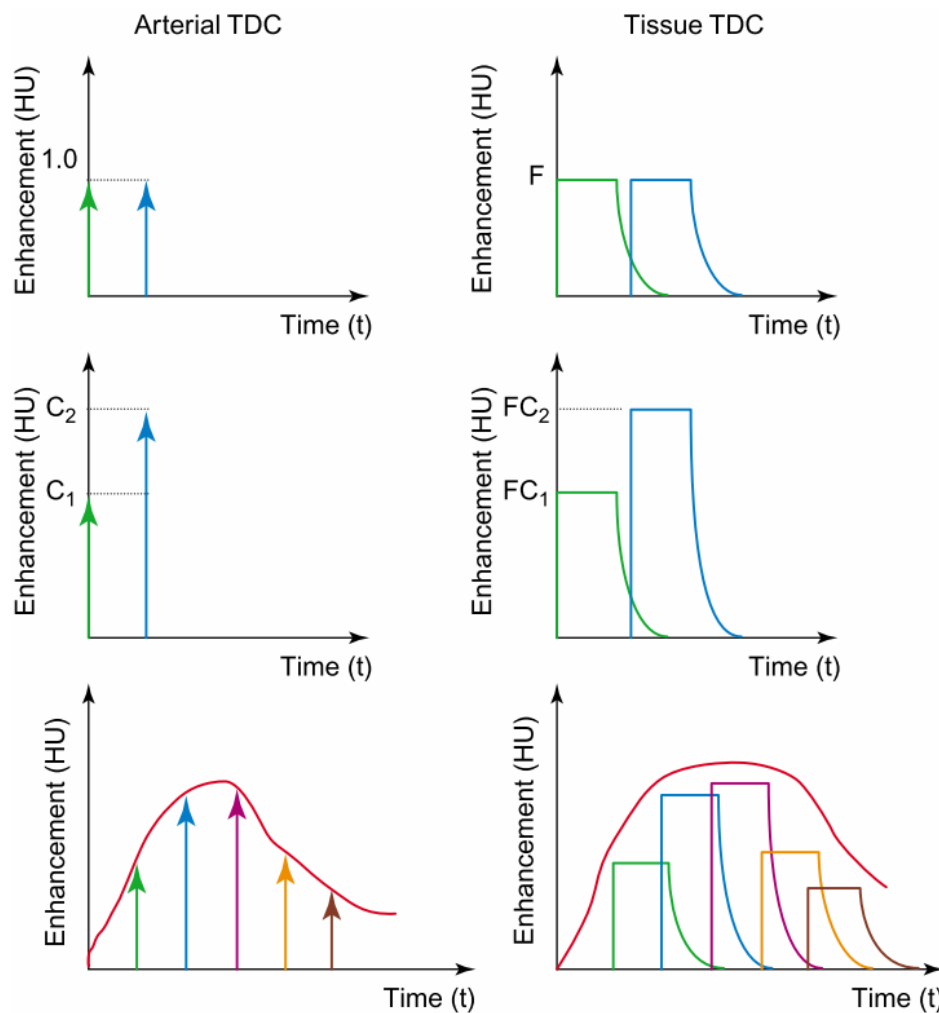


Fig. 1.1: This figure was adapted from ‘Functional CT: Physiological models’, by Ting-Yim Lee published in *Trends in Biotechnology* (2002; 20(8): 3-10)²¹⁰. The left and right columns show arterial TDCs and the corresponding tissue TDCs. The top row illustrates the concept of time invariance; if hemodynamic conditions are constant over the duration of the CTP acquisition, then two impulse arterial inputs of equal height occurring at different times result in two identical IRFs, shifted in time. The middle row illustrates the concept of linearity; if enhancement measured by the CT scanner is linearly related to the concentration of contrast agent, then the height of the IRF will be linearly related to the

arterial enhancement multiplied by the flow (F) delivery. Under these conditions, any general AIF can be represented as a series of delta functions with heights given by the measured arterial contrast concentration versus time curve, and any tissue TDC can be represented as a series of time-shifted IRFs scaled by the measured arterial contrast concentration versus time curve.

Figure 1.2: Graphical representation of CTP deconvolution equation

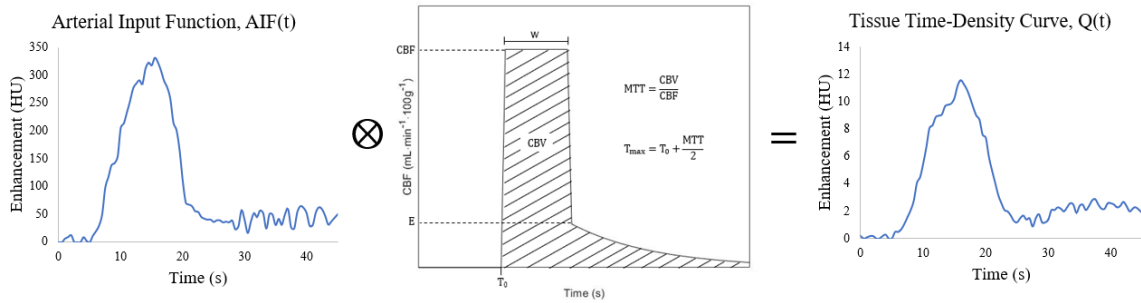


Fig. 1.2: Graphical representation of the operational equation of CTP. $Q(t)$ measured in each voxel of brain tissue is a combination of the arterial delivery of contrast (represented by $AIF(t)$) and the inherent hemodynamics of that voxel of brain tissue (described by $R_F(t)$), therefore $Q(t)$ is a convolution of the AIF and $R_F(t)$.

Deconvolution algorithms solve for $R_F(t)$ in each tissue pixel to approximate the regional tissue hemodynamics that would be measured under ideal injection conditions by removing the effect of $C_a(t)$. The shape of $R_F(t)$ depends on the model used in the CTP software, all work contained in this thesis uses a form based on the Johnson-Wilson model²¹¹. The Johnson-Wilson model allows CBF, CBV, MTT, contrast arrival time (T_0), and T_{max} (Figure 1.3).

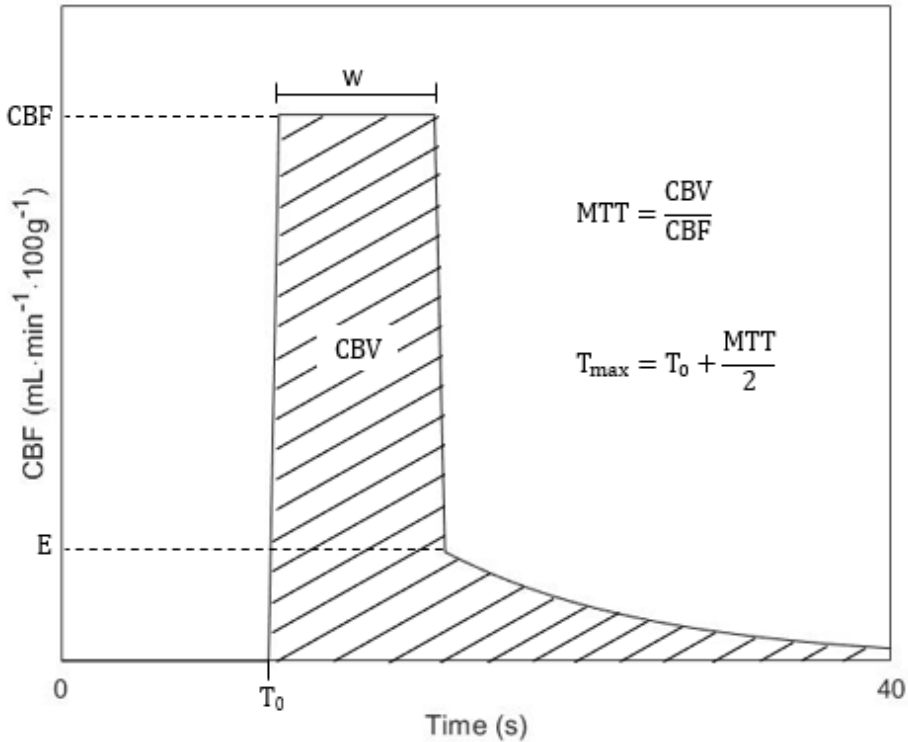
Figure 1.3: Sample IRF

Fig. 1.3: An example of the flow-scaled IRF from the Johnson and Wilson model. The delay between contrast arrival at the AIF and the tissue TDC is the arrival time (T_0), the height of the initial box-shaped portion is equal to CBF, and the area under the IRF is equal to CBV. The width of box (w) is the minimum transit time through the tissue, and E describes the fraction of contrast with transit time equal to w . The remaining fraction of contrast ($1 - E$) with transit times longer than w is described by the tail portion, which is assumed to be an exponential decay function with rate constant k . MTT is calculated as CBV divided by CBF, as required by the central volume principle, and T_{\max} is calculated as T_0 plus half of the MTT ($T_0 + \text{MTT}/2$)²¹⁰.

1.3.3.3.2 Technical Considerations for CTP Acquisition

Current commercially available CTP software packages are almost fully automated, the only user input is reviewing the AIF and venous output function (VOF) automatically selected by the program, or manually selecting them if the software does not have automated post-processing features. The AIF is usually measured from a large cerebral artery that is orthogonal to the image plane to minimize partial volume averaging. Depending on the brain region covered by the scan, the intracranial ICA, or ACA are commonly used for the AIF, and the VOF is usually taken from the posterior superior sagittal sinus²¹². Underestimation of the AIF due to partial volume averaging can be corrected by normalizing the area under the AIF to that of the VOF²¹⁰.

CTP was previously restricted by limited z-axis coverage, but modern 256/320-row multidetector CT scanners can cover 16cm in the z-axis direction, allowing nearly the whole brain to be imaged in a single scan²¹². Scan coverage can be increased further using table-toggling techniques, where the table is moved back and forth so that two adjacent slabs are imaged during the same bolus injection²¹². One limitation of CTP is the ionizing radiation dose to the patient, which depends not only on x-ray tube voltage and current, but also the duration of the scan, the temporal sampling interval, and other factors. CTP scan duration varies from 40-60s when only perfusion is necessary, up to 90-180s when both perfusion and BBB permeability are assessed. Radiation dose increases as sampling interval shortens, so longer scans are divided into multiple phases with progressively longer sampling intervals to reduce radiation dose to the patient. Multiphase scans generally consist of a 30-45s arterial phase with a sampling interval of 1 image per second, then a 30-45s venous phase with a sampling interval of 1 image per 2-3s, and finally a 90-120s

delayed phase with a sampling interval of 1 image per 15s, to limit radiation dose²¹³. When table-toggling is used to increase z-axis coverage the sampling interval must be decreased to 1 image every 2-3s to accommodate table motion. Radiation dose can be decreased by shortening the scan duration, but if the scan is too short to capture the delayed contrast washout from ischemic tissue it can lead to errors in quantitative values. Previous studies have found that shortening the duration of perfusion scans to 40-50s results in underestimated CBV, MTT and T_{max} values in AIS patients, and by extension, under- and overestimated infarct/penumbra volumes derived by T_{max} and CBV thresholds respectively²¹⁴⁻²¹⁷. Further study is required to determine optimal CTP scan duration for AIS applications that can minimize the radiation dose to the patient without affecting quantitative results. Increasing the sampling interval in the first phase of the scan can also decrease the dose, but can lead to errors in quantitative perfusion results, particularly for sampling intervals longer than 1 image every 3s. Studies have found quantitative perfusion results may be over- or underestimated at sampling intervals $\geq 3s$ ^{218,219}, but qualitative lesion appearance, diameter, and volume^{218,219}, and ASPECTS applied to CTP maps are relatively unaffected²¹⁹. Tube voltage of 80kVp is recommended for brain CTP since this results in mean x-ray energy closer to the iodine k-edge, improving iodine detection sensitivity, while also decreasing radiation dose compared to higher tube voltage settings²²⁰. Tube current of 100-200mA is recommended for brain CTP but decreasing tube current to 50mA may reduce effective dose by ~50% without significantly affecting quantitative perfusion values²²¹. Alternative image reconstruction techniques, such as adaptive statistical iterative reconstruction, can also be used to lower radiation dose without impacting image quality²²², or improve quality of CTP maps without increasing radiation

dose²²³. A standard 2-phase CTP study for assessing perfusion and BBB permeability has an effective dose of ~5mSv²²⁴. It is commonly assumed that an effective dose of 1Sv will increase the risk of dying from cancer by 5%²²⁵; extrapolating this to a dose of 5mSv means that a brain CTP study increases the risk of cancer mortality by ~0.025%.

1.3.3.3.3 Applications for Ischemic Stroke

The main application of CT Perfusion in AIS is estimating the volume of irreversibly damaged infarct core and/or salvageable penumbra by applying thresholds to hemodynamic parameter maps. CTP-derived infarct and penumbra volumes may be underestimated for z-axis coverage ≤ 8 and 4cm respectively, compared to what would be measured with 16cm coverage²²⁶. Nevertheless, even with 4cm coverage, studies have found infarct volumes quantified on admission CTP were better correlated with final infarct volume²²⁷ and more predictive of functional outcome than ASPECTS assessed on NCCT^{228,229} and CTP maps, as well as collateral score and clot burden score assessed on CTA²²⁹. Standardization of thresholds used to define infarct and penumbra has been problematic. Studies show infarct volumes derived using different thresholds are significantly different²³⁰, and that even the same threshold applied to maps computed using different software will produce different infarct volumes because of differences in the deconvolution algorithm used by each software²³¹. Based on results from DEFUSE 3 and DAWN, current clinical guidelines recommend CTP with postprocessing by the RAPID software package to determine eligibility for IAT in AIS patients with LVO and either unknown symptom duration, or symptom duration between 6-24h⁵⁸. Patients are selected for IAT based on mismatch between infarct ($\text{CBF} \leq 30\%$ of the contralateral side) and penumbra ($T_{\text{max}} > 6\text{s}$) volumes¹²², or mismatch between infarct volume and severity of

clinical deficit as assessed by NIHSS¹²³ (both mismatch paradigms are described in detail in the Mechanical Thrombectomy section above).

Assessing permeability-surface area product (PS) of the blood-brain barrier with CTP can also be used to predict the risk of hemorrhagic transformation following revascularization therapy. Both the average PS within the ischemic territory and the volume of tissue with elevated PS can predict hemorrhagic transformation with good specificity (83-94%) and moderate sensitivity (51-77%)^{232,233}. In the future PS maps from CTP could be useful for identifying patients with an increased risk of hemorrhagic transformation, where use of thrombolytic agents may be contraindicated. CTP performed after treatment also has the potential to provide additional prognostic information beyond what is available with angiographical imaging. Approximately ~15% of IAT-treated patients from clinical trials had near-complete or complete reperfusion on follow-up DSA (as assessed by the semi-quantitative modified thrombolysis in cerebral infarction scale, or mTICI scale) but still went on to have poor functional outcomes^{113,114,116,117,234}. Reperfusion assessed on follow-up CTP was a better predictor of outcome in AIS patients treated with IV t-PA than recanalization of the occluded vessel on follow-up CTA²³⁵. Follow-up CTP may also be a better predictor of functional outcome in IAT-treated patients than applying the mTICI scale to post-procedural DSA. As further advances are made in neuroprotective drugs and therapies, assessment of reperfusion following treatment of AIS may become important for identifying patients most likely to benefit from additional therapy.

1.4 Animal Models of Ischemic Stroke

Animal models of focal cerebral ischemia have been developed to further our understanding of stroke pathophysiology and develop treatment strategies and novel imaging techniques in a controlled environment. Animal models remove the impact of confounding factors commonly found in the clinical setting (e.g. diabetes, vascular cognitive impairment, previous stroke, etc.) and provide precise control over variables like ischemia duration, something that is impossible to control in a clinical setting. Additionally, radiation dose is less of a concern in animal models than in patients, so multimodal CT or PET imaging can be performed at several time points with less concern for the cumulative radiation dose. Although animal models present many advantages over clinical studies, it should be noted that no animal model completely replicates the complex processes of ischemic stroke in humans, often making translation of results from animal studies to the clinical setting challenging.

Most models of focal cerebral ischemia rely on occlusion of the MCA with an intra-arterial approach. The intraluminal suture procedure involves advancing a filament of surgical suture through the ICA to block the MCA; this model can be used to replicate permanent occlusion or transient occlusion by removing the suture after a predefined time²³⁶. Mechanical abrasion from the filament can result in increased risk of endothelial damage or hemorrhage, but when implemented properly this procedure creates infarcts that increase in volume over time and are highly reproducible between animals. Another option is IA injection of either microspheres or autologous blood clots into the ICA, causing occlusion of the MCA. Using the embolic model with an autologous blood clot is the only model suitable for studying thrombolytic agents²³⁷, but infarct size is also more variable

due to variability of endogenous fibrinolysis between animals. Other models require a craniectomy to expose, and then occlude the MCA using electrocoagulation, clips, or ligatures²³⁸, or by applying the vasoconstrictor endothelin-1 (ET-1) onto the exposed MCA²³⁹. ET-1 can also be injected into the MCA territory to cause vasoconstriction which eventually leads to infarction²⁴⁰.

Animal stroke studies are most commonly performed in mice and rats because they are reproducible and cost-effective. However, rat brains are lissencephalic (smooth surface lacking gyri and sulci), and the proportion of white matter is much lower than in humans, limiting the applicability of results from these models to humans. Therefore, stroke models have also been developed in larger animals such as dogs, pigs, and even primates, all of which have a gyrencephalic brain, and a proportion of gray and white matter more like humans. The disadvantages of using larger animals are increased cost, ethical concerns, and differences in cerebrovascular anatomy. Many large mammals used for biomedical research (e.g. pigs) have a rete mirabile in the extracranial portion of the internal carotid artery – a fine meshwork of blood vessels which reconstitutes into the internal carotid artery further downstream in the carotid canal²⁴¹, making it impossible to employ the intraluminal suture, and embolic stroke models in these animals. Most large animal stroke models require craniectomy of the orbital rim²⁴², or enucleation of the eye²⁴³ so that the MCA can be exposed and occluded. These complex surgical procedures make it difficult to maintain the animal at its basal physiological state throughout the duration of the experiment. Animal models of stroke are an important way of testing new treatment techniques for AIS, a less invasive large animal stroke model could improve clinical

translation by making it easier to test new therapies in models that are more representative of human stroke.

1.5 Future Diagnosis and Treatment of Stroke

Treatment of AIS, and neuroimaging-based triaging and management of AIS patients have progressed rapidly in recent decades, but there are still subgroups of patients where the efficacy of existing treatments have not been confirmed. For example, the benefit of IAT for treating distal MCA (M2 or M3 segment), ACA, and posterior cerebral circulation occlusions is not clear. Meta-analyses of pooled data suggested treating distal occlusions of the MCA (M2 or M3 segments) with mechanical thrombectomy may be beneficial, but statistical significance was not found^{104,244,245}. Occlusion of the ACA and the posterior cerebral circulation are responsible for ~5%²⁴⁶ and 15-20%²⁴⁷ of AIS respectively. There is some evidence that thrombectomy with stent retrievers improves the likelihood of recanalization and good outcome in patients with ACA occlusion^{246,248}, and basilar artery occlusion²⁴⁹, but more study is needed to refine thrombectomy techniques and define appropriate inclusion criteria for treatment. Because of the uncertain benefit of IAT for treating distal occlusions, these patients are currently treated with IV t-PA, but treatment with thrombolysis is restricted by the 4.5h time window, and inability to treat patients with unknown onset times. A recent randomized, placebo-controlled trial showed that patients with unknown stroke onset times who have FLAIR-DWI mismatch benefit from IV t-PA¹⁶⁸, but equivalent CT-based selection criteria should also be studied due to the greater availability of CT outside of major cities.

Research into new thrombolytic drugs and neuroprotective techniques is also ongoing. Alteplase is the only t-PA class drug approved by the FDA but there is some

evidence that IV administration of tenecteplase (TNK), another recombinant t-PA with higher fibrin specificity²⁵⁰ and a longer half-life, could result in greater reperfusion rates²⁵¹ and lower rates of ICH²⁵². TNK may have a role in routine care if the efficacy is shown to be equivalent to alteplase because it is less expensive and easier to administer (one bolus versus a bolus followed by 1h infusion of alteplase)²⁵². Trials comparing IV TNK and alteplase for AIS treatment within 4.5h of onset and treatment of minor stroke or transient ischemic attack within 12 hours of onset are ongoing.

Neuroprotective drugs and therapies are also being studied as method to maximize penumbra salvage by slowing the progression of ischemic tissue toward infarction. One prominent example is the neuroprotective drug NA-1, which acts on the postsynaptic scaffolding protein PSD-95 to inhibit glutamate excitotoxicity. NA-1 reduced final infarct volume by ~40% in a non-human primate model of AIS²⁵³ and was also found to be safe and effective for reducing the number of DWI lesions in humans following endovascular brain aneurysm repair (a procedure where small embolic strokes are common)²⁵⁴. A phase 3 randomized, placebo-controlled trial is currently underway to determine the efficacy of NA-1 for improving functional outcomes in AIS patients treated with IAT. Non-pharmaceutical neuroprotective therapies are also under investigation, including selective brain cooling with intra-arterial infusion of cold saline^{255,256}. Previous research has shown that inducing hypothermia provides neuroprotective effects in the acute phase of stroke by reducing CMRO₂ and excitotoxicity, and in the subacute phase by preserving BBB integrity²⁵⁷. IA infusion of cold saline offers similar neuroprotective effects without the adverse effects associated with hypothermia, such as pneumonia or cardiac arrhythmia²⁵⁸. A recent study of cold saline infusion performed before and after IAT resulted in smaller

final infarct volume and a non-significant trend toward better functional outcomes²⁵⁵. As neuroprotective drugs and therapies continue to be refined, imaging-based selection criteria will need to be studied to identify patients who will be most likely to benefit.

1.6 Research Objectives

The main objective of this work was to identify limitations and potential areas for improvement in current CTP-based methods for guiding AIS treatment and functional outcome prognostication following AIS. The thesis is divided into the following parts:

- 1) Developing a large animal AIS model for deriving CTP parameter thresholds for infarction after 3h of ischemia.
- 2) Assessing the effect of scan duration on perfusion parameters calculated by CTP and determining optimal scan durations for infarction thresholds.
- 3) Determining the association between reperfusion of previously ischemic tissue after IAT, as assessed by follow-up CTP, with good functional outcome in AIS patients.

1.7 References

1. Johnson W, Onuma O, Owolabi M, Sachdev S. Stroke: A global response is needed. *Bull World Health Organ.* 2016;94(9):634A-635A.
doi:10.2471/BLT.16.181636
2. Koton S, Schneider ALC, Rosamond WD, et al. Stroke incidence and mortality trends in US communities, 1987 to 2011. *JAMA - J Am Med Assoc.* 2014;312(3):259-268. doi:10.1001/jama.2014.7692
3. Yang Q, Botto LD, Erickson JD, et al. Improvement in stroke mortality in Canada

and the United States, 1990 to 2002. *Circulation*. 2006;113(10):1335-1343.

doi:10.1161/CIRCULATIONAHA.105.570846

4. Howard G, Moy CS, Howard VJ, et al. Where to focus efforts to reduce the black-white disparity in stroke mortality: Incidence versus case fatality? *Stroke*. 2016;47(7):1893-1898. doi:10.1161/STROKEAHA.115.012631
5. Petrea RE, Beiser AS, Seshadri S, Kelly-Hayes M, Kase CS, Wolf PA. Gender differences in stroke incidence and poststroke disability in the framingham heart study. *Stroke*. 2009;40(4):1032-1037. doi:10.1161/STROKEAHA.108.542894
6. Howard G, Howard VJ, Katholi C, Oli MK, Huston S, Asplund K. Decline in US Stroke Mortality: An Analysis of Temporal Patterns by Sex, Race, and Geographic Region. *Stroke*. 2001;32(10):2213-2220. doi:10.1161/hs1001.096047
7. Lakshminarayan K, Berger AK, Fuller CC, et al. Trends in 10-year survival of patients with stroke hospitalized between 1980 and 2000: The Minnesota stroke survey. *Stroke*. 2014;45(9):2575-2581. doi:10.1161/STROKEAHA.114.005512
8. Howard G, Goff DC. Population shifts and the future of stroke: forecasts of the future burden of stroke. *Ann N Y Acad Sci*. 2012;1268:14-20. doi:10.1111/j.1749-6632.2012.06665.x
9. Hankey GJ, Jamrozik K, Broadhurst RJ, Forbes S, Anderson CS. Long-Term Disability After First-Ever Stroke and Related Prognostic Factors in the Perth Community Stroke Study, 1989 –1990. *Stroke*. 2002;33(4):1034-1040.

10. Krueger H, Koot J, Hall RE, O'Callaghan C, Bayley M, Corbett D. Prevalence of Individuals Experiencing the Effects of Stroke in Canada: Trends and Projections. *Stroke*. 2015;46(8):2226-2231. doi:10.1161/STROKEAHA.115.009616
11. Gloede TD, Halbach SM, Thrift AG, Dewey HM, Pfaff H, Cadilhac DA. Long-term costs of stroke using 10-year longitudinal data from the north east melbourne stroke incidence study. *Stroke*. 2014;45(11):3389-3394. doi:10.1161/STROKEAHA.114.006200
12. Kleindorfer D, Khoury J, Moomaw CJ, et al. Stroke Incidence is Decreasing in Whites, but Not in Blacks: A Population-Based Estimate of Temporal Trends in Stroke Incidence from the Greater Cincinnati/Northern Kentucky Stroke Study. *Stroke*. 2011;41(7):1326-1331. doi:10.1161/STROKEAHA.109.575043.
13. Linfante I, Walker GR, Castonguay AC, et al. Predictors of Mortality in Acute Ischemic Stroke Intervention: Analysis of the North American Solitaire Acute Stroke Registry. *Stroke*. 2015;46(8):2305-2308. doi:10.1161/STROKEAHA.115.009530
14. Hackett ML, Duncan JR, Anderson CS, Broad JB, Bonita R. Health-related quality of life among long-term survivors of stroke: results from the Auckland Stroke Study, 1991-1992. *Stroke*. 2000;31(2):440-447. doi:10.1161/strokeaha.110.598839
15. Ofengeim D, Miyawaki T, Zukin R. Molecular and cellular mechanisms of ischemia-induced neuronal death. In: Mohr J, Wolf P, Grotta J, Moskowitz M, Mayberg M, von Kummer R, eds. *Stroke: Pathophysiology, Diagnosis, and*

Management. Philadelphia: Elsevier; 2011:75-106.

16. Del Zoppo GJ, Hallenbeck JM. Advances in the Vascular Pathophysiology of Ischemic Stroke. *Thromb Res*. 2000;98(3):73-81. doi:10.1016/S0049-3848(00)00218-8
17. Momjian-Mayor I, Baron JC. The pathophysiology of watershed infarction in internal carotid artery disease: Review of cerebral perfusion studies. *Stroke*. 2005;36(3):567-577. doi:10.1161/01.STR.0000155727.82242.e1
18. Wilterdink J, Bendixen B, Adams HJ, Woolson R, Clarke W, Hansen M. Effect of Prior Aspirin Use on Stroke Severity in the Trial of Org 10172 in Acute Stroke Treatment (TOAST). *Stroke*. 2001;32(12):2836-2840.
19. Adams H., Bendixen B., Kappelle L., et al. Classification of Subtype of Acute Ischemic Stroke: Definitions for Use in a Multicenter Clinical Trial. *Stroke*. 1993;24(1):35-41. doi:10.1161/01.STR.24.1.35
20. Puig J, Pedraza S, Demchuk A, et al. Quantification of Thrombus Hounsfield Units on Noncontrast CT Predicts Stroke Subtype and Early Recanalization after Intravenous Recombinant Tissue Plasminogen Activator. *Am J Neuroradiol*. 2012;33(1):90-96. doi:10.3174/ajnr.A2878
21. Choi MH, Park GH, Lee JS, et al. Erythrocyte fraction within retrieved thrombi contributes to thrombolytic response in acute ischemic stroke. *Stroke*. 2018;49(3):652-659. doi:10.1161/STROKEAHA.117.019138

22. Kanekar SG, Zacharia T, Roller R. Imaging of stroke: Part 2, pathophysiology at the molecular and cellular levels and corresponding imaging changes. *Am J Roentgenol*. 2012;198(1):63-74. doi:10.2214/AJR.10.7312
23. Mattson MP. Excitotoxic and excitoprotective mechanisms. *NeuroMolecular Med*. 2003;3(2):65-94. doi:10.1385/NMM:3:2:65
24. Xiong ZG, Zhu XM, Chu XP, et al. Neuroprotection in ischemia: Blocking calcium-permeable acid-sensing ion channels. *Cell*. 2004;118(6):687-698. doi:10.1016/j.cell.2004.08.026
25. Kimelberg HK, MacVicar BA, Sontheimer H. Anion channels in astrocytes: Biophysics, pharmacology, and function. *Glia*. 2006;54(7):747-757. doi:10.1002/glia.20423
26. Aarts MM, Tymianski M. TRPMs and neuronal cell death. *Pflugers Arch Eur J Physiol*. 2005;451(1):243-249. doi:10.1007/s00424-005-1439-x
27. Bano D, Munarriz E, Chen HL, et al. The plasma membrane Na⁺/Ca²⁺ exchanger is cleaved by distinct protease families in neuronal cell death. *Ann N Y Acad Sci*. 2007;1099:451-455. doi:10.1196/annals.1387.006
28. Ankarcrona M, Dypbukt JM, Bonfoco E, Zhivotovsky B, Orrenius S, Lipton SA. Glutamate-Induced Neuronal Death: A Succession of Necrosis or Apoptosis Depending on Mitochondrial Function. *Neuron*. 1995;15(4):961-973.
29. Patel M, Day BJ, Crapo JD, Fridovich I, McNamara JO. Requirement for

- superoxide in excitotoxic cell death. *Neuron*. 1996;16(2):345-355.
doi:10.1016/S0896-6273(00)80052-5
30. Bodalia A, Li H, Jackson MF. Loss of endoplasmic reticulum Ca²⁺ homeostasis: contribution to neuronal cell death during cerebral ischemia. *Acta Pharmacol Sin*. 2013;34(1):49-59. doi:10.1038/aps.2012.139
31. Dohmen C, Sakowitz OW, Fabricius M, et al. Spreading depolarizations occur in human ischemic stroke with high incidence. *Ann Neurol*. 2008;63(6):720-728.
doi:10.1002/ana.21390
32. Hartings JA, Rolli ML, May Lu X, Tortella FC. Delayed secondary phase of peri-infarct depolarizations after focal cerebral ischemia: relation to infarct growth and neuroprotection. *J Neurosci*. 2003;23(37):11602-11610. doi:23/37/11602 [pii]
33. Abbott NJ, Patabendige AAK, Dolman DEM, Yusof SR, Begley DJ. Structure and function of the blood-brain barrier. *Neurobiol Dis*. 2010;37(1):13-25.
doi:10.1016/j.nbd.2009.07.030
34. Liu S, Agalliu D, Yu C, Fisher M. The Role of Pericytes in Blood-Brain Barrier Function and Stroke. *Curr Pharm Des*. 2012;18(25):3653-3662.
doi:10.2174/138161212802002706
35. Gonul E, Duz B, Kahraman S, Kayali H, Kubar A, Timurkaynak E. Early pericyte response to brain hypoxia in cats: An ultrastructural study. *Microvasc Res*. 2002;64(1):116-119. doi:10.1006/mvre.2002.2413

36. McCaffrey G, Willis CL, Staatz WD, et al. Occludin oligomeric assemblies at tight junctions of the blood-brain barrier are altered by hypoxia and reoxygenation stress. *J Neurochem.* 2009;110(1):57-71. doi:doi:10.1111/j.1471-4159.2009.06113.x
37. Jing L, Mai L, Zhang JZ, et al. Diabetes inhibits cerebral ischemia-induced astrocyte activation - An observation in the cingulate corte. *Int J Biol Sci.* 2013;9(9):980-988. doi:10.7150/ijbs.7251
38. Won SJ, Tang XN, Suh SW, Yenari MA, Swanson RA. Hyperglycemia promotes tissue plasminogen activator-induced hemorrhage by Increasing superoxide production. *Ann Neurol.* 2011;70(4):583-590. doi:10.1002/ana.22538
39. Kerényi L, Kardos L, Szász J, et al. Factors influencing hemorrhagic transformation in ischemic stroke: A clinicopathological comparison. *Eur J Neurol.* 2006;13(11):1251-1255. doi:10.1111/j.1468-1331.2006.01489.x
40. Liao CC, Shih CC, Yeh CC, et al. Impact of diabetes on stroke risk and outcomes: Two nationwide retrospective cohort studies. *Med.* 2015;94(52):e2282. doi:10.1097/MD.0000000000002282
41. Saver JL. Time is brain - Quantified. *Stroke.* 2006;37(1):263-266. doi:10.1161/01.STR.0000196957.55928.ab
42. Emberson J, Lees KR, Lyden P, et al. Effect of treatment delay, age, and stroke severity on the effects of intravenous thrombolysis with alteplase for acute ischaemic stroke: A meta-analysis of individual patient data from randomised

- trials. *Lancet*. 2014;384(9958):1929-1935. doi:10.1016/S0140-6736(14)60584-5
43. Saver JL, Goyal M, van der Lugt A, et al. Time to treatment with endovascular thrombectomy and outcomes from ischemic stroke: A meta-analysis. *JAMA - J Am Med Assoc*. 2016;316(12):1279-1288. doi:10.1001/jama.2016.13647
44. Howarth C, Gleeson P, Attwell D. Updated energy budgets for neural computation in the neocortex and cerebellum. *J Cereb Blood Flow Metab*. 2012;32(7):1222-1232. doi:10.1038/jcbfm.2012.35
45. Astrup J, Symon L, Branston NM, Lassen NA. Cortical evoked potential and extracellular K⁺ and H⁺ at critical levels of brain ischemia. *Stroke*. 1977;8(1):51-57. doi:10.1161/01.STR.8.1.51
46. Symon L, Branston NM, Strong AJ, Hope TD. The concepts of thresholds of ischaemia in relation to brain structure and function. *J Clin Pathol*. 1977;11:149-154. doi:10.1136/jcp.s3-11.1.149
47. Mizoi K, Suzuki J, Abiko H, Ogasawara K, Oba M, Yoshimoto T. Experimental study on the reversibility of cerebral ischemia: Residual blood flow and duration of ischemia. *Acta Neurochir*. 1987;88(3-4):126-134.
48. Jones T, Morawetz R, Crowell R, et al. Thresholds of focal cerebral ischemia in awake monkeys. *J Neurosurg*. 1981;54(6):773-782.
doi:10.3171/jns.1981.54.6.0773
49. Powers WJ, Grubb Jr. RL, Darriet D, Raichle ME. Cerebral blood flow and

cerebral metabolic rate of oxygen requirements for cerebral function and viability in humans. *J Cereb Blood Flow Metab.* 1985;5(4):600-608.

doi:10.1038/jcbfm.1985.89

50. Branston NM, Symon L, Crockard HA, Pasztor E. Relationship between the cortical evoked potential and local cortical blood flow following acute middle cerebral artery occlusion in the baboon. *Exp Neurol.* 1974;45(2):195-208.
doi:10.1016/0014-4886(74)90112-5
51. Heiss W, Hayakawa T, Waltz A. Cortical Neuronal Function During Ischemia: Effects of occlusion of one middle cerebral artery on single-unit activity in cats. *Arch Neurol.* 1976;33(12):813-820.
52. Heiss W, Rosner G. Functional Recovery of Cortical Neurons as Related to Degree and Duration of Ischemia. *Ann Neurol.* 1983;14(3):294-301.
doi:10.1002/ana.410140307
53. Drake R, Vogl AW, Mitchell A. *Gray's Anatomy for Students.* 3rd editio. Philadelphia: Churchill Livingstone; 2014.
54. Leenders KL, Perani D, Lammertsma A, et al. Cerebral blood flow, blood volume and oxygen utilization. Normal values and effect of age. *Brain.* 1990;113(1):27-47.
doi:10.1093/brain/113.1.27
55. Harris JJ, Attwell D. The energetics of central nervous system white matter. *J Neurosci.* 2012;32(1):356-371. doi:10.1523/JNEUROSCI.3430-11.2012.The

56. Chen C, Bivard A, Lin L, Levi CR, Spratt NJ, Parsons MW. Thresholds for infarction vary between gray matter and white matter in acute ischemic stroke: A CT perfusion study. *J Cereb Blood Flow Metab.* 2017;0(00):1-11.
doi:10.1177/0271678X17744453
57. NINDS. Tissue plasminogen activator for acute ischemic stroke. *N Engl J Med.* 1995;333(24). <http://www.nejm.org/doi/full/10.1056/NEJM1996052333342114>. Accessed September 10, 2014.
58. Powers WJ, Rabinstein AA, Ackerson T, et al. 2018 Guidelines for the Early Management of Patients With Acute Ischemic Stroke: A Guideline for Healthcare Professionals From the American Heart Association/American Stroke Association. *Stroke.* 2018;49(3):e46-e110. doi:10.1161/STR.0000000000000158
59. Lin CB, Peterson ED, Smith EE, et al. Emergency medical service hospital prenotification is associated with improved evaluation and treatment of acute ischemic stroke. *Circ Cardiovasc Qual Outcomes.* 2012;5(4):514-522.
doi:10.1161/CIRCOUTCOMES.112.965210
60. Spokoyny I, Raman R, Ernstrom K, et al. Pooled assessment of computed tomography interpretation by vascular neurologists in the STRoKE DOC telestroke network. *J Stroke Cerebrovasc Dis.* 2014;23(3):511-515.
doi:10.1016/j.jstrokecerebrovasdis.2013.04.023.Pooled
61. Xian Y, Xu H, Lytle B, et al. Use of Strategies to Improve Door-to-Needle Times with Tissue-Type Plasminogen Activator in Acute Ischemic Stroke in Clinical

- Practice: Findings from Target: Stroke. *Circ Cardiovasc Qual Outcomes*. 2017;10(1):e003227. doi:10.1161/CIRCOUTCOMES.116.003227
62. Broos K, Feys HB, De Meyer SF, Vanhoorelbeke K, Deckmyn H. Platelets at work in primary hemostasis. *Blood Rev*. 2011;25(4):155-167. doi:10.1016/j.blre.2011.03.002
63. Furie B. Pathogenesis of thrombosis. *Hematol Am Soc Hematol Educ Progr*. 2009;255-258. doi:10.1182/asheducation-2009.1.255
64. Chapin J, Hajjar KA. Fibrinolysis and the control of blood coagulation. *Blood Rev*. 2015;29(1):17-24. doi:10.1016/j.blre.2014.09.003.Fibrinolysis
65. del Zoppo GJ, Kalafut M. Mechanisms of thrombosis and thrombolysis. In: Mohr J, Wolf PA, Grotta J, Moskowitz M, Mayberg M, von Kummer R, eds. *Stroke: Pathophysiology, Diagnosis, and Management*. Philadelphia: Elsevier; 2011:29-43.
66. Tomkins AJ, Schleicher N, Murtha L, et al. Platelet rich clots are resistant to lysis by thrombolytic therapy in a rat model of embolic stroke. *Exp Transl Stroke Med*. 2015;7(2):1-9. doi:10.1186/s13231-014-0014-y
67. Rohan V, Baxa J, Tupy R, et al. Length of occlusion predicts recanalization and outcome after intravenous thrombolysis in middle cerebral artery stroke. *Stroke*. 2014;45(7):2010-2017. doi:10.1161/STROKEAHA.114.005731
68. Moftakhar P, English JD, Cooke DL, et al. Density of thrombus on admission CT

- predicts revascularization efficacy in large vessel occlusion acute ischemic stroke. *Stroke*. 2013;44(1):243-245. doi:10.1161/STROKEAHA.112.674127
69. Molina CA, Montaner J, Arenillas JF, Ribo M, Rubiera M, Alvarez-Sabín J. Differential Pattern of Tissue Plasminogen Activator-Induced Proximal Middle Cerebral Artery Recanalization among Stroke Subtypes. *Stroke*. 2004;35(2):486-490. doi:10.1161/01.STR.0000110219.67054.BF
70. Schmitz ML, Simonsen CZ, Svendsen ML, et al. Ischemic stroke subtype is associated with outcome in thrombolysed patients. *Acta Neurol Scand*. 2017;135(2):176-182. doi:10.1111/ane.12589
71. Vandelli L, Marietta M, Gambini M, et al. Fibrinogen decrease after intravenous thrombolysis in ischemic stroke patients is a risk factor for intracerebral hemorrhage. *J Stroke Cerebrovasc Dis*. 2015;24(2):394-400. doi:10.1016/j.jstrokecerebrovasdis.2014.09.005
72. Whiteley WN, Emberson J, Lees KR, et al. Risk of intracerebral haemorrhage with alteplase after acute ischaemic stroke: a secondary analysis of an individual patient data meta-analysis. *Lancet Neurol*. 2016;15(9):925-933. doi:10.1016/S1474-4422(16)30076-X
73. Kaur J, Zhao Z, Klein GM, Lo EH, Buchan AM. The neurotoxicity of tissue plasminogen activator? *J Cereb Blood Flow Metab*. 2004;24(9):945-963. doi:10.1097/01.WCB.0000137868.50767.E8
74. Wardlaw JM, Seymour J, Cairns J, Keir S, Lewis S, Sandercock P. Immediate

computed tomography scanning of acute stroke is cost-effective and improves quality of life. *Stroke*. 2004;35(11):2477-2483.

doi:10.1161/01.STR.0000143453.78005.44

75. Hill MD, Buchan AM. Thrombolysis for acute ischemic stroke: results of the Canadian Alteplase for Stroke Effectiveness Study (CASES). *CMAJ*. 2005;172(10):1307-1312. doi:10.1503/cmaj.1041561
76. Wahlgren N, Ahmed N, Dávalos A, et al. Thrombolysis with alteplase for acute ischaemic stroke in the Safe Implementation of Thrombolysis in Stroke-Monitoring Study (SITS-MOST): an observational study. *Lancet (London, England)*. 2007;369(9558):275-282. doi:10.1016/S0140-6736(07)60149-4
77. Schumacher HC, Bateman BT, Boden-Albala B, et al. Use of Thrombolysis in Acute Ischemic Stroke: Analysis of the Nationwide Inpatient Sample 1999 to 2004. *Ann Emerg Med*. 2007;50(2):99-107. doi:10.1016/j.annemergmed.2007.01.021
78. Fang MC, Cutler DM, Rosen AB. Trends in thrombolytic use for ischemic stroke in the United States. *J Hosp Med*. 2011;5(7):406-409. doi:10.1002/jhm.689.Trends
79. O'Connor RE, McGraw P, Edelsohn L. Thrombolytic therapy for acute ischemic stroke: Why the majority of patients remain ineligible for treatment. *Ann Emerg Med*. 1999;33(1):9-14. doi:10.1016/S0196-0644(99)70411-7
80. Hacke W, Kaste M, Fieschi C, et al. Intravenous Thrombolysis With Recombinant Tissue Plasminogen Activator for Acute Hemispheric Stroke: The European

- Cooperative Acute Stroke Study (ECASS). *JAMA J Am Med Assoc.* 1995;274(13):1017-1025. doi:10.1001/jama.1995.03530130023023
81. Hacke W, Kaste M, Fieschi C, et al. Randomised double-blind placebo-controlled trial of thrombolytic therapy with intravenous alteplase in acute ischaemic stroke (ECASS II). *Lancet.* 1998;352(9136):1245-1251. doi:10.1016/S0140-6736(98)08020-9
82. Clark WM, Wissman S, Albers GW, et al. Recombinant Tissue-Type Plasminogen Activator (Alteplase) for Ischemic Stroke 3 to 5 Hours After Symptom: The ATLANTIS Study: A Randomized Controlled Trial. *JAMA.* 1999;282(21):2019-2026. doi:10.1001/jama.282.21.2019
83. The ATLANTIS, ECASS and N rt-PSGI. Association of outcome with early stroke treatment: Pooled analysis of ATLANTIS, ECASS, and NINDS rt-PA stroke trials. *Lancet.* 2004;363(9411):768-774. doi:10.1016/S0140-6736(04)15692-4
84. Hacke W, Kaste M, Bluhmki E, et al. Thrombolysis with alteplase 3 to 4.5 hours after acute ischemic stroke. *N Engl J Med.* 2008;359(13):1317-1329. doi:10.1056/NEJMoa1215817
85. Reiff T, Michel P. Reasons and evolution of non-thrombolysis in acute ischaemic stroke. *Emerg Med J.* 2017;34(4):219-226. doi:10.1136/emered-2015-205140
86. Yamaguchi T, Mori E, Minematsu K, et al. Alteplase at 0.6 mg/kg for acute ischemic stroke within 3 hours of onset: Japan Alteplase Clinical Trial (J-ACT).

- Stroke*. 2006;37(7):1810-1815. doi:10.1161/01.STR.0000227191.01792.e3
87. Clua-Espuny JL, Ripolles-Vicente R, Forcadell-Arenas T, et al. Sex Differences in Long-Term Survival after a First Stroke with Intravenous Thrombolysis: Ebrictus Study. *Cerebrovasc Dis Extra*. 2015;5(3):95-102. doi:10.1159/000440734
88. Agrawal N, Jamshed N, Aggarwal P, Ekka M. Severe hypoglycemia masquerading as cerebellar stroke. *J Fam Med Prim Care*. 2014;3(4):440-442. doi:10.4103/2249-4863.148144
89. Ribo M, Molina C, Montaner J, et al. Acute hyperglycemia state is associated with lower tPA-induced recanalization rates in stroke patients. *Stroke*. 2005;36(8):1705-1709. doi:10.1161/01.STR.0000173161.05453.90.9f
90. Snarska KK, Bachórzewska-Gajewska H, Kapica-Topczewska K, et al. Hyperglycemia and diabetes have different impacts on outcome of ischemic and hemorrhagic stroke. *Arch Med Sci*. 2017;13(1):100-108. doi:10.5114/aoms.2016.61009
91. Jaillard A, Cornu C, Durieux A, et al. Hemorrhagic Transformation in Acute Ischemic Stroke: The MAST-E Study. *Stroke*. 1999;30(7):1326-1333.
92. Capes SE, Hunt D, Malmberg K, Pathak P, Gerstein HC. Stress hyperglycemia and prognosis of stroke in non diabetic and diabetic patients: A systemic overview. *Stroke*. 2001;32(10):2426-2432. <http://stroke.ahajournals.org/content/32/10/2426.long>.

93. Reiter M, Teuschl Y, Matz K, Seyfang L, Brainin M. Diabetes and thrombolysis for acute stroke: A clear benefit for diabetics. *Eur J Neurol*. 2014;21(1):5-10. doi:10.1111/ene.12263
94. Ahmed N, Wahlgren N, Brainin M, et al. Relationship of blood pressure, antihypertensive therapy, and outcome in ischemic stroke treated with intravenous thrombolysis: Retrospective analysis from safe implementation of thrombolysis in stroke-international stroke thrombolysis register (SITS-ISTR). *Stroke*. 2009;40(7):2442-2449. doi:10.1161/STROKEAHA.109.548602
95. Bhatia R, Hill MD, Shobha N, et al. Low rates of acute recanalization with intravenous recombinant tissue plasminogen activator in ischemic stroke: Real-world experience and a call for action. *Stroke*. 2010;41(10):2254-2258. doi:10.1161/STROKEAHA.110.592535
96. Malhotra K, Gornbein J, Saver JL. Ischemic Strokes Due to Large-Vessel Occlusions Contribute Disproportionately to Stroke-Related Dependence and Death: A Review. *Front Neurol*. 2017;8(651):1-5. doi:10.3389/fneur.2017.00651
97. Zeumer H, Hacke W, Ringelstein EB. Local intraarterial thrombolysis in vertebrobasilar thromboembolic disease. *Am J Neuroradiol*. 1983;4(3):401-404.
98. Furlan A, Higashida R, Wechsler L, et al. Intra-arterial Prourokinase for Acute Ischemic Stroke. The PROACT II Study: A Randomized Controlled Trial. *JAMA*. 1999;282(21):2003-2011. doi:10.1001/jama.282.21.2003
99. Ogawa A, Mori E, Minematsu K, et al. Randomized trial of intraarterial infusion

- of urokinase within 6 hours of middle cerebral artery stroke: The Middle Cerebral Artery Embolism Local Fibrinolytic Intervention Trial (MELT) Japan. *Stroke*. 2007;38(10):2633-2639. doi:10.1161/STROKEAHA.107.488551
100. Lewandowski CA, Frankel M, Tomsick TA, et al. Combined intravenous and intra-arterial r-TPA versus intra-arterial therapy of acute ischemic stroke: Emergency management of stroke (EMS) bridging trial. *Stroke*. 1999;30(12):2598-2605. doi:10.1161/01.STR.30.12.2598
101. The IMS Study Investigators. Combined Intravenous and Intra-Arterial Recanalization for Acute Ischemic Stroke: The Interventional Management of Stroke Study. *Stroke*. 2004;35(4):904-912. doi:10.1161/01.STR.0000121641.77121.98
102. The IMS II Trial Investigators. The Interventional Management of Stroke (IMS) II study. *Stroke*. 2007;38(7):2127-2135. doi:10.1161/STROKEAHA.107.483131
103. del Zoppo GJ, Higashida RT, Furlan AJ, Pessin MS, Rowley HA, Gent M. PROACT: A Phase II Randomized Trial of Recombinant Pro-Urokinase by Direct Arterial Delivery in Acute Middle Cerebral Artery Stroke. *Stroke*. 1998;29(1):4-11. doi:10.1161/01.STR.29.1.4
104. Goyal M, Menon BK, Van Zwam WH, et al. Endovascular thrombectomy after large-vessel ischaemic stroke: A meta-analysis of individual patient data from five randomised trials. *Lancet*. 2016;387(10029):1723-1731. doi:10.1016/S0140-6736(16)00163-X

105. Smith WS, Furlan AJ. Brief History of Endovascular Acute Ischemic Stroke Treatment. *Stroke*. 2016;47(2):e23-e26. doi:10.1161/STROKEAHA.115.010863
106. Smith WS, Sung G, Starkman S, et al. Safety and efficacy of mechanical embolectomy in acute ischemic stroke: Results of the MERCI trial. *Stroke*. 2005;36(7):1432-1440. doi:10.1161/01.STR.0000171066.25248.1d
107. Smith WS, Sung G, Saver J, et al. Mechanical thrombectomy for acute ischemic stroke: Final results of the multi MERCI trial. *Stroke*. 2008;39(4):1205-1212. doi:10.1161/STROKEAHA.107.497115
108. Saver JL, Jahan R, Levy EI, et al. Solitaire flow restoration device versus the Merci Retriever in patients with acute ischaemic stroke (SWIFT): A randomised, parallel-group, non-inferiority trial. *Lancet*. 2012;380(9849):1241-1249. doi:10.1016/S0140-6736(12)61384-1
109. Nogueira RG, Lutsep HL, Gupta R, et al. Trevo versus Merci retrievers for thrombectomy revascularisation of large vessel occlusions in acute ischaemic stroke (TREVO 2): A randomised trial. *Lancet*. 2012;380(9849):1231-1240. doi:10.1016/S0140-6736(12)61299-9
110. Broderick JP, Palesch YY, Demchuk AM, et al. Endovascular Therapy after Intravenous t-PA versus t-PA Alone for Stroke. *N Engl J Med*. 2013;368(10):893-903. doi:10.1056/NEJMoa1214300
111. Ciccone A, Valvassori L, Nichelatti M, et al. Endovascular Treatment for Acute Ischemic Stroke. *N Engl J Med*. 2013;368(10):904-913.

doi:10.1056/NEJMoa1213701

112. Kidwell CS, Jahan R, Gornbein J, et al. A Trial of Imaging Selection and Endovascular Treatment for Ischemic Stroke. *N Engl J Med*. 2013;368(10):914-923. doi:10.1056/NEJMoa1212793
113. Saver JL, Goyal M, Bonafe A, et al. Stent-Retriever Thrombectomy after Intravenous t-PA vs. t-PA Alone in Stroke. *N Engl J Med*. 2015;372(24):2285-2295. doi:10.1056/NEJMoa1415061
114. Goyal M, Demchuk AM, Menon BK, et al. Randomized Assessment of Rapid Endovascular Treatment of Ischemic Stroke. *N Engl J Med*. 2015;372(11):1019-1030. doi:10.1056/NEJMoa1414905
115. Campbell BCV, Mitchell PJ, Kleinig TJ, et al. Endovascular Therapy for Ischemic Stroke with Perfusion-Imaging Selection. *N Engl J Med*. 2015;372(11):1009-1018. doi:10.1056/NEJMoa1414792
116. Berkhemer OA, Fransen PSS, Beumer D, et al. A Randomized Trial of Intraarterial Treatment for Acute Ischemic Stroke. *N Engl J Med*. 2015;372(1):11-20. doi:10.1056/NEJMoa1411587
117. Jovin TG, Chamorro A, Cobo E, et al. Thrombectomy within 8 Hours after Symptom Onset in Ischemic Stroke. *N Engl J Med*. 2015;372(24):2296-2306. doi:10.1056/NEJMoa1503780
118. Barber PA, Demchuk AM, Zhang J, Buchan AM. Validity and reliability of a

- quantitative computed tomography score in predicting outcome of hyperacute stroke before thrombolytic therapy. *Lancet*. 2000;355(9216):1670-1674.
doi:10.1016/S0140-6736(00)02237-6
119. Menon BK, D'Esterre CD, Qazi EM, et al. Multiphase CT Angiography: A New Tool for the Imaging Triage of Patients with Acute Ischemic Stroke. *Radiology*. 2015;275(2):510-520. doi:10.1148/radiol.15142256
120. Abou-Chebl A. Endovascular treatment of acute ischemic stroke may be safely performed with no time window limit in appropriately selected patients. *Stroke*. 2010;41(9):1996-2000. doi:10.1161/STROKEAHA.110.578997
121. Chalouhi N, Ghobrial G, Tjoumakaris S, et al. CT perfusion-guided versus time-guided mechanical recanalization in acute ischemic stroke patients. *Clin Neurol Neurosurg*. 2013;115(12):2471-2475. doi:10.1016/j.clineuro.2013.09.036
122. Albers GW, Marks MP, Kemp S, et al. Thrombectomy for Stroke at 6 to 16 Hours with Selection by Perfusion Imaging. *N Engl J Med*. 2018;378(8):708-718.
doi:10.1056/NEJMoa1713973
123. Nogueira RG, Jadhav AP, Haussen DC, et al. Thrombectomy 6 to 24 Hours after Stroke with a Mismatch between Deficit and Infarct. *N Engl J Med*. 2018;378(1):11-21. doi:10.1056/NEJMoa1706442
124. Kidwell CS, Chalela JA, Saver JL, et al. Comparison of MRI and CT for Detection of Acute Intracerebral Hemorrhage. *JAMA*. 2014;292(15):1823-1830.

125. Boellaard R. Standards for PET Image Acquisition and Quantitative Data Analysis. *J Nucl Med.* 2009;50(Suppl_1):11S-20S.
doi:10.2967/jnumed.108.057182
126. Powers WJ, Grubb RL, Darriet D, Raichle ME. Cerebral Blood Flow and Cerebral Metabolic Rate of Oxygen Requirements for Cerebral Function and Viability in Humans. *J Cereb Blood Flow Metab.* 1985;5(4):600-608.
doi:10.1038/jcbfm.1985.89
127. Marchal G, Serrati C, Rioux P, et al. PET imaging of cerebral perfusion and oxygen consumption in acute ischaemic stroke: relation to outcome. *Lancet.* 1993;341(8850):925-927. <http://www.ncbi.nlm.nih.gov/pubmed/8096267>.
128. Heiss W-D. Ischemic Penumbra: Evidence From Functional Imaging in Man. *J Cereb Blood Flow Metab.* 2000;20(9):1276-1293. doi:10.1097/00004647-200009000-00002
129. Baron JC. Mapping the ischemic penumbra with PET: implications for acute stroke treatment. *Cerebrovasc Dis.* 1999;9(4):193-201. doi:10.1159/000015955
130. Young AR, Sette G, Touzani O, et al. Relationships between high oxygen extraction fraction in the acute stage and final infarction in reversible middle cerebral artery occlusion: An investigation in anesthetized baboons with positron emission tomography. *J Cereb Blood Flow Metab.* 1996;16(6):1176-1188.
doi:10.1097/00004647-199611000-00012
131. Touzani O, Young AR, Derlon JM, Baron JC, MacKenzie ET. Progressive

- impairment of brain oxidative metabolism reversed by reperfusion following middle cerebral artery occlusion in anaesthetized baboons. *Brain Res.* 1997;767(1):17-25. doi:10.1016/S0006-8993(97)00515-5
132. Zanzonico P. Positron Emission Tomography: A Review of Basic Principles, Scanner Design and Performance, and Current Systems. *Semin Nucl Med.* 2004;34(11):87-111. doi:10.1053/j.semnuclmed.2003.12.002
133. Sette G, Baron J-C, Young AR, et al. In Vivo Mapping of Brain Benzodiazepine Receptor Changes by Positron Emission Tomography After Focal Ischemia in the Anesthetized Baboon. *Stroke.* 1993;24(12):2046-2058.
134. Heiss W-D, Grond M, Thiel A, et al. Permanent Cortical Damage Detected by Flumazenil Positron Emission Tomography in Acute Stroke. *Stroke.* 1998;29(2):454-461.
135. Heiss WD, Kracht L, Grond M, et al. Early [11C]flumazenil/H2O positron emission tomography predicts irreversible ischemic cortical damage in stroke patients receiving acute thrombolytic therapy. *Stroke.* 2000;31(2):366-369. doi:10.1161/01.STR.31.2.366
136. Heiss W-D, Sobesky J, Smekal U V, et al. Probability of cortical infarction predicted by flumazenil binding and diffusion-weighted imaging signal intensity: a comparative positron emission tomography/magnetic resonance imaging study in early ischemic stroke. *Stroke.* 2004;35(8):1892-1898. doi:10.1161/01.STR.0000134746.93535.9b

137. Levêque P, Sanabria-Bohorquez S, Bol A, et al. Quantification of human brain benzodiazepine receptors using [18F]fluoroethylflumazenil: a first report in volunteers and epileptic patients. *Eur J Nucl Med Mol Imaging*. 2003;30(12):1630-1636. doi:10.1007/s00259-003-1304-0
138. Gründer G, Siessmeier T, Lange-Asschenfeldt C, et al. [18F]Fluoroethylflumazenil: A novel tracer for PET imaging of human benzodiazepine receptors. *Eur J Nucl Med*. 2001;28(10):1463-1470. doi:10.1007/s002590100594
139. Richards JG, Möhler H, Schoch P, Häring P, Takacs B, Stähli C. The visualization of neuronal benzodiazepine receptors in the brain by autoradiography and immunohistochemistry. *J Recept Signal Transduct*. 1984;4(1-6):657-669. doi:10.3109/10799898409042579
140. Krohn KA, Link JM, Mason RP. Molecular imaging of hypoxia. *J Nucl Med*. 2008;49(Suppl 2):129S-48S. doi:10.2967/jnumed.107.045914
141. Saita K, Chen M, Spratt NJ, et al. Imaging the Ischemic Penumbra with 18F-Fluoromisonidazole in a Rat Model of Ischemic Stroke. *Stroke*. 2004;35(4):975-980. doi:10.1161/01.STR.0000121647.01941.ba
142. Takasawa M, Beech JS, Fryer TD, et al. Imaging of brain hypoxia in permanent and temporary middle cerebral artery occlusion in the rat using 18F-fluoromisonidazole and positron emission tomography: a pilot study. *J Cereb Blood Flow Metab*. 2007;27(4):679-689. doi:10.1038/sj.jcbfm.9600405

143. Markus R, Reutens DC, Kazui S, et al. Topography and Temporal Evolution of Hypoxic Viable Tissue Identified by 18F-Fluoromisonidazole Positron Emission Tomography in Humans After Ischemic Stroke. *Stroke*. 2003;34(11):2646-2652. doi:10.1161/01.STR.0000094422.74023.FF
144. Spratt NJ, Donnan GA, Howells DW. Characterisation of the timing of binding of the hypoxia tracer FMISO after stroke. *Brain Res*. 2009;1288:135-142. doi:10.1016/j.brainres.2009.06.102
145. Spratt NJ, Donnan GA, McLeod DD, Howells DW. Salvaged stroke ischaemic penumbra shows significant injury: Studies with the hypoxia tracer FMISO. *J Cereb Blood Flow Metab*. 2011;31(3):934-943. doi:10.1038/jcbfm.2010.174
146. Agarwal A, Vijay K, Thamburaj K, Kanekar S, Kalapos P. Sensitivity of 3D gradient recalled echo susceptibility-weighted imaging technique compared to computed tomography angiography for detection of middle cerebral artery thrombus in acute stroke. *Neurol Int*. 2014;6(4):61-65. doi:10.4081/ni.2014.5521
147. Naggara O, Raymond J, Domingo Ayllon M, et al. T2* “Susceptibility Vessel Sign” Demonstrates Clot Location and Length in Acute Ischemic Stroke. *PLoS One*. 2013;8(10):2-10. doi:10.1371/journal.pone.0076727
148. Liebeskind DS, Sanossian N, Yong WH, et al. CT and MRI Early Vessel Signs Reflect Clot Composition in Acute Stroke. *Stroke*. 2011;42(5):1237-1243. doi:10.1161/STROKEAHA.110.605576.CT
149. Alfke K, Jensen U, Pool C, et al. Contrast-enhanced magnetic resonance

- angiography in stroke diagnostics : Additional information compared with time-of-flight magnetic resonance angiography? *Clin Neuroradiol.* 2011;21(1):5-10.
doi:10.1007/s00062-010-0039-0
150. Lövblad KO, Baird AE, Schlaug G, et al. Ischemic lesion volumes in acute stroke by diffusion-weighted magnetic resonance imaging correlate with clinical outcome. *Ann Neurol.* 1997;42(2):164-170. doi:10.1002/ana.410420206
151. Schaefer PW, Grant PE, Gonzalez RG. DW-MRI imaging of the brain. *Radiology.* 2000;217(2):331-345. doi:10.1016/j.acra.2009.10.014
152. Simonsen CZ, Madsen MH, Schmitz ML, Mikkelsen IK, Fisher M, Andersen G. Sensitivity of diffusion-and perfusion-weighted imaging for diagnosing acute ischemic stroke is 97.5%. *Stroke.* 2015;46(1):98-101.
doi:10.1161/STROKEAHA.114.007107
153. Campbell BCV, Purushotham A, Christensen S, et al. The infarct core is well represented by the acute diffusion lesion: Sustained reversal is infrequent. *J Cereb Blood Flow Metab.* 2012;32(1):50-56. doi:10.1038/jcbfm.2011.102
154. Inoue M, Mlynash M, Christensen S, et al. Early DWI Reversal Following Endovascular Reperfusion Is Typically Transient in Patients Imaged 3-6 Hours After Onset. *Stroke.* 2014;45(4):1024-1028.
doi:10.1161/STROKEAHA.113.002135
155. Copen WA, Schaefer PW, Wu O. MR Perfusion Imaging in Acute Ischemic Stroke. *Neuroimaging Clin N Am.* 2011;21(2):259-283.

doi:10.1016/j.nic.2011.02.007. MR

156. Bergamino M, Bonzano L, Levrero F, Mancardi GL, Roccatagliata L. A review of technical aspects of T1-weighted dynamic contrast-enhanced magnetic resonance imaging (DCE-MRI) in human brain tumors. *Phys Medica*. 2014;30(6):635-643. doi:10.1016/j.ejmp.2014.04.005
157. Olivot J-M, Mlynash M, Thijs VN, et al. Optimal Tmax threshold for predicting penumbral tissue in acute stroke. *Stroke*. 2009;40(2):469-475. doi:10.1161/STROKEAHA.108.526954
158. Zhang S, Tang H, Yu YN, Yan SQ, Parsons MW, Lou M. Optimal Magnetic Resonance Perfusion Thresholds Identifying Ischemic Penumbra and Infarct Core: A Chinese Population-based Study. *CNS Neurosci Ther*. 2015;21(3):289-295. doi:10.1111/cns.12367
159. Perthen JE, Calamante F, Gadian DG, Connelly A. Is quantification of bolus tracking MRI reliable without deconvolution? *Magn Reson Med*. 2002;47(1):61-67. doi:10.1002/mrm.10020
160. Wouters A, Christensen S, Straka M, et al. A comparison of relative time to peak and Tmax for mismatch-based patient selection. *Front Neurol*. 2017;8(539). doi:10.3389/fneur.2017.00539
161. Zaro-Weber O, Moeller-Hartmann W, Heiss WD, Sobesky J. Maps of time to maximum and time to peak for mismatch definition in clinical stroke studies validated with positron emission tomography. *Stroke*. 2010;41(12):2817-2821.

doi:10.1161/STROKEAHA.110.594432

162. Straka M, Albers GW, Bammer R. Real-time diffusion-perfusion mismatch analysis in acute stroke. *J Magn Reson Imaging*. 2010;32(5):1024-1037.
doi:10.1002/jmri.22338
163. Huang Y-C, Liu H-L, Lee J-D, et al. Comparison of Arterial Spin Labeling and Dynamic Susceptibility Contrast Perfusion MRI in Patients with Acute Stroke. *PLoS One*. 2013;8(7):e69085. doi:10.1371/journal.pone.0069085
164. Brant-Zawadzki M, Atkinson D, Detrick M, Bradley WG, Scidmore G. Fluid-Attenuated Inversion Recovery (FLAIR) for Assessment of Cerebral Infarction: Initial Clinical Experience in 50 Patients. *Stroke*. 1996;27(7):1187-1191.
doi:10.1161/01.STR.27.7.1187
165. Moseley ME, Kucharczyk J, Mintorovitch J, et al. Diffusion-weighted MR imaging of acute stroke: correlation with T2-weighted and magnetic susceptibility-enhanced MR imaging in cats. *AJNR Am J Neuroradiol*. 1990;11(3):423-429.
<http://stroke.ahajournals.org/cgi/doi/10.1161/01.STR.27.7.1187>.
166. Thomalla G, Rossbach P, Rosenkranz M, et al. Negative fluid-attenuated inversion recovery imaging identifies acute ischemic stroke at 3 hours or less. *Ann Neurol*. 2009;65(6):724-732. doi:10.1002/ana.21651
167. Thomalla G, Cheng B, Ebinger M, et al. DWI-FLAIR mismatch for the identification of patients with acute ischaemic stroke within 4.5 h of symptom

- onset (PRE-FLAIR): A multicentre observational study. *Lancet Neurol.* 2011;10(11):978-986. doi:10.1016/S1474-4422(11)70192-2
168. Thomalla G, Simonsen CZ, Boutitie F, et al. MRI-Guided Thrombolysis for Stroke with Unknown Time of Onset. *N Engl J Med.* 2018;379(7):611-622. doi:10.1056/NEJMoa1804355
169. Fink JN, Kumar S, Horkan C, et al. The Stroke Patient Who Woke Up. Clinical and Radiological Features, Including Diffusion and Perfusion MRI. *Stroke.* 2002;33(4):988-993.
170. Mackey J, Kleindorfer D, Sucharew H, et al. Population-based study of wake-up strokes. *Neurology.* 2011;76(19):1662-1667. doi:10.1212/WNL.0b013e318219fb30
171. Hansen CK, Christensen A, Rodgers H, et al. CT and MRI-based door-needle-times for acute stroke patients a quasi-randomized clinical trial. *Clin Neurol Neurosurg.* 2017;159(March):42-49. doi:10.1016/j.clineuro.2017.05.011
172. Ginde AA, Foianini A, Renner DM, Valley M, Camargo CA. Availability and quality of computed tomography and magnetic resonance imaging equipment in U.S. emergency departments. *Acad Emerg Med.* 2008;15(8):780-783. doi:10.1111/j.1553-2712.2008.00192.x
173. Pexman JHW, Barber PA, Hill MD, et al. Use of the Alberta Stroke Program Early CT Score (ASPECTS) for assessing CT scans in patients with acute stroke. *Am J Neuroradiol.* 2001;22(8):1534-1542.

174. Demchuk AM, Hill MD, Barber PA, Silver B, Patel SC, Levine SR. Importance of early ischemic computed tomography changes using ASPECTS in NINDS rtPA stroke study. *Stroke*. 2005;36(10):2110-2115.
doi:10.1161/01.STR.0000181116.15426.58
175. Dzialowski I, Hill MD, Coutts SB, et al. Extent of early ischemic changes on computed tomography (CT) before thrombolysis: Prognostic value of the Alberta Stroke Program early CT score in ECASS II. *Stroke*. 2006;37(4):973-978.
doi:10.1161/01.STR.0000206215.62441.56
176. Yoo AJ, Zaidat OO, Chaudhry ZA, et al. Impact of pretreatment noncontrast CT Alberta stroke program early ct score on clinical outcome after intra arterial stroke therapy. *Stroke*. 2014;45(3):746-751. doi:10.1161/STROKEAHA.113.004260
177. Yoo AJ, Berkhemer OA, Fransen PSS, et al. Effect of baseline Alberta Stroke Program Early CT Score on safety and efficacy of intra-arterial treatment: a subgroup analysis of a randomised phase 3 trial (MR CLEAN). *Lancet Neurol*. 2016;15(7):685-694. doi:10.1016/S1474-4422(16)00124-1
178. Jiang S, Peng Y, Jing C-H, et al. Endovascular thrombectomy can be beneficial to acute ischemic stroke patients with large infarcts. *J Neurosurg*. 2018:1-8.
doi:10.3171/2017.11.JNS171297.10.3171/2017.11.JNS171297
179. Mair G, Boyd E V., Chappell FM, et al. Sensitivity and specificity of the hyperdense artery sign for arterial obstruction in acute ischemic stroke. *Stroke*. 2015;46(1):102-107. doi:10.1161/STROKEAHA.114.007036

180. Kim EY, Lee SK, Kim DJ, et al. Detection of thrombus in acute ischemic stroke: Value of thin-section noncontrast-computed tomography. *Stroke*. 2005;36(12):2745-2747. doi:10.1161/01.STR.0000185720.03803.41
181. Riedel CH, Zoubie J, Ulmer S, Gierthmuehlen J, Jansen O. Thin-slice reconstructions of nonenhanced CT images allow for detection of thrombus in acute stroke. *Stroke*. 2012;43(9):2319-2323. doi:10.1161/STROKEAHA.112.649921
182. Lim J, Magarik JA, Froehler MT. The CT-Defined Hyperdense Arterial Sign as a Marker for Acute Intracerebral Large Vessel Occlusion. *J Neuroimaging*. 2018;28(2):212-216. doi:10.1111/jon.12484
183. Riedel CH, Jensen U, Rohr A, et al. Assessment of thrombus in acute middle cerebral artery occlusion using thin-slice nonenhanced computed tomography reconstructions. *Stroke*. 2010;41(8):1659-1664. doi:10.1161/STROKEAHA.110.580662
184. Shobha N, Bal S, Boyko M, et al. Measurement of Length of Hyperdense MCA Sign in Acute Ischemic Stroke Predicts Disappearance after IV tPA. *J Neuroimaging*. 2014;24(1):7-10. doi:10.1111/j.1552-6569.2012.00761.x
185. Man S, Hussain MS, Wisco D, et al. The Location of Pretreatment Hyperdense Middle Cerebral Artery Sign Predicts the Outcome of Intraarterial Thrombectomy for Acute Stroke. *J Neuroimaging*. 2015;25(2):263-268. doi:10.1111/jon.12115
186. Lell MM, Anders K, Uder M, et al. New Techniques in CT Angiography.

- RadioGraphics*. 2006;26(suppl_1):S45-S62. doi:10.1148/rg.26si065508
187. Shrier DA, Tanaka H, Numaguchi Y, Konno S, Patel U, Shibata D. CT angiography in the evaluation of acute stroke. *AJNR Am J Neuroradiol*. 1997;18(6):1011-1020. <http://www.ncbi.nlm.nih.gov/pubmed/9194426>.
188. Bash S, Villablanca JP, Jahan R, et al. Intracranial vascular stenosis and occlusive disease: Evaluation with CT angiography, MR angiography, and digital subtraction angiography. *AJNR Am J Neuroradiol*. 2005;26(5):1012-1021. doi:26/5/1012 [pii]
189. Tian H, Parsons MW, Levi CR, et al. Intravenous thrombolysis may not improve clinical outcome of acute ischemic stroke patients without a baseline vessel occlusion. *Front Neurol*. 2018;9(405):1-7. doi:10.3389/fneur.2018.00405
190. Demchuk AM, Goyal M, Yeatts SD, et al. Recanalization and Clinical Outcome of Occlusion Sites at Baseline CT Angiography in the Interventional Management of Stroke III Trial. *Radiology*. 2014;273(1):202-210. doi:10.1148/radiol.14132649
191. Mishra SM, Dykeman J, Sajobi TT, et al. Early Reperfusion rates with IV tPA Are determined by CTA clot characteristics. *AJNR Am J Neuroradiol*. 2014;35(12):2265-2272. doi:10.3174/ajnr.A4048
192. Ahn SH, D'Esterre CD, Qazi EM, et al. Occult Anterograde Flow Is an Under-Recognized but Crucial Predictor of Early Recanalization with Intravenous Tissue-Type Plasminogen Activator. *Stroke*. 2015;46(4):968-975. doi:10.1161/STROKEAHA.114.008648

193. Puetz V, Dzialowski I, Hill MD, et al. Intracranial thrombus extent predicts clinical outcome, final infarct size and hemorrhagic transformation in ischemic stroke: The clot burden score. *Int J Stroke*. 2008;3(4):230-236. doi:10.1111/j.1747-4949.2008.00221.x
194. Tan IYL, Demchuk AM, Hopyan J, et al. CT angiography clot burden score and collateral score: Correlation with clinical and radiologic outcomes in acute middle cerebral artery infarct. *AJNR Am J Neuroradiol*. 2009;30(3):525-531. doi:10.3174/ajnr.A1408
195. Treurniet KM, Yoo AJ, Berkhemer OA, et al. Clot Burden Score on Baseline Computerized Tomographic Angiography and Intra-Arterial Treatment Effect in Acute Ischemic Stroke. *Stroke*. 2016;47(12):2972-2978. doi:10.1161/STROKEAHA.116.014565
196. Simon J, Roland W, Jan G, Richard M, Heinrich MP, David L. Relevance of the cerebral collateral circulation in ischaemic stroke: Time is brain, but collaterals set the pace. *Swiss Med Wkly*. 2017;147(w14538):1-7. doi:10.4414/smw.2017.14538
197. Elijevich L, Goyal N, Mainali S, et al. CTA collateral score predicts infarct volume and clinical outcome after endovascular therapy for acute ischemic stroke: A retrospective chart review. *J Neurointerv Surg*. 2016;8(6):559-562. doi:10.1136/neurintsurg-2015-011731
198. Menon BK, Qazi E, Nambiar V, et al. Differential effect of baseline computed tomographic angiography collaterals on clinical outcome in patients enrolled in the

- Interventional management of stroke III trial. *Stroke*. 2015;46(5):1239-1244.
doi:10.1161/STROKEAHA.115.009009.Differential
199. Kim JJ, Fischbein NJ, Lu Y, Pham D, Dillon WP. Regional angiographic grading system for collateral flow: Correlation with cerebral infarction in patients with middle cerebral artery occlusion. *Stroke*. 2004;35(6):1340-1344.
doi:10.1161/01.STR.0000126043.83777.3a
200. Christoforidis GA, Mohammad Y, Kehagias D, Avutu B, Slivka AP. Angiographic assessment of pial collaterals as a prognostic indicator following intra-arterial thrombolysis for acute ischemic stroke. *AJNR Am J Neuroradiol*. 2005;26(7):1789-1797.
201. Maas MB, Lev MH, Ay H, et al. Collateral Vessels on CTA Predict Outcome in Acute Ischemic Stroke. *Stroke*. 2009;40(9):3001-3005.
doi:10.1161/STROKEAHA.109.552513.Collateral
202. Miteff F, Levi CR, Bateman GA, Spratt N, McElduff P, Parsons MW. The independent predictive utility of computed tomography angiographic collateral status in acute ischaemic stroke. *Brain*. 2009;132(8):2231-2238.
doi:10.1093/brain/awp155
203. Menon BK, Smith EE, Modi J, et al. Regional Leptomeningeal Score on CT Angiography Predicts Clinical and Imaging Outcomes in Patients with Acute Anterior Circulation Occlusions. *AJNR Am J Neuroradiol*. 2011;32(9):1640-1645.
doi:10.3174/ajnr.A2564

204. Menon BK, O'Brien B, Bivard A, et al. Assessment of leptomeningeal collaterals using dynamic CT angiography in patients with acute ischemic stroke. *J Cereb Blood Flow Metab.* 2013;33(3):365-371. doi:10.1038/jcbfm.2012.171
205. Seker F, Potreck A, Möhlenbruch M, Bendszus M, Pham M. Comparison of four different collateral scores in acute ischemic stroke by CT angiography. *J Neurointerv Surg.* 2016;8(11):1116-1118. doi:10.1136/neurintsurg-2015-012101
206. García-Tornel A, Carvalho V, Boned S, et al. Improving the Evaluation of Collateral Circulation by Multiphase Computed Tomography Angiography in Acute Stroke Patients Treated with Endovascular Reperfusion Therapies. *Interv Neurol.* 2016;5(3-4):209-217. doi:10.1159/000448525
207. Smit EJ, Vonken E, van Seeters T, et al. Timing-invariant imaging of collateral vessels in acute ischemic stroke. *Stroke.* 2013;44(8):2194-2199. doi:10.1161/STROKEAHA.111.000675
208. Konstas AA, Goldmakher G V., Lee TY, Lev MH. Theoretic basis and technical implementations of CT perfusion in acute ischemic stroke, part 1: Theoretic basis. *Am J Neuroradiol.* 2009;30(4):662-668. doi:10.3174/ajnr.A1487
209. Lee T-Y. Scientific basis and validation. In: Miles KA, Eastwood JD, Konig M, eds. *Multidetector Computed Tomography in Cerebrovascular Disease: CT Perfusion Imaging.* 1st editio. Milton: CRC Press; 2007:13-27.
210. Lee TY. Functional CT: Physiological models. *Trends Biotechnol.* 2002;20(8):3-10. doi:10.1016/S0167-7799(02)02035-8

211. St. Lawrence K, Lee T-Y. An Adiabatic Approximation to the Tissue Homogeneity Model for Water Exchange in the Brain: II. Experimental Validation. *J Cereb Blood Flow Metab.* 1998;18(12):1378-1385. doi:10.1097/00004647-199812000-00012
212. Krishnan P, Murphy A, Aviv RI. CT-based Techniques for Brain Perfusion. *Top Magn Reson Imaging.* 2017;26(3):113-119. doi:10.1097/RMR.0000000000000129
213. Konostas A, Goldmakher G, Lee T, Lev M. Theoretic basis and technical implementations of CT perfusion in acute ischemic stroke, part 2: technical implementations. *AJNR Am J Neuroradiol.* 2009;30(5):885-892. doi:10.3174/ajnr.A1492
214. Borst J, Marquering HA, Beenen LFM, et al. Effect of extended CT perfusion acquisition time on ischemic core and penumbra volume estimation in patients with acute ischemic stroke due to a large vessel occlusion. *PLoS One.* 2015;10(3):e0119409. doi:10.1371/journal.pone.0119409
215. Copen WA, Deipolyi AR, Schaefer PW, Schwamm LH, González RG, Wu O. Exposing hidden truncation-related errors in acute stroke perfusion imaging. *Am J Neuroradiol.* 2015;36(4):638-645. doi:10.3174/ajnr.A4186
216. d'Esterre CD, Aviv RI, Lee T-Y. The evolution of the cerebral blood volume abnormality in patients with ischemic stroke: A CT perfusion study. *Acta radiol.* 2012;53(4):461-467. doi:10.1258/ar.2012.110582
217. Deipolyi AR, Wu O, Macklin EA, et al. Reliability of cerebral blood volume maps

- as a substitute for diffusion-weighted imaging in acute ischemic stroke. *J Magn Reson Imaging*. 2012;36(5):1083-1087. doi:10.2217/nmm.12.167.Gene
218. Kämena A, Streitparth F, Grieser C, et al. Dynamic perfusion CT: Optimizing the temporal resolution for the calculation of perfusion CT parameters in stroke patients. *Eur J Radiol*. 2007;64(1):111-118. doi:10.1016/j.ejrad.2007.02.025
219. Abels B, Klotz E, Tomandl BF, Villablanca JP, Kloska SP, Lell MM. CT perfusion in acute ischemic stroke: a comparison of 2-second and 1-second temporal resolution. *AJNR American J Neuroradiol*. 2011;32(9):1632-1639. doi:10.3174/ajnr.A2576; 10.3174/ajnr.A2576
220. Wintermark M, Maeder P, Verdun FR, et al. Using 80 kVp versus 120 kVp in perfusion CT measurement of regional cerebral blood flow. *Am J Neuroradiol*. 2000;21(10):1881-1884. doi:10.2214/AJR.10.5705
221. Murphy A, So A, Lee T-Y, et al. Low dose CT perfusion in acute ischemic stroke. *Neuroradiology*. 2014;56(12):1055-1062. doi:10.1007/s00234-014-1434-z
222. Østerås BH, Heggen KL, Pedersen HK, Andersen HK, Martinsen ACT. Can use of adaptive statistical iterative reconstruction reduce radiation dose in unenhanced head CT? An analysis of qualitative and quantitative image quality. *Acta Radiol Open*. 2016;5(8):1-10. doi:10.1177/2058460116645831
223. Flottmann F, Kabath J, Illies T, et al. Iterative reconstruction improves both objective and subjective image quality in acute stroke CTP. *PLoS One*. 2016;11(3):e0150103. doi:10.1371/journal.pone.0150103

224. Mnyusiwalla A, Aviv RI, Symons SP. Radiation dose from multidetector row CT imaging for acute stroke. *Neuroradiology*. 2009;51(10):635-640.
doi:10.1007/s00234-009-0543-6
225. Lin EC. Radiation risk from medical imaging. *Mayo Clin Proc*. 2010;85(12):1142-1146. doi:10.4065/mcp.2010.0260
226. Lin L, Bivard A, Krishnamurthy V, Levi CR, Parsons MW. Whole-Brain CT Perfusion to Quantify Acute Ischemic Penumbra and Core. *Radiology*. 2016;279(3):876-887. doi:10.1148/radiol.2015150319
227. Haussen DC, Dehkharghani S, Rangaraju S, et al. Automated CT Perfusion Ischemic Core Volume and Noncontrast CT ASPECTS (Alberta Stroke Program Early CT Score): Correlation and Clinical Outcome Prediction in Large Vessel Stroke. *Stroke*. 2016;47(9):2318-2322. doi:10.1161/STROKEAHA.116.014117
228. Demeestere J, Garcia-Esperon C, Garcia-Bermejo P, et al. Evaluation of hyperacute infarct volume using ASPECTS and brain CT perfusion core volume. *Neurology*. 2017;88(24):2248-2253. doi:10.1212/WNL.0000000000004028
229. Dehkharghani S, Bammer R, Straka M, et al. Performance and predictive value of a user-independent platform for CT perfusion analysis: Threshold-derived automated systems outperform examiner-driven approaches in outcome prediction of acute ischemic stroke. *Am J Neuroradiol*. 2015;36(8):1419-1425.
doi:10.3174/ajnr.A4363
230. Huang X, Kalladka D, Cheripelli BK, Moreton FC, Muir KW. The Impact of CT

- Perfusion Threshold on Predicted Viable and Nonviable Tissue Volumes in Acute Ischemic Stroke. *J Neuroimaging*. 2017;27(6):602-606. doi:10.1111/jon.12442
231. Kamalian S, Kamalian S, Maas MB, et al. CT cerebral blood flow maps optimally correlate with admission diffusion-weighted imaging in acute stroke but thresholds vary by postprocessing platform. *Stroke*. 2011;42(7):1923-1928. doi:10.1161/STROKEAHA.110.610618
232. Aviv RI, d'Esterre CD, Murphy BD, et al. Hemorrhagic Transformation of Ischemic Stroke: Prediction with CT Perfusion. *Radiology*. 2009;250(3):867-877. doi:10.1148/radiol.2503080257
233. Puig J, Blasco G, Daunis-I-Estadella P, et al. High-permeability region size on perfusion CT predicts hemorrhagic transformation after intravenous thrombolysis in stroke. *PLoS One*. 2017;12(11):e0188238. doi:10.1371/journal.pone.0188238
234. Bracard S, Ducrocq X, Mas JL, et al. Mechanical thrombectomy after intravenous alteplase versus alteplase alone after stroke (THRACE): a randomised controlled trial. *Lancet Neurol*. 2016;15(11):1138-1147. doi:10.1016/S1474-4422(16)30177-6
235. Eilaghi A, Brooks J, d'Esterre C, et al. Reperfusion Is a Stronger Predictor of Good Clinical Outcome than Recanalization in Ischemic Stroke. *Radiology*. 2013;269(1):240-248. doi:10.1148/radiol.13122327
236. Belayev L, Alonso OF, Busto R, Zhao W, Ginsberg MD, Hsu CY. Middle Cerebral Artery Occlusion in the Rat by Intraluminal Suture: Neurological and

- Pathological Evaluation of an Improved Model. *Stroke*. 1996;27(9):1616-1623.
doi:10.1161/01.STR.27.9.1616
237. Fan X, Qiu J, Yu Z, et al. A rat model of studying tissue-type plasminogen activator thrombolysis in ischemic stroke with diabetes. *Stroke*. 2012;43(2):567-570. doi:10.1161/STROKEAHA.111.635250
238. Tamura A, Graham DI, McCulloch J, Teasdale GM. Focal Cerebral Ischaemia in the Rat: 1. Description of Technique and Early Neuropathological Consequences following Middle Cerebral Artery Occlusion. *J Cereb Blood Flow Metab*. 1981;1(1):53-60. doi:10.1038/jcbfm.1981.6
239. Fuxe K, Bjelke B, Andbjør B, Grahn H, Rimondini R, Agnati LF. Endothelin-1 induced lesions of the frontoparietal cortex of the rat. A possible model of focal cortical ischemia. *Neuroreport*. 1997;8(11):2623-2629. doi:10.1097/00001756-199707280-00040
240. Hughes PM, Anthony DC, Ruddin M, et al. Focal lesions in the rat central nervous system induced by endothelin-1. *J Neuropathol Exp Neurol*. 2003;62(12):1276-1286. doi:10.1093/jnen/62.12.1276
241. Burbridge B, Matte G, Remedios A. Complex intracranial arterial anatomy in swine is unsuitable for cerebral infarction projects. *Can Assoc Radiol J*. 2004;55(5):326-329.
242. Imai H, Konno K, Nakamura M, et al. A new model of focal cerebral ischemia in the miniature pig. *J Neurosurg*. 2006;104(2 Suppl):123-132.

doi:10.3171/ped.2006.104.2.123

243. O'Brien MD, Waltz AG. Transorbital approach for occluding the middle cerebral artery without craniectomy. *Stroke*. 1973;4(2):201-206.
doi:10.1161/01.STR.4.2.201
244. Campbell BCV, Hill MD, Rubiera M, et al. Safety and Efficacy of Solitaire Stent Thrombectomy. *Stroke*. 2016;47(3):798-806.
doi:10.1161/STROKEAHA.115.012360
245. Lemmens R, Hamilton S, Liebeskind D, et al. Effect of endovascular reperfusion in relation to site of arterial occlusion. *Stroke*. 2016;86(8):762-770.
doi:10.1212/WNL.0000000000002399
246. Pfaff J, Herweh C, Pham M, et al. Mechanical Thrombectomy of Distal Occlusions in the Anterior Cerebral Artery: Recanalization Rates, Periprocedural Complications, and Clinical Outcome. *Am J Neuroradiol*. 2016;37(4):673-678.
doi:10.3174/ajnr.A4594
247. Demel SL, Broderick JP. Basilar Occlusion Syndromes: An Update. *The Neurohospitalist*. 2015;5(3):142-150. doi:10.1177/1941874415583847
248. Kurre W, Vorlaender K, Aguilar-Perez M, Schmid E, Bözne H, Henkes H. Frequency and relevance of anterior cerebral artery embolism caused by mechanical thrombectomy of middle cerebral artery occlusion. *Am J Neuroradiol*. 2013;34(8):1606-1611. doi:10.3174/ajnr.A3462

249. Alonso De Leciñana M, Kawiorski MM, Ximénez-Carrillo Á, et al. Mechanical thrombectomy for basilar artery thrombosis: A comparison of outcomes with anterior circulation occlusions. *J Neurointerv Surg*. 2017;9(12):1173-1178. doi:10.1136/neurintsurg-2016-012797
250. Huang X, MacIsaac R, Thompson JLP, et al. Tenecteplase versus alteplase in stroke thrombolysis: An individual patient data meta-analysis of randomized controlled trials. *Int J Stroke*. 2016;11(5):534-543. doi:10.1177/1747493016641112
251. Parsons M, Spratt N, Bivard A, et al. A Randomized Trial of Tenecteplase versus Alteplase for Acute Ischemic Stroke. *N Engl J Med*. 2012;366(12):1099-1107. doi:10.1056/NEJMoa1109842
252. Huang X, Cheripelli BK, Lloyd SM, et al. Alteplase versus tenecteplase for thrombolysis after ischaemic stroke (ATTEST): A phase 2, randomised, open-label, blinded endpoint study. *Lancet Neurol*. 2015;14(4):368-376. doi:10.1016/S1474-4422(15)70017-7
253. Cook DJ, Teves L, Tymianski M. Treatment of stroke with a PSD-95 inhibitor in the gyrencephalic primate brain. *Nature*. 2012;483(7388):213-217. doi:10.1038/nature10841
254. Hill MD, Martin RH, Mikulis D, et al. Safety and efficacy of NA-1 in patients with iatrogenic stroke after endovascular aneurysm repair (ENACT): A phase 2, randomised, double-blind, placebo-controlled trial. *Lancet Neurol*.

2012;11(11):942-950. doi:10.1016/S1474-4422(12)70225-9

255. Wu C, Zhao W, An H, et al. Safety, feasibility, and potential efficacy of intraarterial selective cooling infusion for stroke patients treated with mechanical thrombectomy. *J Cereb Blood Flow Metab.* 2018;271678X18790139. doi:10.1177/0271678X18790139
256. Chen J, Liu L, Zhang H, et al. Endovascular hypothermia in acute ischemic stroke: A pilot study of selective intra-arterial cold saline infusion. *Stroke.* 2016;47(7):1933-1935. doi:10.1038/leu.2016.282.Dynamic
257. Karnatovskaia L V., Wartenberg KE, Freeman WD. Therapeutic Hypothermia for Neuroprotection: History, Mechanisms, Risks, and Clinical Applications. *The Neurohospitalist.* 2014;4(3):153-163. doi:10.1177/1941874413519802
258. Piironen K, Tiainen M, Mustanoja S, et al. Mild Hypothermia After Intravenous Thrombolysis in Patients With Acute Stroke: A Randomized Controlled Trial. *Stroke.* 2014;45(2):486-491. doi:10.1161/STROKEAHA.113.003180

Chapter 2

2 Absolute Cerebral Blood Flow Infarction Threshold for 3-hour Ischemia Time Determined with CT Perfusion and ^{18}F -FFMZ-PET Imaging in a Porcine Model of Cerebral Ischemia

2.1 Introduction

Both MRI and CT are highly sensitive for infarct core. Generally, CT is used preferentially for stroke diagnosis/prognosis because of availability, cost and speed. Along with NCCT and CTA, CTP is now consistently acquired at many institutes. CTP based time-dependent thresholds for infarct core have been recently derived using data from ischemic stroke patients¹. These thresholds will have important implications for patient triaging and will be useful in wake-up and late presenting strokes. Predicting the infarct core evolution could help identify patients who will benefit most from transfer to tertiary centers capable of IAT, the new standard of care.

However, many threshold derivation studies used follow-up imaging performed 1-7 days after symptom onset to define the infarct core²⁻⁸, introducing uncertainty caused by infarct expansion in the time between admission and follow-up imaging. Furthermore, some of these studies used DWI to define the infarct core^{5,6,8}. DWI lesion reversal has been observed in both human and animal ischemic stroke^{9,10}, though it should be noted that clinical instances of DWI lesion reversal are rare¹¹ and should not deter anyone from using MRI if it is logistically feasible to acquire in the acute setting.

One alternative, which may circumvent uncertainties caused by infarct expansion and DWI, is to use large animal stroke models to derive time-dependent thresholds for

infarction. The logistical complexity of producing and using radiotracers in the clinical acute stroke setting are not a factor, and radiation dose is less of a concern in animal models, so the infarct can be defined using PET imaging with radiolabeled FMZ, or its fluorinated analog, FFMZ. This gold standard method reliably predicts the final infarct and is less prone to false positives than DWI¹². Furthermore, animal models provide greater control over the time interval between symptom onset and tissue status determination, allowing infarction thresholds to be determined for many different ischemia durations.

Porcine models are more useful than small animal models since the gyrencephalic brain is more similar to a human brain in terms of grey/white matter composition and size¹³. However, the rete mirabile makes it impossible to use intra-arterial catheter-based methods commonly used to initiate cerebral ischemia in small animal models¹⁴. As a result, most porcine models of stroke rely on complex and invasive surgical procedures to access the middle cerebral artery, so a clip or ligature can be applied^{15,16}. Using ET-1 to cause transient cerebral ischemia does not require complicated surgical procedures and has been well established in rodents and lower primates^{17,18}. ET-1 binds to endothelin receptors type A and B in cerebral vascular smooth muscle cells, triggering a potent vasoconstriction that induces changes in CBF severe enough to induce infarction, with minimal tissue edema¹⁹. Recently, the ET-1 method was used in a porcine model of cerebral ischemia²⁰.

In this study, we presented an ET-1 based porcine model of cerebral ischemia for determining time dependent CBF thresholds for infarction using CTP and ¹⁸F-FFMZ-PET imaging, and we determined a CBF threshold for infarction after 3hrs of ischemia.

2.2 Methods

2.2.1 Acute Cerebral Ischemia Model

All animal experiments were conducted following the guidelines of the Canadian Council on Animal Care and approved by the Animal Use Subcommittee at the University of Western Ontario (Protocol #2007-050). Duroc Cross Pigs were picked up from a nearby farm on the day of the experiment and were not housed at the laboratory prior to experiments. Out of the 11 animals (average weight 26 ± 5 kg) used in this study, 7 were female and 4 were male. Anesthesia was induced in the animals using 4-5% isoflurane. Anesthesia was maintained by mask with 3-4% isoflurane until intubation. Propofol (16-22 mg/kg) was given IV for intubation. The pig was ventilated (10-15 cc/stroke volume, 20-30 breath per minute) with 2.5-3.5% isoflurane with oxygen and medical air (2:1 medical air to oxygen ratio) for the duration of the experiment. A 22G cephalic vein catheter was placed for injection of CT contrast (Isovue 370) and ^{18}F -FFMZ. One femoral artery was cannulated with a catheter for measuring blood pressure, blood gases (pO_2 and pCO_2), glucose and pH throughout the experiment. In addition, heart rate, arterial oxygen saturation, end-tidal carbon dioxide tension (CO_2), respiration rate and blood pressure were continuously monitored (Surgivet). The animal was wrapped in a circulating hot water blanket and rectal temp were monitored continuously throughout the experiment.

A CT scan was done to identify sixteen contiguous 2.5mm thick slices which included the largest coronal sections of the brain, then a baseline CTP study was performed using the procedures outlined in the next section. A target slice location showing the maximal extent of the MCA territory was selected following the baseline CTP scan. This target slice was marked on the pig's head using the CT scanner laser positioning light, the

scalp was incised (silver nitrate sticks used to control bleeding) and a 1-2mm diameter burr hole was made with a Dremel hand tool through the skull. A 27G 1 ¼” long needle attached to a 1mL saline syringe with PE 40 tubing was preloaded with ET-1 and inserted through the burr hole into the brain. An axial CT scan was then acquired to verify that the needle tip is within the cerebral cortex in the target slice. 33µg of ET-1 in 150µL of sterile water was injected at 50 µL/min using an infusion pump. CT Perfusion studies were performed 10 and 30min after the ET-1 injection, and then every 30min for the remainder of the 3hr monitoring period.

Animals were under anesthetic for the entire study to reduce unnecessary animal suffering. If anything seriously detrimental had happened during surgery or scanning, the animal would have been euthanized immediately by intravenous potassium chloride overdose under full deep anesthetic, however there were no serious incidents so early termination of experiments was not necessary. At the conclusion of the experiment animals were euthanized by intravenous potassium chloride overdose under full deep isoflurane anesthetic.

2.2.2 On-line CBF Monitoring with CT Perfusion

CTP studies were acquired on the GE Healthcare Discovery VCT PET/CT scanner using the following protocol: 80kV, 200mA, 16 slices of 2.5mm thickness, 1 scan per second for 60s with a 5s delay from the start of contrast injection (370mg Iodine/mL) at a dosage of 1mL/kg body weight and at an injection rate of 3mL/s. CTP studies were completed at baseline, 10 and 30min post ET-1 injection and then every 30min until 3hr post ischemia. Quantitative CBF maps from each acquired CTP study, calculated within 5min of acquisition, were used to evaluate the perfusion in the ET-1 injection territory. If

reperfusion caused CBF to rise above the target range of $\sim 20 \text{ mL}\cdot\text{min}^{-1}\cdot 100\text{g}^{-1}$ (infarction threshold with permanent occlusion²¹), a second dose of ET-1 was injected and perfusion was checked 10min after, before perfusion monitoring went back to half-hourly intervals. Physiological parameters that have an impact on CBF were monitored throughout the experiment.

2.2.3 ^{18}F -FFMZ-PET Imaging for Detecting Cerebral Infarction

FMZ is a selective, high-affinity ligand for the central benzodiazepine receptor of the GABA-A receptor complex²². Since cortical neurons have a high concentration of GABA-A receptors, and they are sensitive to early ischemic damage, their activity within the brain is an indicator of neuronal integrity²³. Previous studies in humans and animals have shown that irreversibly damaged cortical tissue can be detected by decreased binding of carbon-11 (^{11}C) labeled FMZ^{22,23}. FFMZ is a fluorinated analogue of flumazenil with similar pharmacokinetics. FFMZ can be labelled with fluorine-18 (^{18}F), which is advantageous because of the longer half-life²⁴. Previous studies have shown that PET imaging with ^{18}F -FFMZ can be used to map the activity of GABA-A receptors in the human brain in the same way as ^{11}C -FMZ²⁵.

^{18}F -FFMZ-PET imaging was performed on the GE Healthcare Discovery VCT PET/CT scanner in the 3D acquisition mode. 370MBq of the tracer was injected 25min before the start of the PET imaging (160min after first ET-1 injection). A CT scan was acquired for attenuation correction. For the PET imaging, 5 frames of 300s duration each (25min total time) were acquired on forty-seven 3.3mm thick slices. The 5 frames were averaged together at all slice locations.

2.2.4 Data Analysis

For consistency, all CTP functional maps were calculated by one author using delay-insensitive deconvolution software (CT Perfusion 5 GE Healthcare, Waukesha, WI) as described previously²⁶. For each pig, CBF maps from each CTP imaging time point were co-registered, and the median value of each pixel was found using Matlab, to generate a median CBF map. The median CBF map was then co-registered with the PET images, average images (perfusion-weighted maps) from the baseline CTP study, and blood volume (BV) maps at 10min after the first ET-1 injection. All image registration was manually performed with rigid 3D registration in Analyze 11 (Mayo Clinic, Biomedical Engineering). The average image was used to draw regions of interest (ROIs) covering the cortex on the affected and contralateral sides on all slices containing a defect in ¹⁸F-FFMZ uptake. These ROIs were then superimposed onto all other co-registered images. Infarct pixels were identified on PET images as having signal less than the average minus 2 standard deviations from the contralateral ROI. Since GABA-A receptors are located primarily in the grey matter²⁷, the average image was used to segment out white matter by removing any pixels where the CT number was less than 40 HU. To avoid the influence of large blood vessels on parenchymal perfusion, the BV map was used to exclude blood vessel pixels if they had a BV greater than the average plus 2 standard deviations from the affected side ROI. Additionally, pixels with median CBF greater than $100 \text{ mL} \cdot \text{min}^{-1} \cdot 100\text{g}^{-1}$ were also considered to be blood vessels and excluded from analysis. The remaining infarct and non-infarct grey matter ROIs were then superimposed onto the median CBF map and pixel values were imported into an in-house Matlab program for logistic regression and ROC analysis (Figure 2.1). This process was repeated for each animal that

had a defect in ^{18}F -FFMZ uptake. The CBF values that corresponded to the optimal operating point of the ROC curve (the point closest to the top left corner)²⁸ for each animal were averaged together to determine the CBF threshold for infarction after 3h of ischemia. All analysis of images and data was performed by one author (EAW).

Figure 2.1: Image analysis method

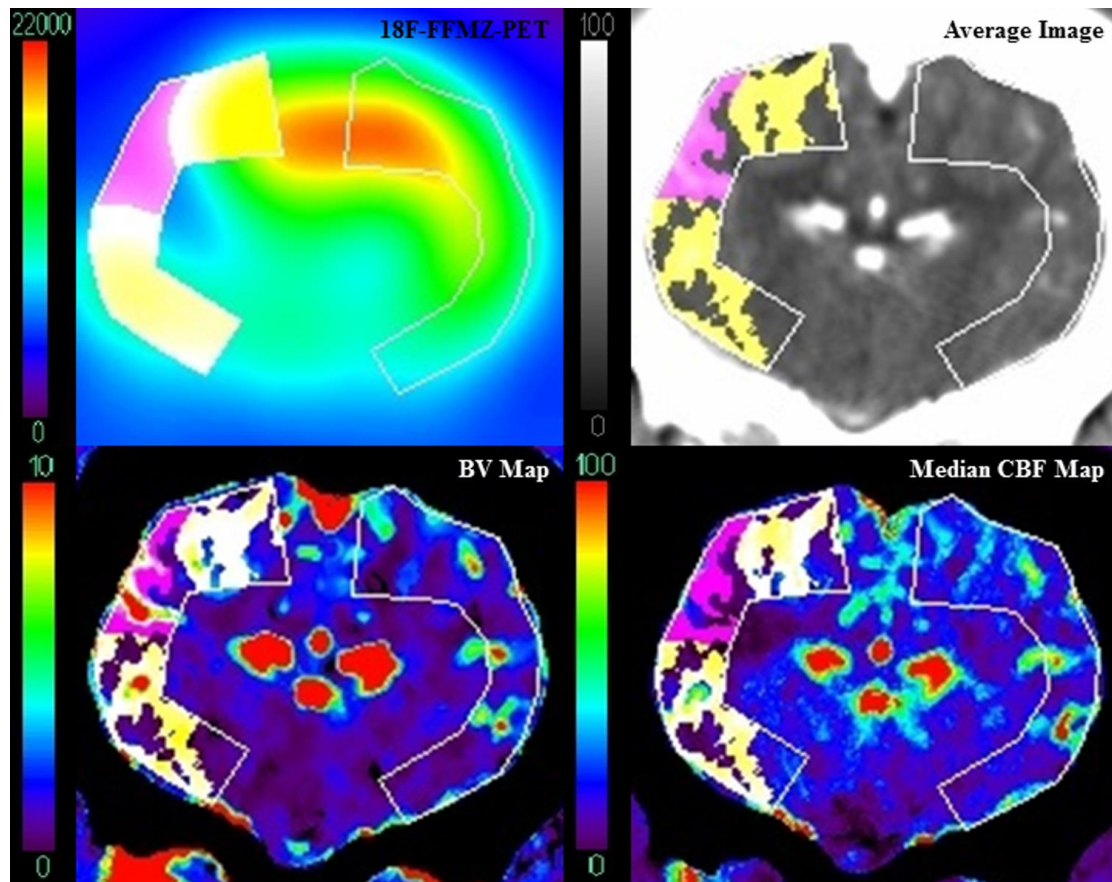


Fig. 2.1 Infarct (pink) was identified on a PET image (top left) acquired 160-185min after ET-1 injection as pixels in the affected side ROI with signal below the infarction threshold derived from the contralateral ROI. Pixels with signal above this threshold were classified as non-infarct (yellow). The average image (top right) was used to segment out white matter. Blood vessels were identified on the BV map (bottom left) using a threshold derived from the affected side ROI (see text). Grey matter, vessel-less infarct and non-infarct ROIs were then superimposed onto the median CBF map (bottom right).

2.3 Results

6 out of 11 animals had irreversible tissue damage (i.e. uptake defect upon ^{18}F -FFMZ imaging) and were included in the analysis. After removing vessel pixels, the volumes of grey matter infarct determined by the PET threshold for these animals were 2.96, 0.74, 2.30, 0.96, 0.97, and 0.80mL, giving an average grey matter infarct volume of $1.46 \pm 0.38\text{mL}$. 3 of the 6 animals that developed infarction required a second ET-1 injection to maintain depressed CBF in the ischemic territory.

The average relative CBF (rCBF normalized to contralateral grey matter) in the grey matter infarct region was calculated at each CTP imaging time point, for each animal. The average relative CBF value in the infarct regions over all animals and CTP imaging time points was $42 \pm 16\%$. Figure 2.2 shows the average rCBF in the infarct region over time. On average, 60min after the 1st ET-1 injection rCBF dropped to $\sim 40\%$ and remained there for the duration of the experiment.

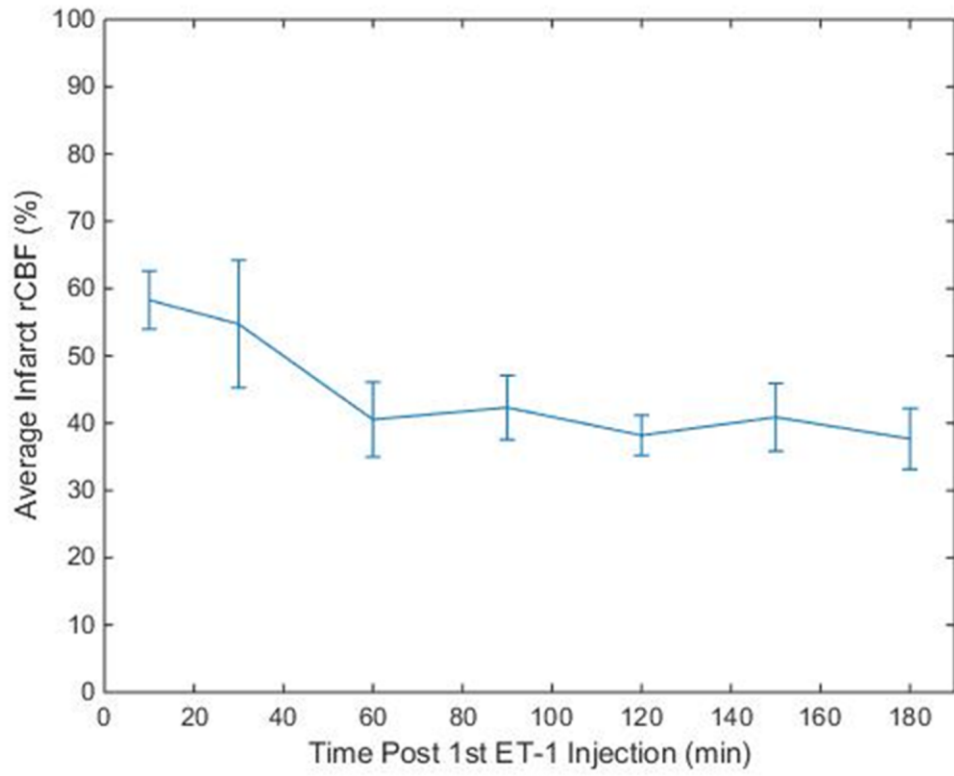
Figure 2.2: Average relative CBF of infarct ROIs

Fig. 2.2: Average relative CBF value from the infarct regions of the 6 animals at each time point. Error bars indicate standard error.

The infarct CBF histograms for each animal were normalized by scaling the number of infarct pixels in each bin up by the ratio of the total penumbra/oligemia pixels to the total infarct pixels (this scaling operation equalized the number of pixels in the infarct and penumbra/oligemia histograms). This normalization did not affect the ROC analysis because the relative frequencies of the CBF values were not changed, but it was necessary to prevent bias in the logistic regression caused by having a much greater number of pixels in the penumbra/oligemia group than in the infarct group. CBF histograms for each animal, and ^{18}F -FFMZ-PET and CBF maps from the slice with the largest extent of infarct for each animal can be found in Appendix A. Matlab was used to perform a binary logistic regression on the normalized histogram data for each animal. The probability of infarction predicted by logistic regression is plotted against CBF for each animal in Figure 2.3. The average of the 6 CBF values that corresponded to a 75% predicted probability of infarction in each animal was $4.5 \pm 2.6 \text{ mL}\cdot\text{min}^{-1}\cdot 100\text{g}^{-1}$.

Figure 2.3: Predicted probability of infarction versus CBF

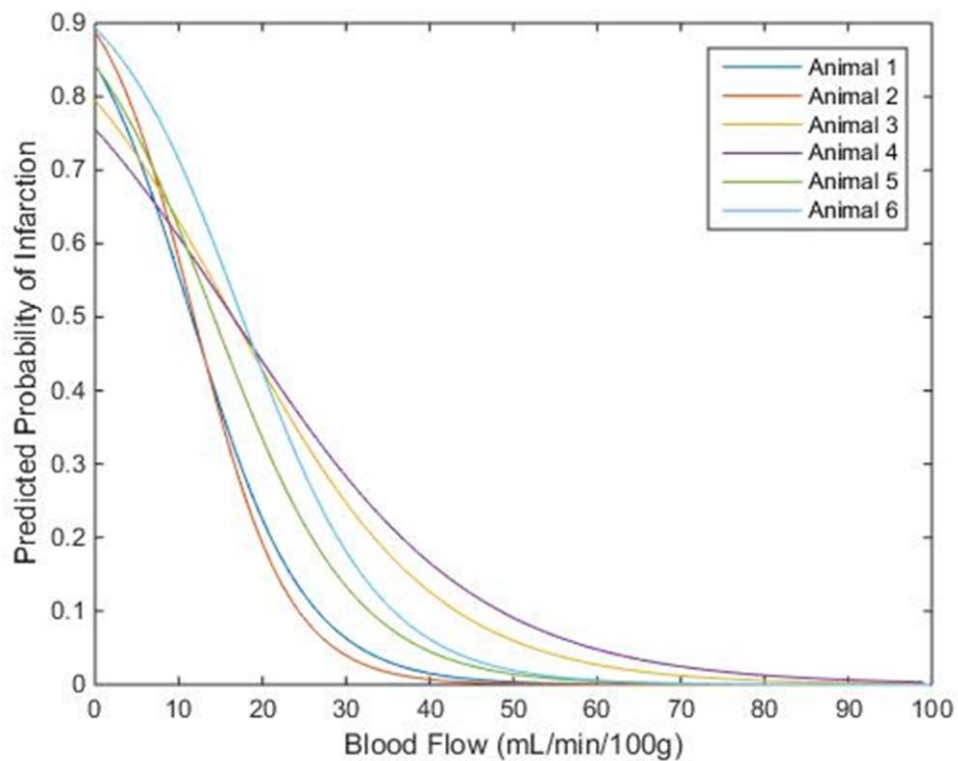


Fig. 2.3: Predicted probability of infarction from logistic regression plotted against CBF for each animal. The average of the CBF values that corresponded to a 75% predicted probability of infarction was approximately $4.5 \pm 2.6 \text{ mL} \cdot \text{min}^{-1} \cdot 100\text{g}^{-1}$.

Figure 2.4 shows the ROC curve for each animal. The average of the CBF values corresponding to the optimal operating points of the ROC curves²⁸ was $12.6 \pm 2.8 \text{ mL} \cdot \text{min}^{-1} \cdot 100\text{g}^{-1}$. The sensitivity, specificity, and accuracy for infarct detection corresponding to the threshold in each animal, and the area under curve (AUC) can be found in Table 2.1.

Figure 2.4: ROC curves for each animal

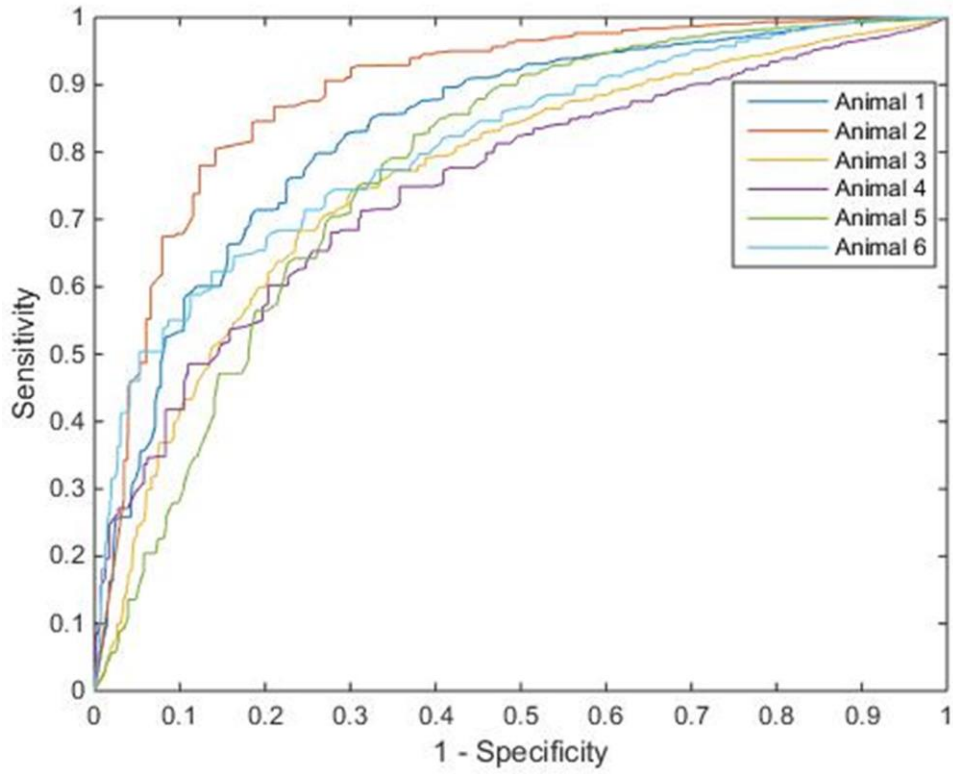


Fig. 2.4: ROC curves plotted for each of the 6 animals. Table 1 lists the CBF threshold derived from the optimal operating point of the ROC curve for each animal, and the corresponding sensitivity, specificity, accuracy, and AUC.

Table 2.1: ROC parameters for each animal

Animal	Threshold (mL·min⁻¹·100g⁻¹)	Sensitivity	Specificity	Accuracy	AUC
1	10.1	0.80	0.74	0.77	0.8333
2	8.9	0.80	0.86	0.83	0.8908
3	15.0	0.74	0.70	0.72	0.7650
4	13.2	0.68	0.72	0.70	0.7528
5	12.1	0.75	0.69	0.72	0.7750
6	16.2	0.71	0.75	0.73	0.8110

The relevant parameters from the ROC analysis for each animal. The CBF threshold for infarction was the CBF value that corresponded to the optimal operating point of the ROC curve. AUC stands for area-under-curve.

2.4 Discussion

This study used a porcine model of ET-1 induced cerebral ischemia to determine a CTP-derived CBF threshold for infarction as determined by ^{18}F -FFMZ-PET imaging after 3 hours of ischemia. A threshold of $12.6 \text{ mL}\cdot\text{min}^{-1}\cdot 100\text{g}^{-1}$ was determined using ROC analysis. Previous animal studies have shown that the threshold for infarction is time dependent, dropping from $17\text{-}24 \text{ mL}\cdot\text{min}^{-1}\cdot 100\text{g}^{-1}$ for permanent occlusion to $12 \text{ mL}\cdot\text{min}^{-1}\cdot 100\text{g}^{-1}$ for occlusion lasting only 3 hours^{21,29}.

CTP-based time dependent thresholds for infarct core could be important for identifying late presenting or wake-up ischemic stroke patients that may still benefit from therapy¹. Furthermore, time-dependent thresholds for infarction could be used to predict infarct growth in the time between admission imaging and reperfusion. This knowledge would be useful when deciding whether it is worthwhile to transfer a patient from a regional hospital to an IAT capable tertiary care hospital.

Prior perfusion threshold derivation studies could be affected by methodological problems. Many studies measure CBF during the acute phase of stroke, but do not determine the tissue outcome until several days or even weeks later³⁻⁵ introducing the uncertainty of infarct expansion in the interim. Furthermore, some studies use sub-optimal imaging data sets where the degree of reperfusion is not known⁴. With the experimental procedure used in this study CBF measurements and tissue outcome can be determined contemporaneously, eliminating the error caused by infarct expansion. This model also allows consistent monitoring of CBF using CTP, which gives information about the extent of reperfusion in the ischemic tissue.

The experimental model used in this study has several advantages over other animal models. The model used by Jones et al involved surgery to expose the MCA, so it could be occluded using a ligature²⁹. This is an example of a broader category of models which induce ischemia by occluding the MCA, generally using either an intra-arterial catheter³⁰ or by exposing the MCA and applying a clip or ligature²⁹. Implementing these models of acute ischemia in pigs can be problematic for several reasons; the rete mirabile makes it impossible to use an intra-arterial catheter¹⁴, and using a clip or ligature requires very invasive surgical procedures such as an osteotomy on the orbital rim¹⁵ or removal of an eye¹⁶. The ET-1 insult used in this study circumvents these difficulties since the only surgeries required are an incision on the scalp and a small burr hole in the skull (~2mm diameter). The less traumatic approach increases the ability to maintain the animal at its basal physiological state throughout the experiment. This is supported by the fact that in the Jones study 13 of the 33 monkeys had to be excluded from the data analysis because of subarachnoid hemorrhage, problems with the ligature or other technical issues²⁹ whereas in this study none of the 11 animals experienced these problems.

In animals 1, 2, and 6 the first dose, administered at the start of the experiment, was able to maintain rCBF in the final infarct region below 50% for most of the experiment. However, in animals 3, 4, and 5 the effect of the first dose was transient and a second dose was required. The second dose was given 90min after the first dose in animal 4 and 30min after the first dose in animal 5, the average rCBF for the remainder of the experiments dropped to ~37% and ~32% respectively in the final infarct regions. In animal 3, the second dose was given 90min into the experiment, causing a transient decrease in rCBF to 43% before it rose above 50% again 150min into the experiment. In this animal the second

dose may have been given too late to counteract the reactive hyperemia associated with reperfusion^{31,32}. There was some variation in response to ET-1 injections, but variation in CBF reduction is to be expected in animal models of stroke. In the study by Jones et al where cerebral ischemia was initiated in monkeys by ligating the MCA, the average CBF after ligation in the insular cortex was $17 \pm 16 \text{ mL}\cdot\text{min}^{-1}\cdot 100\text{g}^{-1}$ ²⁹, in this study the average CBF across all animals and time points after the first ET-1 injection was $15 \pm 5 \text{ mL}\cdot\text{min}^{-1}\cdot 100\text{g}^{-1}$. On average, rCBF in the final infarct tissue dropped to 56% for the first 30min of the experiment, from the 1hr time point until the end of the experiment rCBF was maintained at ~40%. Although the cerebral ischemia caused by ET-1 injections does not always replicate clinical cases of stroke, the model is still suitable for this study, where the objective is to cause a reduction in CBF leading to infarction, then determine a CBF threshold for distinguishing salvaged tissue from tissue which progressed to infarction.

Reperfusion and subsequent reactive hyperemia of the ischemic tissue after the first ET-1 injection is problematic in this model for several reasons. Premature reperfusion prevents ischemic tissue from progressing to infarction, this was the main reason that 5 of 11 animals did not develop irreversible tissue damage. When reperfusion occurs midway through the experiment it can be difficult to accurately define the ischemia duration. Lastly, some tissue progresses to infarction despite having a relatively high CBF at many time points during the experiment, either due to a weak response to the first injection or premature reperfusion and associated reactive hyperemia after the first injection wears off. This can result in high median CBF in the infarct regions leading to overestimation of the infarction threshold. For example, the average rCBF in the final infarct region for animal 6 was below 30% between the 30min and 120min time points and above 40% in the final

three time points. It is possible that infarction was due to CBF dropping to an average value of $9.4 \text{ mL}\cdot\text{min}^{-1}\cdot 100\text{g}^{-1}$ for 30-90min in the middle of the experiment, and the higher CBF at the other time points resulted in an overestimated threshold of $16.2 \text{ mL}\cdot\text{min}^{-1}\cdot 100\text{g}^{-1}$ being derived. Using the median CBF value rather than the average CBF lessens the effect that reperfusion has on the derivation of a threshold.

In our experiments, reperfusion was partially mitigated by using semi-continuous CBF monitoring with CTP at 30min intervals to identify when reperfusion had started, so that another dose of ET-1 could be given. At each CTP imaging time point the CBF maps were calculated on a work station in the CT scanner suite within ~5-8min of completing the scanning, to monitor for reperfusion from the ET-1 effects wearing off. This method effectively limited reperfusion of the ischemic tissue, as the average rCBF in the final infarct region was below 50% for the duration of the experiment in 5 of 6 animals, and the average infarct rCBF across all animals and time points was $42 \pm 16\%$.

2.5 Conclusion

The objective of this study was to determine a CBF threshold for infarction after 3 hours of ischemia. ROC analysis was used to find a threshold of $12.6 \text{ mL}\cdot\text{min}^{-1}\cdot 100\text{g}^{-1}$, which agrees well with the value of $12 \text{ mL}\cdot\text{min}^{-1}\cdot 100\text{g}^{-1}$ determined by Jones et al in 1981²⁹. The ET-1 model of acute stroke used in this study is easier to implement than other large animal stroke models. Despite some variation in response to ET-1 injections and instances of premature reperfusion, the model is comparable to other animal stroke models for the study objective.

2.6 References

1. d'Esteire CD, Boesen ME, Hwan S, Pordeli P, Najm M, Minhas P, et al. Time-dependent computed tomographic perfusion thresholds for patients with acute ischemic stroke. *Stroke*. 2015; 46(12): 3390-3397.
2. Qiao Y, Zhu G, Patrie J, Xin W, Michel P, Eskandari A, et al. Optimal perfusion computed tomographic thresholds for ischemic core and penumbra are not time dependent in the clinically relevant time window. *Stroke*. 2014; 45(5): 1355-1362.
3. Murphy BD, Fox AJ, Lee DH, Sahlas DJ, Black SE, Hogan MJ, et al. Identification of penumbra and infarct in acute ischemic stroke using computed tomography perfusion-derived blood flow and blood volume measurements. *Stroke*. 2006; 37(7): 1771-1777.
4. Murphy BD, Fox AJ, Lee DH, Sahlas DJ, Black SE, Hogan MJ, et al. White matter thresholds for ischemic penumbra and infarct core in patients with acute stroke: CT perfusion study. *Radiology*. 2008; 247(3): 818-825.
5. Bao DZ, Bao HY, Yao LZ, Pan YG, Zhu XR, Yang XS, et al. 64-slice spiral CT perfusion combined with vascular imaging of acute ischemic stroke for assessment of infarct core and penumbra. *Exp Ther Med*. 2013; 6(1): 133-139.
6. Pan J, Zhang J, Huang W, Cheng X, Ling Y, Dong Q, et al. Value of perfusion computed tomography in acute ischemic stroke: diagnosis of infarct core and penumbra. *J Comput Assist Tomogr*. 2013; 37(5): 645-649.
7. Eilaghi A, d'Esteire CD, Lee TY, Jakobovic R, Brooks J, Liu RTK, et al. Toward patient-tailored perfusion thresholds for prediction of stroke outcome. *AJNR Am J Neuroradiol*. 2014; 35(3): 472-477.

8. Yu Y, Han Q, Ding X, Chen Q, Ye K, Zhang S, et al. Defining core and penumbra in ischemic stroke: a voxel- and volume-based analysis of whole brain CT perfusion. *Sci Rep.* 2016; 10(6): 1-7.
9. Labeyrie MA, Turc G, Hess A, Hervo P, Mas JL, Meder JF, et al. Diffusion lesion reversal after thrombolysis: a MR correlate of early neurological improvement. *Stroke.* 2012; 43(11): 2986-2991.
10. Olivot JM, Mlynash M, Thijs VN, Purushotham A, Kemp S, Lansberg MG, et al. Relationships between cerebral perfusion and reversibility of acute diffusion lesions in DEFUSE: insights from RADAR. *Stroke.* 2009; 40(5): 1692-1697.
11. Freeman JW, Luby M, Merino JG, Latour LL, Auh S, Song SS, et al. Negative diffusion weighted imaging after IV tPA is rare and unlikely to indicate averted infarction. *Stroke.* 2013; 44(6): 1629-1634.
12. Heiss WD, Sobesky J, Smekal UV, Kracht LW, Lehnhardt FG, Thiel A, et al. Probability of cortical infarction predicted by flumazenil binding and diffusion-weighted imaging signal intensity: a comparative positron emission tomography/magnetic resonance imaging study in early ischemic stroke. *Stroke.* 2004; 35(8): 1892-1898.
13. Platt SR, Holmes SP, Howerth EW, Duberstein KJJ, Dove CR, Kinder HA, et al. Development and characterization of a Yucatan miniature biomedical pig permanent middle cerebral artery occlusion stroke model. *Exp Transl Stroke Med.* 2014; 6(1): 1-14.

14. Burbridge B, Matte G, Remedios A. Complex intracranial arterial anatomy in swine is unsuitable for cerebral infarction projects. *Can Assoc Radiol J.* 2004; 55(5): 326-329.
15. O'Brien MD, Waltz AG. Transorbital approach for occluding the middle cerebral artery without craniectomy. *Stroke.* 1973; 4(2): 201-206.
16. Imai H, Konno K, Nakamura M, Shimizu T, Kubota C, Seki K, et al. A new model of focal cerebral ischemia in the miniature pig. *J Neurosurg.* 2006; 104(2 Suppl): 123-132.
17. Nikolova S, Moyanova S, Hughes S, Bellyou-Camilleri M, Lee TY, Bartha R. Endothelin-1 induced MCAO: dose dependency of cerebral blood flow. *J Neurosci Methods.* 2009; 179(1): 22-28.
18. Virley D, Hadingham SJ, Roberts JC, Farnfield B, Elliot H, Whelan G, et al. A new primate model of focal stroke: endothelin-1-induced middle cerebral artery occlusion and reperfusion in the common marmoset. *J Cereb Blood Flow Metab.* 2004; 24(1): 24-41.
19. Grell A, Thigarajah L, Edvinsson L, Samraj AK. Regulatory mechanism of endothelin receptor b in the cerebral arteries after focal cerebral ischemia. *PLoS One.* 2014; 9(12): e113624.
20. d'Esterre CD, Aviv RI, Morrison L, Fainardi E, Lee TY. Acute multi-modal neuroimaging in a porcine model of endothelin-1-induced cerebral ischemia: defining the acute infarct core. *Transl Stroke Res.* 2015; 6(3): 234-241.
21. Hossmann KA. Viability thresholds and the penumbra of focal ischemia. *Ann Neurol.* 1994; 36(4): 557-565.

22. Sette G, Baron JC, Young AR, Miyazawa H, Tillet I, Barré L, et al. In vivo mapping of brain benzodiazepine receptor changes by positron emission tomography after focal ischemia in the anesthetized baboon. *Stroke*. 1993; 24(12): 2046-2058.
23. Heiss WD, Grond M, Thiel A, Ghaemi M, Sobesky J, Rudolf J, et al. Permanent cortical damage detected by flumazenil positron emission tomography in acute stroke. *Stroke*. 1998; 29(2): 454-461.
24. Gründer G, Siessmeier T, Lange-Asschenfeldt C, Vernaleken I, Buchholz HG, Stoeter P, et al. [¹⁸F]Fluoroethylflumazenil: a novel tracer for PET imaging of human benzodiazepine receptors. *Eur J Nucl Med*. 2001; 28(10): 1463-1470.
25. Levêque P, Sanabria-Bohorquez S, Bol A, De Volder A, Labar D, Van Rijckevorsel K, et al. Quantification of human brain benzodiazepine receptors using [¹⁸F]fluoroethylflumazenil: a first report in volunteers and epileptic patients. *Eur J Nucl Med Mol Imaging*. 2003; 30(12): 1630-1636.
26. Konstas AA, Goldmakher GV, Lee TY, Lev MH. Theoretic basis and technical implementations of CT perfusion in acute ischemic stroke, part 2: technical implementations. *AJNR Am J Neuroradiol*. 2009; 30(5): 885-892.
27. Richards JG, Möhler H, Schoch P, Häring P, Takacs B, Stähli C. The visualization of neuronal benzodiazepine receptors in the brain by autoradiography and immunohistochemistry. *J Recept Res*. 1984; 4(1-6): 657-669.
28. Gallop RJ, Crits-Christoph P, Muenz LR, Tu XM. Determination and interpretation of the optimal operating point for ROC curves derived through generalized linear models. *Understand Stat*. 2003; 2(4): 219-242.

29. Jones TH, Morawetz RB, Crowell RM, Marcoux FW, FitzGibbon SJ, DeGirolami U, et al. Thresholds of focal cerebral ischemia in awake monkeys. *J Neurosurg.* 1981; 54(6): 773-782.
30. Van Winkle JA, Chen B, Lei IF, Pereira B, Raiput PS, Lyden PD. Concurrent middle cerebral artery occlusion and intra-arterial drug infusion via ipsilateral common carotid artery catheter in the rat. *J Neurosci Methods.* 2013; 213(1): 63-69.
31. Onetti Y, Dantas AP, Pérez B, Cugota R, Chamorro A, Planas AM, et al. Middle cerebral artery remodeling following transient brain ischemia is linked to early postischemic hyperemia: a target of uric acid treatment. *Am J Physiol Heart Circ Physiol.* 2015; 308(8): H862-H874.
32. Traupe H, Kruse E, Heiss WD. Reperfusion of focal ischemia of varying duration: postischemic hyper- and hypo-perfusion. *Stroke.* 1982; 13(5): 615-622.

Chapter 3

3 Impact of Truncation Artifacts on CT Perfusion-derived CBV, CBF, and Time-to-Maximum Measurements in Ischemic Stroke Patients

3.1 Introduction

CTP has become common in AIS as a tool for quantifying the extent of irreversibly damaged infarct core and salvageable penumbra^{1,2}. CT is advantageous in AIS since it is more accessible than MRI³ and can be performed without screening patients for metal implants and other MRI contraindications, thereby reducing door-to-needle times⁴. Applying thresholds to CTP-parameter maps can provide estimates of infarct core volume which are comparable to infarct volumes from DWI and follow-up CT⁵⁻⁷. These infarct core volumes from thresholded CTP maps have been used to determine eligibility for endovascular therapy^{1,2,8,9} or predicting outcome after endovascular therapy.

However, there is still a lack of consensus about the optimal scan duration for ischemic stroke applications. Scan durations vary from 40s to 120s from center-to-center¹⁰, despite recommendations to use a 90s-acquisition time¹¹. Shorter scan durations are desirable due to the decreased radiation dose to the patient, but shortened scan durations can also lead to truncation of time-density curves from ischemic tissue if the scan duration is not long enough to capture the complete wash-in and wash-out of the contrast agent. In AIS patients, since the contrast agent must travel through stenotic arteries or collateral circulation, the arrival time at ischemic tissue can be longer than 35s¹². Furthermore, once contrast reaches the ischemic tissue, decreased perfusion pressure can cause the washout to take 10-20s longer than in normal tissue¹³. The delayed wash-in and washout of contrast

agent in ischemic tissue could result in truncated ischemic tissue time-density curves in 44 to 67% of cases^{10,14}, particularly for scan durations shorter than 60s (Figure 3.1).

Figure 3.1: Truncation of ischemic tissue TDCs

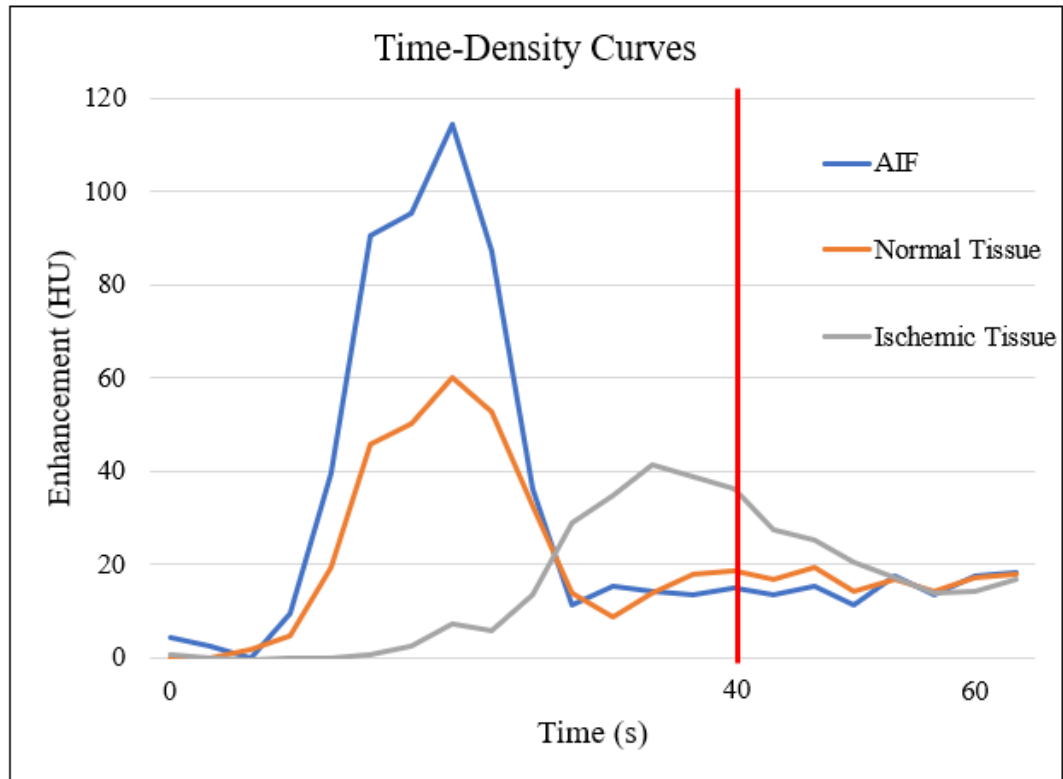


Fig 3.1: Illustration of contrast washout from ischemic tissue being missed when short (e.g. 40 seconds, red line) scan durations are used for brain CTP in stroke patients.

Deconvolution of truncated TDCs can lead to errors in calculation of hemodynamic parameters, and by extension, over- or underestimated infarct volumes when thresholds are applied to parameter maps.

Previous studies showed that truncation artifacts can result in underestimated CTP parameters^{12,15-17}, and therefore, under/over-estimated infarct volumes derived by applying thresholds^{9,12,15,17,18}.

In a previous publication, CTP infarction thresholds for different times from admission to reperfusion were derived using commercially available perfusion software (CTP4D, GE Healthcare, Waukesha, WI)⁵. The effects of truncation on perfusion parameters and the optimal scan duration¹⁸ to avoid such effects could be dependent on the details of the deconvolution algorithm used to analyze the acquired data. To investigate the impact of truncation on CTP parameters calculated by this software and clarify the optimal scan duration to be used with these previously derived thresholds, CTP parameter maps were computed in AIS patients for five scan durations ranging from 40-150s, using the same software and processing procedures as in the previous publication⁵. Median values in ischemic and unaffected tissue were found for each scan duration, and the shortest scan duration that provided volume estimates within $\pm 2\text{mL}$ of the volume from the 150s scan duration was determined for two CBF thresholds.

3.2 Methods

3.2.1 Patients

Inclusion criteria were as follows: a) ischemic stroke symptoms, b) age > 18 years, c) baseline imaging including CTP performed within 12 hours of symptom onset, and before initiation of therapy, and d) follow-up MRI or CT performed at 24 hours to delineate infarct extent. Exclusion criteria were as follows: a) intracranial hemorrhage at baseline CT, b) previous stroke in ipsilateral hemisphere, c) participation in investigational drug or

therapy trial, d) motion in admission CTP not amenable to correction. Retrospective review of consecutive patients from the PROVE-IT database (NCT02184936) identified 65 patients meeting the inclusion and exclusion criteria for the study. The local ethics board approved this retrospective data review study.

3.2.2 Image Acquisition

CT imaging was performed on a 64-slice CT scanner (Lightspeed; General Electric Healthcare, Waukesha, WI). 45mL of contrast material (68% ioversol, Optiray 320; Mallinckrodt Pharmaceuticals, St Louis, Mo) was injected at 4.5mL/s followed by a 40mL saline chaser at 6mL/s. Axial shuttle mode was used to cover an 8cm section of the brain with a 5mm slice thickness. A two-phase scanning protocol was used where scanning started 5s after contrast injection⁵, in the first phase images were acquired every 2.8s for 60s, and in the second phase images were acquired every 15s for 90s. Other acquisition parameters were 80kV, 350mA, standard reconstruction filter, and 23cm display field of view. NCCT or DWI was acquired for final infarct delineation in all patients between 24 and 48h post symptom onset⁵.

3.2.3 CTP Postprocessing

CBV, CBF, and T_{\max} maps were computed using a commercially available delay-insensitive software package (CTP4D, GE Healthcare, Waukesha, WI). The AIF was obtained from a 2x2 voxel ROI in the basilar artery and corrected for partial volume averaging using the VOF, obtained from an ROI in the posterior superior sagittal sinus. In cases where the AIF could not be obtained from the basilar artery it was selected from the contralateral anterior or middle cerebral artery. In-plane patient motion was corrected using automated software (CTP4D, GE Healthcare, Waukesha, WI). Maps of CBF

($\text{mL}\cdot\text{min}^{-1}\cdot 100\text{g}^{-1}$), cerebral blood volume (CBV) ($\text{mL}/100\text{g}$), and T_{max} (seconds) were calculated by deconvolving the partial volume corrected AIF from the tissue time-density curves (TDCs). Dynamic CTP images over the first pass of contrast were averaged to create average maps, which were used as source images for co-registration with follow-up NCCT or DWI. Shorter scan durations were simulated by sequentially deleting frames from the end of the CTP acquisitions to create 40, 60, 90, and 120s versions of each 150s CTP study. For each patient, CBV, CBF, and T_{max} maps were computed for all scan durations. ROIs used to define the arterial input function and venous output function were saved, so that the arterial input function, venous output function, and all other post-processing variables could be kept the same for computing maps from all scan durations.

3.2.4 Image Analysis

Follow-up CT or MR images were co-registered with average images from the admission CTP, details of the registration were published elsewhere¹⁹. ROIs drawn using the follow-up CT/MR images to delineate the infarct, ipsilateral non-infarct (tissue in ipsilateral hemisphere outside infarct ROI), and contralateral tissue⁵, were superimposed onto CBV, CBF, and T_{max} maps from all scan durations. Median CBV, CBF, and T_{max} values from each ROI were found for all scan durations.

For CBF maps from all scan durations for each patient, one infarction threshold for onset to reperfusion time $<4.5\text{h}$ ($\text{CBF}<7 \text{ mL}\cdot\text{min}^{-1}\cdot 100\text{g}^{-1}$) and one infarction threshold for onset to reperfusion time $>4.5\text{-}6\text{h}$ ($7<\text{CBF}<13 \text{ mL}\cdot\text{min}^{-1}\cdot 100\text{g}^{-1}$)⁵ were applied to each 5mm slice, and the total infarct volume quantified by each threshold was calculated.

3.2.5 Statistical Analysis

Statistical analysis was performed in SPSS (IBM SPSS Statistics for Windows, version 20.0, IBM Corporation, Armonk, NY), $p < 0.05$ was considered significant. One-way repeated measures ANOVA was used to assess the effect of scan duration on median CBV, CBF, and T_{\max} values in the infarct, ipsilateral non-infarct, and contralateral ROIs. Mauchly's test was used to test the assumption of sphericity for all one-way repeated measures ANOVAs²⁰. In case of non-sphericity, the degrees of freedom were adjusted using the Greenhouse and Geisser method²¹ to reduce the risk of type I error. Adjusted degrees of freedom were reported in brackets with the F-statistic for all one-way repeated measures ANOVA. If the effect of scan duration was significant, then pairwise paired t-tests with the Bonferroni correction for multiple comparisons were performed²².

Infarct volumes derived by previously mentioned CBF thresholds from the 120, 90, 60, and 40s scans were tested for statistical equivalence with their corresponding volumes from the 150s scan using two one-sided t-test (TOST). In TOST, volumes measured from two different scan durations are equivalent if their difference (Δ) is significantly lower than a predetermined upper equivalence bound (Δ_u), and significantly higher than a predetermined lower equivalence bound (Δ_l)²³⁻²⁵. For this study Δ_l and Δ_u were defined as $\pm 2\text{mL}$, since this corresponded to 10% of the smallest infarct volume threshold used to determine eligibility for endovascular therapy in the DAWN trial (20mL)¹. The optimal scan duration for each threshold was defined as the shortest scan duration where the infarct volume was statistically equivalent, within $\pm 2\text{mL}$, to the infarct volume from the 150s scan in a TOST procedure. Additionally, the number of patients where infarct volume derived by each threshold fluctuated by more than $\pm 2\text{mL}$ relative to that patient's corresponding

infarct volume from the 150s scan was reported for all shortened scan durations. Median CBV, CBF, and T_{\max} values were reported as the average \pm standard error, and average differences in threshold-derived volume between scan durations were reported with their 95% CIs unless indicated otherwise. Error bars on all figures indicate standard error unless stated otherwise in the figure caption.

3.3 Results

3.3.1 Patients

65 patients were included in the study, 46% were male and 54% were female. The average age was 70.0 ± 12.4 (standard deviation) years. 8 patients without infarct on follow-up images were not included in the infarct region analysis, while all patients were included in the ipsilateral non-infarct and contralateral region analysis and TOST of threshold-derived volumes.

3.3.2 Median Parameter Values

3.3.2.1 CBV

Scan duration had a significant effect on median CBV in the infarct ROI ($F_{[2,99]} = 120.1$, $p < 0.001$), ipsilateral non-infarct ROI ($F_{[3,174]} = 85.0$, $p < 0.001$), and contralateral ROI ($F_{[3,159]} = 118.2$, $p < 0.001$). Panel A of Figure 3.2 shows the average median CBV value in the three ROIs for each scan duration, post-hoc paired samples t-tests with the Bonferroni correction showed that for all three ROIs, median CBV was different for all pairwise scan duration comparisons ($p < 0.01$).

Truncation had the greatest effect in the infarct ROI, where decreasing the scan duration to 120, 90, 60, and 40s underestimated median CBV by 0.2 ± 0.04 , 0.7 ± 0.1 , 1.1

± 0.1 , and 1.6 ± 0.1 mL/100g respectively, relative to that from the 150s scan duration. In the ipsilateral non-infarct and contralateral ROIs decreasing the scan duration from 150 to 40s underestimated median CBV by 1.3 ± 0.1 and 1.2 ± 0.1 mL/100g respectively.

3.3.2.2 CBF

The effect of scan duration on median CBF was not significant for the infarct ($F_{[3,155]} = 2.3$, $p = 0.086$), ipsilateral non-infarct ($F_{[3,185]} = 2.4$, $p = 0.075$) or contralateral ($F_{[3,197]} = 0.742$, $p = 0.531$) ROI. Median CBF for each of the three ROIs is plotted against scan duration in Panel B of Figure 3.2.

3.3.2.3 T_{\max}

Median T_{\max} was significantly affected by scan duration in the infarct ($F_{[1,80]} = 108.0$, $p < 0.001$), ipsilateral non-infarct ($F_{[2,110]} = 156.1$, $p < 0.001$), and contralateral ($F_{[2,150]} = 116.5$, $p < 0.001$) ROI. Median T_{\max} from each ROI is plotted against scan duration in Panel C of Figure 3.2. Post-hoc paired t-tests with the Bonferroni correction showed that for all three ROIs, all pairwise comparisons of median T_{\max} from different scan duration were significantly different ($p < 0.001$).

For the infarct ROI, decreasing the scan duration from 150s to 120, 90, 60, and 40s underestimated median T_{\max} value by 1.1 ± 0.2 , 3.2 ± 0.4 , 6.4 ± 0.6 , and 9.8 ± 0.9 s relative to that from the 150s scan duration. For the ipsilateral non-infarct and contralateral ROI, decreasing the scan duration from 150 to 40s underestimated median T_{\max} by 2.5 ± 0.2 and 1.5 ± 0.1 s respectively, relative to that from 150s scan duration.

Figure 3.2: Median CBV, CBF, and T_{max} versus scan duration in infarct, ipsilateral non-infarct, and contralateral ROIs

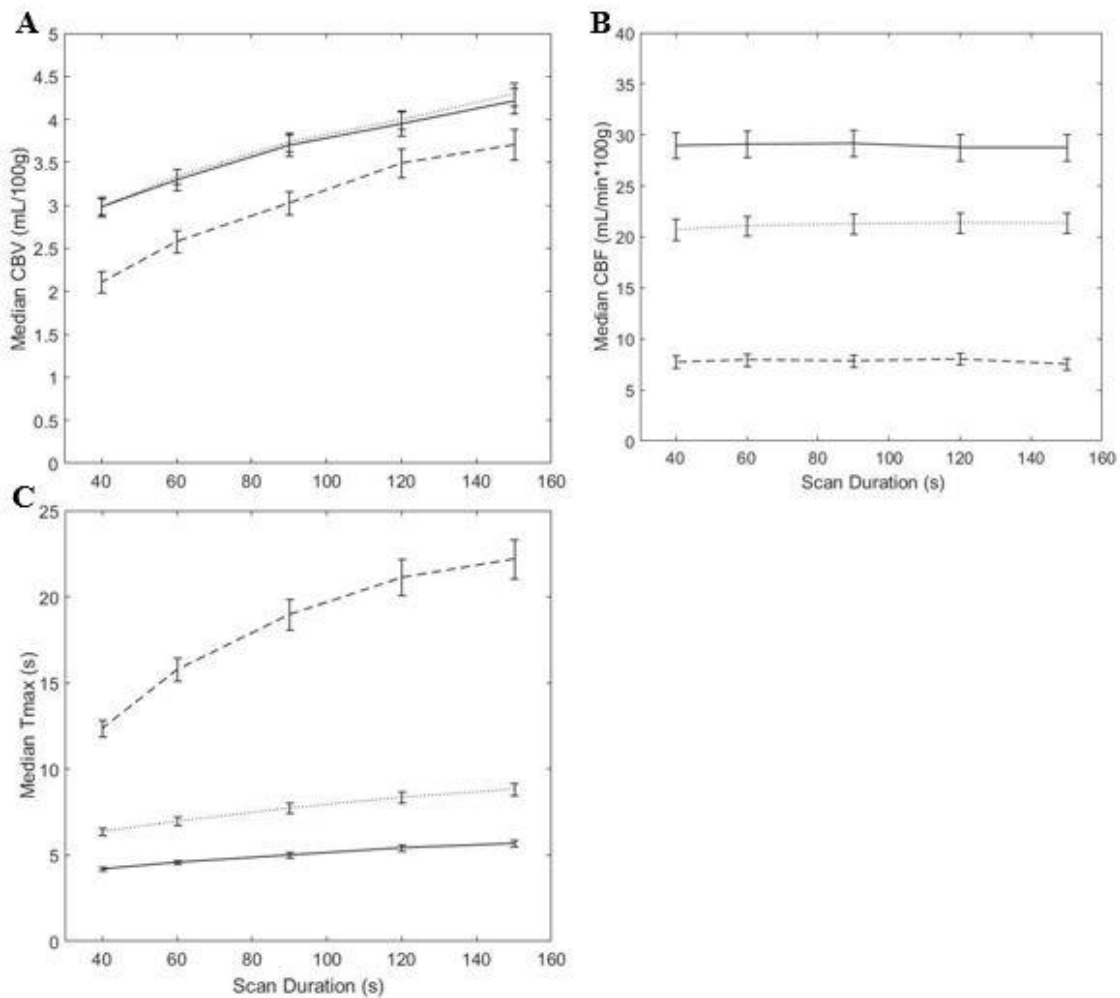


Fig. 3.2: CBV (A), CBF (B), and time-to-maximum (T_{max}) (C) in infarct (dashed), ipsilateral non-infarct (dotted), and contralateral (solid) ROIs at each scan duration. Scan duration had a significant effect on median CBV and T_{max} in all three ROIs ($p < 0.001$) but the effect on median CBF was not significant for any of the ROIs ($p > 0.05$). Error bars represent standard error.

3.3.3 Threshold-derived Infarct Volumes

The volume of infarct core for onset to reperfusion time $<4.5\text{h}$ identified by the $\text{CBF}<7\text{ mL}\cdot\text{min}^{-1}\cdot 100\text{g}^{-1}$ threshold was equivalent to the volume from the 150s scan in TOST for all shorter scan durations ($p<0.001$). The infarct volume for onset to reperfusion time $>4.5\text{-}6\text{h}$ derived by the thresholds $7<\text{CBF}<13\text{ mL}\cdot\text{min}^{-1}\cdot 100\text{g}^{-1}$ was also equivalent to the volume from the 150s scan in TOST for all shorter scan durations ($p<0.01$). For $\text{CBF}<7\text{ mL}\cdot\text{min}^{-1}\cdot 100\text{g}^{-1}$, changing the scan duration from 150s to 120, 90, 60, and 40s decreased infarct volume (mL) by (mean (95% CI)): -0.20 (-0.31 to -0.10), -0.13 (-0.28 to -0.02), -0.28 (-0.46 to -0.11), and -0.61 (-1.00 to -0.22) respectively, and resulted in 0 (0%), 0 (0%), 2 (3%), and 11 (17%) patients where the infarct volume changed by more than $\pm 2\text{mL}$ relative to their value from the 150s scan. When scan duration was decreased from 150s to 120, 90, 60, and 40s the infarct volume (mL) for onset to reperfusion time $>4.5\text{-}6\text{h}$ defined by $7<\text{CBF}<13\text{ mL}\cdot\text{min}^{-1}\cdot 100\text{g}^{-1}$ changed by -0.29 (-0.52 to -0.05), -0.40 (-0.65 to -0.15), -0.69 (-1.10 to -0.27), and -1.31 (-1.83 to -0.78) respectively, and resulted in 3 (5%), 3 (5%), 8 (12%), and 23 (35%) patients where the infarct volume changed by more than $\pm 2\text{mL}$ relative to their value from the 150s scan. Figure 3.3 shows the 95% CIs, and range of infarct volume changes relative to the volume from the 150s duration for both thresholds. Table 3.1 shows the average infarct volume derived by each threshold for all scan durations.

Figure 3.3: Confidence intervals and range of volume differences relative to 150s scan for $CBF < 7 \text{ mL} \cdot \text{min}^{-1} \cdot 100\text{g}^{-1}$ and $7 < CBF < 13 \text{ mL} \cdot \text{min}^{-1} \cdot 100\text{g}^{-1}$

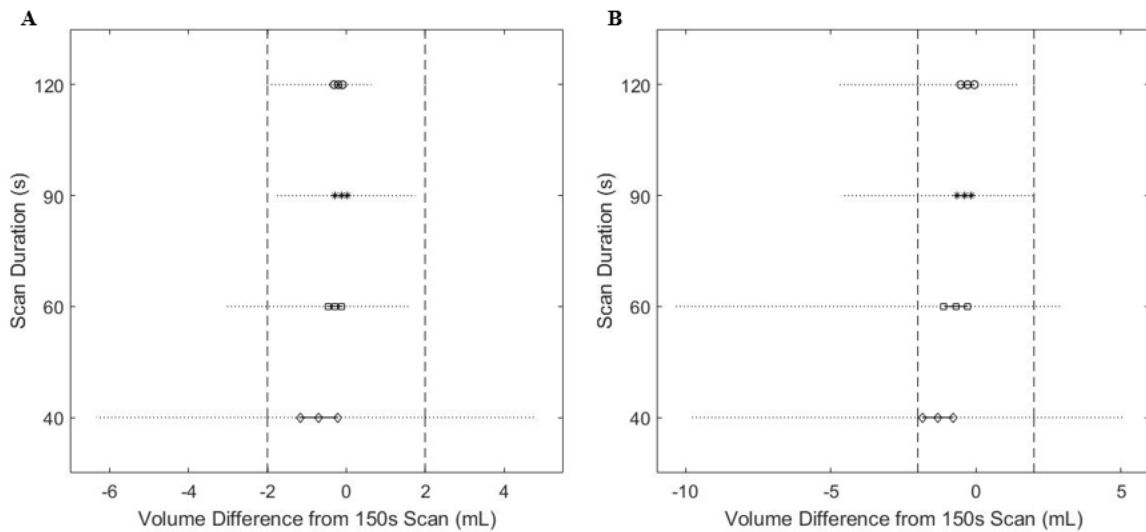


Fig. 3.3: Average and 95% CIs (solid lines with markers), and range (dotted lines) of differences in infarct volume relative to the 150s scan for $CBF < 7 \text{ mL} \cdot \text{min}^{-1} \cdot 100\text{g}^{-1}$ (A) and $CBF < 13 \text{ mL} \cdot \text{min}^{-1} \cdot 100\text{g}^{-1}$ (B). Scan durations of 120, 90, 60, and 40s indicated by circles, stars, squares, and diamonds respectively, and vertical dashed lines represent the equivalence boundaries for the two-one-sided t-test procedures ($\pm 2\text{mL}$). The volumes derived by $CBF < 7 \text{ mL} \cdot \text{min}^{-1} \cdot 100\text{g}^{-1}$ ($p < 0.001$) and $CBF < 13 \text{ mL} \cdot \text{min}^{-1} \cdot 100\text{g}^{-1}$ ($p < 0.01$) were equivalent to the 150s scan within $\pm 2\text{mL}$ for all shorter scan durations.

Table 3.1: Average \pm S.E. tissue volumes specified by CBF thresholds

Threshold	Infarct Volume at Each Scan Duration				
	150s	120s	90s	60s	40s
CBF < 7 mL·min ⁻¹ ·100g ⁻¹	17.01 \pm	16.81 \pm	16.88 \pm	16.73 \pm	16.41 \pm
	1.91	1.92*	1.92*	1.91*	1.91*
7 < CBF < 13 mL·min ⁻¹ ·100g ⁻¹	37.06 \pm	36.77 \pm	36.66 \pm	36.37 \pm	35.75 \pm
	2.52	2.52*	2.53*	2.55*	2.55*

Table 3.1: Average infarct volumes for onset to reperfusion time <4.5h (cerebral blood flow (CBF) < 7 mL·min⁻¹·100g⁻¹), and onset to reperfusion time >4.5-6h (7 < CBF < 13 mL·min⁻¹·100g⁻¹) for each scan duration. Volumes that were statistically equivalent (p < 0.01), within \pm 2mL, as evaluated by two-one-sided tests, to the corresponding volume measured from the 150s scan duration are indicated by an asterisk (*).

3.4 Discussion

CTP is used in AIS to estimate the volume of infarct core and salvageable tissue at admission to the hospital by applying thresholds to parameter maps, however the optimal duration of CTP scans for AIS applications is not yet clear. The results of this study show that CBV and T_{\max} calculated by GE Healthcare's CTP4D software are dependent on scan duration, whereas CBF calculations by this software, and therefore infarct volumes quantified by previously derived CBF thresholds⁵, are independent of scan duration. Truncation effects on median CBV and T_{\max} were most severe in the infarct ROI due to delayed bolus arrival and slow contrast washout^{12,13}, but significant truncation effects were also seen in the ipsilateral-salvaged and contralateral ROIs. This agrees with results from prior studies which found that truncation artifacts result in underestimated CBV in PWI¹⁵ and CTP scans¹⁶, and by extension, overestimated infarct volumes when CBV thresholds are applied. Contrastingly, median CBF changed by only 1.4-6.5% of values from the 150s scan, and similarly, time-dependent infarct volumes for onset to reperfusion time <4.5h and >4.5-6h derived using CBF thresholds from scan durations ranging from 40 to 120s were all equivalent to the volumes derived from the 150s scan in TOST procedures, within $\pm 2\text{mL}$ ($p < 0.025$). This means that when CBF thresholds are used to define the infarct core, scan duration can be reduced to 40s without affecting treatment decisions made based on infarct volume. For the 2-phase CTP protocol used in this study, this would remove the entire 2nd phase and one-third of the 1st phase of the scan, or 13 out of 27 total time points. This would have decreased radiation dose by ~48%, from ~5mSv²⁶ to ~2.6mSv.

These results agree with prior CTP¹⁷ and PWI¹² studies using deconvolution based on standard singular value decomposition, oscillation-index regulated singular value

decomposition¹², and circular singular value decomposition¹⁷. These studies which found CBF lesion volumes were independent of scan duration within the clinically relevant range of scan durations (>40s)¹⁷, and that reversal of CBF lesions occurred in only ~3% of cases when scan duration was decreased from 110 to 40s¹². Although these studies established the effect of truncation on CTP parameters and threshold-derived volumes, optimal minimum scan durations that result in stable infarct/penumbra volume estimates were not reported. A prior study by Kasasbeh et al, which used a research version of RAPID (RAPID, iSchemaView, Menlo Park, CA), proposed calculating personalized minimum scan durations depending on the arrival time and width of a patient's venous output function¹⁸. However, the shape of the venous output function is determined by venous drainage of contrast from both ischemic and normal tissue. This could be an issue when determining the optimal scan duration for AIS patients since it is likely that the arrival time and width of the venous output function is not representative of the wash-in and washout of contrast from ischemic tissue. Furthermore, calculating the patient's optimal CTP scan duration based on venous output function shape requires an additional pre-scan with a bolus injection of contrast to measure the venous output function. This extra radiation dose is counter-productive to using a shortened scan duration to limit radiation dose. In addition to personalized scan durations, this study also recommended a population-based optimal CTP scan duration of 70s, since infarct (relative CBF<30%) and penumbra ($T_{max}>6s$) volumes quantified with RAPID (iSchemaView, Menlo Park, CA) from a 70s scan remained within $\pm 10\%$ of their respective volumes from a 90s scan¹⁸. The results of this study suggest that if CTP4D (GE Healthcare, Waukesha, WI) is used for map computation, and previously derived time-dependent CBF thresholds are used to determine tissue

viability, then scan duration can be decreased to 40s, further reducing radiation dose, without affecting tissue volumes by more than an average of $\pm 2\text{mL}$.

Relatively conservative equivalence bounds of $\pm 2\text{mL}$ were chosen for TOST in this study because they were equal to 10% of the smallest CTP-derived infarct volume used to determine eligibility for endovascular therapy in the DAWN trial¹. In addition to performing TOST we also reported the number of patients where infarct volumes determined by each threshold changed by more than $\pm 2\text{mL}$ relative to the 150s for each scan duration. Although infarct volumes derived from 40s scans by the thresholds $\text{CBF} < 7$ and $13 \text{ mL}\cdot\text{min}^{-1}\cdot 100\text{g}^{-1}$ were equivalent to the 150s scan by TOST, there were 11 (17%) and 23 (35%) patients respectively where the infarct volume derived by each threshold changed by more than $\pm 2\text{mL}$ relative to the 150s scan, however only 2 (3%) and 4 (6%) patients experienced a change of greater than 4mL. Therefore, shortening scan duration to 40s may cause small infarct volume fluctuations in up to 35% of patients, but these fluctuations are smaller than 4mL in most cases, and the average infarct volume change is less than $\pm 2\text{mL}$.

Under- or over-estimation of the infarct or penumbra volume due to truncation is problematic when mismatch criteria are used to determine treatment eligibility for AIS patients. Penumbra volumes¹ quantified by $T_{\text{max}} > 6\text{s}$ could be underestimated at short scan durations due to truncation, causing patients to be misclassified as ineligible for endovascular therapy due to lack of salvageable tissue when they may have still benefited from reperfusion. Similarly, infarct volumes²⁷ determined by $\text{CBV} < 2\text{mL}/100\text{g}$ may be overestimated with short scan durations, resulting in patients being incorrectly classified as ineligible for endovascular therapy. Our results indicate that AIS triaging will not be

affected by truncation artifacts for scan durations longer than 40s if maps are computed with GE Healthcare's CTP4D (CTP4D, GE Healthcare, Waukesha, WI) and previously derived time-dependent CBF thresholds for infarction⁵ are used to define tissue viability.

CBF is determined by the upslope of the tissue time-density curve²⁸, so unless truncation affects this upslope, CBF is estimated relatively error free. Based on conservation of mass, CBV can be calculated as the area under the tissue time-density curve divided by the area under the arterial input function²⁹. With truncation, the area under the time-density curve of ischemic tissue with delayed contrast wash-in and washout decreases more rapidly than the area under the arterial input function resulting in underestimated CBV. MTT is equal to the CBV divided by CBF, as required by the Central Volume Principle³⁰, therefore MTT also decreases with shorter scan durations. This also applies to T_{\max} , since the software used in this study calculates T_{\max} as T_0 plus half the MTT⁵. These theoretical considerations explain why CBV and T_{\max} were affected by truncation artifacts while CBF was not. It also explains why the limited truncation effect on CBF observed in this study was similar to what was seen in studies using other deconvolution software packages^{10,12}, since CBF is dependent on the upslope of the tissue time-density curve, regardless of what software is used to produce maps.

This study had several limitations. As mentioned before, CTP maps vary depending on the software used to compute them³¹, therefore optimal scan durations from this study may not be directly applicable to other software packages. However, we expect the general conclusion that CBF is relatively independent of scan duration, would remain the same since it is calculated based on the upslope of the tissue time-density curve regardless of software. CTP was acquired using a 2-phase protocol where images were

acquired once every 15s in the second phase, this made it impossible to investigate scan durations in between time points in the second phase. Analysis was also limited only to scan durations longer than 40s since this is the shortest scan duration used clinically for brain CTP. Lastly, this was a retrospective study with a relatively small group of patients. The results of this study should be confirmed in a prospectively designed study with a larger group of patients.

3.5 Conclusion

CBF remains constant and infarct volumes estimated using previously derived⁵ CBF thresholds are equivalent within $\pm 2\text{mL}$ for scan durations ranging from 40 to 150s, whereas CBV and T_{max} decrease at shorter scan durations due to truncation errors. If these CBF thresholds are used to determine treatment eligibility, then scan duration can be decreased to 40s to reduce radiation dose to AIS patients by ~48% without triaging being affected by truncation artifacts.

3.6 References

1. Nogueira RG, Jadhav AP, Haussen DC, et al. Thrombectomy 6 to 24 hours after stroke with a mismatch between deficit and infarct. *N Engl J Med* 2018;378:11-21.
2. Albers GW, Marks MP, Kemp S, et al. Thrombectomy for stroke at 6 to 16 hours with selection by perfusion imaging. *N Engl J Med* 2018;378:708-718.
3. Nabavi DG, Cenic A, Henderson S, et al. Perfusion mapping using computed tomography allows accurate prediction of cerebral infarction in experimental brain ischemia. *Stroke* 2001;32:175-183.
4. Campbell BC, Yassi N, Ma H, et al. Imaging selection in ischemic stroke: feasibility of automated CT-perfusion analysis. *Int J Stroke* 2015;10:51-54.

5. d'Este CD, Boesen ME, Ahn SH, et al. Time-dependent computed tomographic perfusion thresholds for patients with acute ischemic stroke. *Stroke* 2015;46:3390-3397.
6. Campbell BC, Christensen S, Levi CR, et al. Comparison of computed tomography perfusion and magnetic resonance imaging perfusion-diffusion mismatch in ischemic stroke. *Stroke* 2012;43:2648-2653.
7. Schaefer PW, Barak ER, Kamalian S, et al. Quantitative assessment of core/penumbra mismatch in acute stroke: CT and MR perfusion imaging are strongly correlated when sufficient brain volume is imaged. *Stroke* 2008;39:2986-2992.
8. Campbell BC, Mitchell PJ, Kleinig TJ, et al. Endovascular therapy for ischemic stroke with perfusion-imaging selection. *N Engl J Med* 2015;372:1009-1018.
9. Saver JL, Goyal M, Bonafe A, et al. Stent-retriever thrombectomy after intravenous t-PA vs. t-PA alone in stroke. *N Engl J Med* 2015;372:2285-2295.
10. Borst J, Marquering HA, Beenen LF, et al. Effect of extended CT perfusion acquisition time on ischemic core and penumbra volume estimation in patients with acute ischemic stroke due to large vessel occlusion. *PLoS One* 2015;10:e0119409.
11. Wintermark M, Albers GW, Alexandrov AV, et al. Acute stroke imaging research roadmap. *AJNR Am J Neuroradiol* 2008;29:e23-30.
12. Copen WA, Deipolyi AR, Schaefer PW, et al. Exposing hidden truncation-related errors in acute stroke perfusion imaging. *AJNR Am J Neuroradiol* 2015;36:638-645.

13. Carrera E, Jones PS, Iglesias S, et al. The vascular mean transit time: a surrogate for the penumbra flow threshold? *J Cereb Blood Flow Metab* 2011;31:1027-1035.
14. d'Esterre CD, Roversi G, Padroni M, et al. CT perfusion cerebral blood volume does not always predict infarct core in acute ischemic stroke. *Neurol Sci* 2015;36:1777-1783.
15. Deipolyi AR, Wu O, Macklin EA, et al. Reliability of cerebral blood volume maps as a substitute for diffusion-weighted imaging in acute ischemic stroke. *J Magn Reson Imaging* 2012;36:1083-1087.
16. d'Esterre CD, Aviv RI, Lee TY. The evolution of the cerebral blood volume abnormality in patients with ischemic stroke: a CT perfusion study. *Acta Radiol* 2012;53:461-467.
17. Mikkelsen IK, Jones PS, Ribe LR, et al. Biased visualization of hypoperfused tissue by computed tomography due to short imaging duration: improved classification by image down-sampling and vascular models. *Eur Radiol* 2015;25:2080-2088.
18. Kasasbeh AS, Christensen S, Straka M, et al. Optimal computed tomographic perfusion scan duration for assessment of acute stroke lesion volumes. *Stroke* 2016;47:2966-2971.
19. Studholme C, Hill DL, Hawkes DJ. Automated 3-D registration of MR and CT images of the head. *Med Image Anal* 1996;1:163-175.
20. Mauchly JW. Significance test for sphericity of a normal n-vare distribution. *Ann Math Stat* 1940;11:204-209.

21. Greenhouse SW, Geisser S. On methods in the analysis of profile data. *Psychometrika* 1959;24:95-112.
22. Dunn OJ. Multiple comparisons among means. *J Am Stat Assoc* 1961;56:52-64.
23. Ahn S, Park SH, Lee KH. How to demonstrate similarity by using noninferiority and equivalence statistical testing in radiology research. *Radiology* 2013;267:328-338.
24. Jones B, Jarvis P, Lewis JA, et al. Trials to assess equivalence: the importance of rigorous methods. *BMJ* 1996;313:36-39.
25. Lakens D. Equivalence tests: a practical primer for t tests, correlations, and meta-analyses. *Soc Psychol Personal Sci* 2017;8:355-362.
26. Mnyusiwalla A, Aviv R, Symons S. Radiation dose from multidetector row CT imaging for acute stroke. *Neuroradiology* 2009;51:635-640.
27. Wintermark M, Flanders AE, Velthuis B, et al. Perfusion-CT assessment of infarct core and penumbra: receiver operating characteristic curve analysis in 130 patients suspected of acute hemispheric stroke. *Stroke* 2006;37:979-985.
28. Konstas AA, Goldmakher GV, Lee TY, et al. Theoretic basis and technical implementations of CT perfusion in acute ischemic stroke, part 1: theoretic basis. *AJNR Am J Neuroradiol* 2009;30:662-668.
29. Axel L. Cerebral blood flow determination by rapid-sequence computed tomography: theoretical analysis. *Radiology* 1980;137:679-686.
30. Lee TY. Functional CT: physiological models. *Trends Biotechnol* 2002;20:S3-S10.

31. Kudo K, Sasaki M, Yamada K, et al. Differences in CT perfusion maps generated by different commercial software: quantitative analysis by using identical source data of acute stroke patients. *Radiology* 2010;254:200-209.

Chapter 4

4 Reperfusion Assessed by CT Perfusion is a More Specific and Accurate Predictor of Functional Outcome than Modified Thrombolysis in Cerebral Infarction Score in Ischemic Stroke Patients Treated with Intra-Arterial Therapy

4.1 Introduction

IAT has become the standard of care for acute ischemic stroke patients with large vessel occlusion after multiple clinical trials demonstrated superior efficacy compared to thrombolysis alone¹⁻⁶. More recently, results from the DEFUSE-3 and DAWN trials have shown that IAT performed in patients selected by perfusion imaging within 16h⁷ and 24h⁸ post symptom onset is superior to medical management alone. One secondary outcome of these trials was a mTICI score of 2b or 3 on post-procedural DSA, representing reperfusion of 50-99% and 100% of the affected vascular territory respectively⁹. Although mTICI 2b/3 is a commonly accepted criterion for good reperfusion, ~15-20% of patients in the treatment arm of earlier trials²⁻⁶ had a poor 90-day functional outcome (90-day mRS>2) despite post-procedural mTICI scores of 2b/3; this number increased to ~30-35% in the DEFUSE-3 and DAWN trials^{7,8}. There is a need to better measure poor reperfusion after IAT, to allow other treatment to be instituted as soon as possible. A more quantitative, less subjective alternative to the mTICI score could be the percentage change in ischemic volume from admission to shortly after IAT, calculated by applying thresholds for ischemia¹⁰ to CTP maps obtained at admission and post-IAT¹¹. Prior studies have shown that post-procedural mTICI scores were independently associated with functional outcome¹²⁻¹⁴, and improved outcome prediction accuracy¹⁵. However, relatively few

studies have directly compared reperfusion assessed by follow-up CTP to post-procedural mTICI scores as measures of post-IAT reperfusion, and as prognosticators of outcome after IAT.

The objectives for this study were therefore: 1) to compare mTICI scores and a CTP-based reperfusion metric and 2) to determine which of these two measures of reperfusion was better associated with 90-day functional outcome. We hypothesized that the CTP-based reperfusion metric would have a stronger association with 90-day functional outcome than mTICI scores.

4.2 Methods

4.2.1 Patient Selection

The institutional review board approved this study and informed consent was obtained from each patient contributing data to the study. Eligible patients were ischemic stroke patients treated by IAT, received non-contrast CT, CT Angiography, and CTP at hospital admission, and follow-up CTP approximately 24 hours post symptom onset, functional evaluation 90-days post onset with mRS, and a complete record of demographic, clinical and imaging variables, including mTICI score from post-procedural DSA. Retrospective review of consecutive acute ischemic stroke patients admitted to the Neuroscience Department of Azienda Ospedaliero-Universitaria di Ferrara (Italy) from June 2008 to September 2015 identified 118 IAT-treated patients. Patients without onset CTP (n=2), 24h CTP (n=11), 90-day mRS evaluation (n=2), or those with motion in either onset or 24h CTP that was not amenable to correction with in-plane rigid registration (n=7) were excluded, leaving 96 patients for the final patient cohort (Figure 4.1).

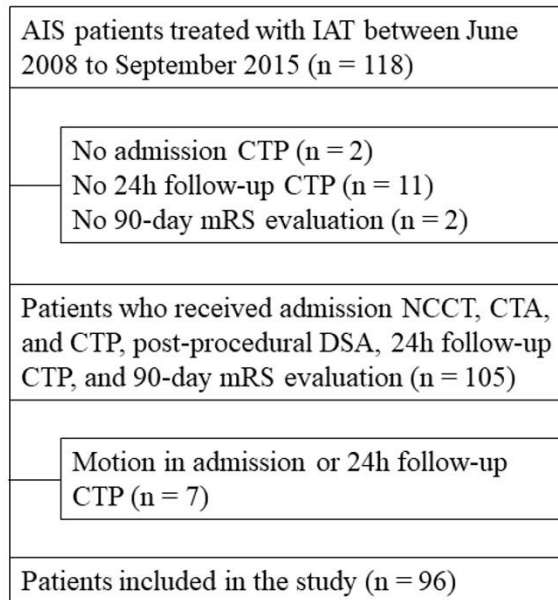
Figure 4.1: Patient exclusion flow chart

Fig. 4.1: Flow diagram that highlights exclusions of patients after retrospective review of all acute ischemic stroke (AIS) patients treated with intra-arterial therapy (IAT) between June 2008 and September 2015. CTA indicates CT Angiography; CTP, CT Perfusion; DSA, digital subtraction angiography; mRS, modified Rankin Scale; NCCT, non-contrast CT.

4.2.2 Imaging Protocol

Patients underwent non-contrast CT, CT angiography, and CTP at admission, DSA after the IAT procedure concluded, and follow-up CTP at ~24h post admission (median (IQR) = 25 (22-28) hours). All CT imaging were performed on a Lightspeed VCT scanner (GE Healthcare, Waukesha, WI). Non-contrast CT and CT angiography imaging protocols have been described previously¹⁶. Briefly, helical NCCT scans covered from the skull base to the vertex with the following parameters: 120kV, 340mA, 4 x 5 collimation, 1s rotation time, and table speed of 15mm/rotation¹⁶. CTA covering from the carotid bifurcation to the vertex were acquired with the following parameters: 0.7mL/kg contrast (up to a maximum of 90mL) injected at 4mL/s, 5-10s delay from injection to start of scanning, 120kV, 270mA, 1s rotation time, 1.25mm thick slices, and table speed of 3.75mm/rotation¹⁶. CTP scanning was initiated 5s after 40mL of CT contrast agent was power-injected at 4mL/s into an antecubital vein. Most patients (n = 65) were scanned using a 2-phase protocol without axial shuttle mode; volume (4cm coverage) acquired every 0.5s for 50s in first phase, and every 15s for 150s in second phase, 80kV, 100mAs, 5mm slice thickness. Fifteen patients (n = 15) were scanned using a 2-phase protocol with axial shuttle mode; volume (8cm coverage) acquired every 2.8s for 60s in first phase, and every 15s for 135s in second phase, 80kV, 140mAs, 5mm slice thickness. Sixteen patients (n = 16) were scanned with a 1-phase protocol without shuttle mode; volume (4cm coverage) acquired every 0.5s for 50s, 80kV, 100mAs, 5mm slice thickness. All CTP source images were reconstructed with the standard filter and DFOV of 25cm.

4.2.3 Image Analysis

Admission CT angiography were reviewed by two neuroradiologists (AB and EF; 5 and 20 years of experience respectively) and assigned rLMC scores, clot burden scores, and pre-treatment mTICI scores. Post-procedural mTICI scores were assessed on DSA. The rLMC score has been described previously¹⁷; the degree of contrast opacification of cerebral blood vessels is assessed in the six ASPECTS cortical regions, parasagittal anterior cerebral artery territory, and basal ganglia and assigned a score of 0 (artery is not visible), 1 (artery is less prominent compared to contralateral side), or 2 (artery is equal or more prominent compared to contralateral side) is assigned to each region. Scores can range from 0-20, with increasing rLMC score indicating better collateral circulation status. The clot burden score has also been described previously¹⁸; starting from a 10-point scale, 2 points were subtracted for lack of contrast opacification across the full cross-section in any part of the supraclinoid ICA, proximal M1 segment, and distal M1 segment, and 1 point was subtracted for each M2 branch, A1 segment and infraclinoid ICA. Clot burden scores range from 0-10, with decreasing scores indicating greater thrombus extent.

CBV, CBF, and T_{\max} maps for admission and follow-up CTP studies were computed by one author (EW; 5 years of experience) using commercially available delay-insensitive perfusion software (CTP4D, GE Healthcare, Waukesha, WI). In-plane patient motion was corrected using an automated registration program included in the perfusion software. The AIF and VOF were measured from regions of interest (ROIs) in the basilar artery, and superior sagittal sinus respectively. If the AIF could not be measured from the basilar artery, it was measured from an ROI in the contralateral anterior cerebral artery or middle cerebral artery. The VOF was used to correct for partial volume averaging in the

AIF, then CBF ($\text{mL}\cdot\text{min}^{-1}\cdot 100\text{g}^{-1}$), CBV ($\text{mL}/100\text{g}$), and T_{max} (seconds) maps were computed by deconvolving the AIF from tissue TDCs. Dynamic images from the first pass of contrast were averaged to create average maps, which were used to exclude cerebrospinal fluid and skull using HU thresholds.

An ROI was drawn on the average image covering the ipsilateral hemisphere (excluding ventricles and old infarct, if present), this ROI was superimposed onto cerebral blood flow, cerebral blood volume, and time-to-maximum maps. Blood vessel pixels were removed by applying thresholds to cerebral blood flow ($>100 \text{ mL}\cdot\text{min}^{-1}\cdot 100\text{g}^{-1}$), cerebral blood volume ($>8\text{mL}/100\text{g}$) maps, and any remaining cerebrospinal fluid or skull was removed by applying thresholds to the average image. Ischemic tissue volume was then quantified using the threshold time-to-maximum $>10\text{s}$ (derived in a previous study)¹⁰. This process was repeated for admission and follow-up CTP studies to acquire admission (V_{adm}), and 24h ischemic tissue volumes ($V_{24\text{h}}$) for all patients. To quantify tissue reperfusion measured by CTP, the reperfusion score (S_{CTP}) was defined as the percentage change in ischemic volume from admission to 24h follow-up¹¹.

$$[1] \quad S_{\text{CTP}} = \frac{V_{\text{adm}} - V_{24\text{h}}}{V_{\text{adm}}} \cdot 100\%$$

The maximum value of the reperfusion score was 100% ($V_{24\text{h}} = 0\text{mL}$), a reperfusion score of 0% corresponds to no reperfusion between admission and 24h ($V_{\text{adm}} = V_{24\text{h}}$), and a negative reperfusion score indicates the ischemic tissue volume increased between onset and 24h ($V_{24\text{h}} > V_{\text{adm}}$).

4.2.4 Statistical Analysis

4.2.4.1 Comparison of mTICI Scores to S_{CTP}

Ordinal regression of post-procedural mTICI scores on S_{CTP} was performed to assess the association between reperfusion predicted by post-procedural mTICI scores and reperfusion seen on follow-up CTP. One-way ANOVA and post-hoc t-tests with the Bonferroni correction¹⁹ were used to compare the mean S_{CTP} at different levels of post-procedural mTICI score. A one-sample t-test was also performed to determine if the mean S_{CTP} from mTICI 3 patients was significantly less than 100%, since mTICI 3 is meant to indicate reperfusion of 100% of the affected vascular territory⁹.

4.2.4.2 Comparison of mTICI Scores and S_{CTP} for Predicting Functional Outcome

S_{CTP} and other variables were compared between patients with good (mRS \leq 2) and poor (mRS $>$ 2) outcomes using either independent samples t-test (continuous variable), or Mann-Whitney U test (categorical variable). Variables that were significantly different between good and poor outcome groups were included in a logistic regression model for predicting outcome with backwards, stepwise elimination of variables. Removal of variables was based on the significance of the Wald statistic; the cut-off value for variable removal was $p > 0.05$.

ROC analysis was then performed to compare S_{CTP} and the mTICI score in ability to determine good outcome at 90 days. AUC was compared using methods described by Hanley and McNeil²⁰. Optimal thresholds for separating patients with good and poor outcomes were defined using Youden's J statistic²¹. The corresponding sensitivity, specificity, accuracy, PPV, and NPV of these optimal thresholds were determined.

Statistical analysis was performed in SPSS version 20 (IBM Corporation, Armonk, NJ), $p < 0.05$ was considered significant. Values were reported as mean \pm SE unless indicated otherwise, error bars on figures are SE unless indicated otherwise in the figure caption.

4.3 Results

4.3.1 Comparison of mTICI Scores to S_{CTP}

Out of the 96 patients included, 48% (46/96) were female (mean age (\pm SD) =70 \pm 11y) and 52% (50/96) were male (mean age (\pm SD) =69 \pm 11y). The most common TOAST stroke subtype was cardioembolic (50/96), followed by atherothrombotic (36/96), undetermined (8/96), and other (dissection) (2/96). Of the 96 patients, 32% (31/96) received intravenous tissue plasminogen activator (IV-tPA). The number of patients with post-procedural mTICI scores of 0, 1, 2a, 2b, and 3 were 17, 6, 5, 19, and 49 respectively.

The association between post-procedural mTICI score and S_{CTP} was significant in the ordinal logistic regression, but only 36% of the variation in S_{CTP} was explained by the post-procedural mTICI score (Nagelkerke $R^2=0.36$, $p < 0.001$). S_{CTP} in patients with mTICI scores of 2b (72.8 \pm 6.5%) and 3 (82.6 \pm 2.7) was significantly higher than in patients with mTICI scores of 0 (27.0 \pm 12.2%) ($p < 0.001$ for both mTICI 2b and 3) and 1 (16.7 \pm 6.8%) ($p \leq 0.001$ and $p < 0.001$ for mTICI 2b and 3 respectively) in post-hoc t-tests with the Bonferroni correction. However, S_{CTP} in patients with mTICI scores of 2a (67.7 \pm 10.9%), 2b, and 3 were not significantly different from each other ($p=1.00$ for all pairwise comparisons) (Figure 4.2). S_{CTP} in mTICI 3 patients (82.6 \pm 2.7%) was also significantly lower than the expected value of 100% ($p < 0.001$).

Figure 4.2: Mean S_{CTP} at each level of post-procedural mTICI score

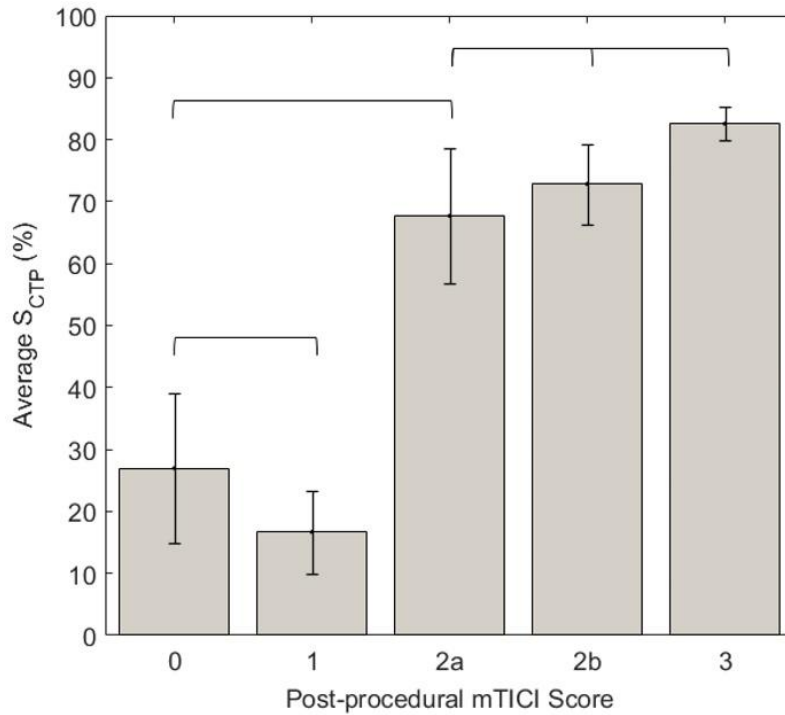


Fig. 4.2: Mean \pm standard error reperfusion score (S_{CTP}) at each level of the modified thrombolysis in cerebral infarction (mTICI) score. Square brackets indicate lack of significance ($p > 0.05$) difference in S_{CTP} between 2 or more levels of post-procedural mTICI score.

Interestingly, 26% (6/23) of patients with post-procedural mTICI \leq 1 had S_{CTP}>50%, even though mTICI scores of 0 and 1 are meant to indicate no reperfusion, with no flow past the occlusion site and limited flow past the occlusion site respectively⁹. These patients had S_{CTP} ranging from 50.8-100% with an average of 84.0 \pm 8.3%, 4 of the 6 patients had good 90-day functional outcomes. 18% (9/49) of patients with post-procedural mTICI scores of 3 had S_{CTP}<67%, despite mTICI 3 being defined as full reperfusion without any flow defects⁹. These patients had S_{CTP} ranging from 18.5-66.7% with an average of 50.0 \pm 6.0%, 6 of the 9 patients had poor 90-day functional outcomes (Figure 4.3).

Figure 4.3: Ischemic lesion on 24h follow-up T_{max} map for patient with post-procedural mTICI score of 3

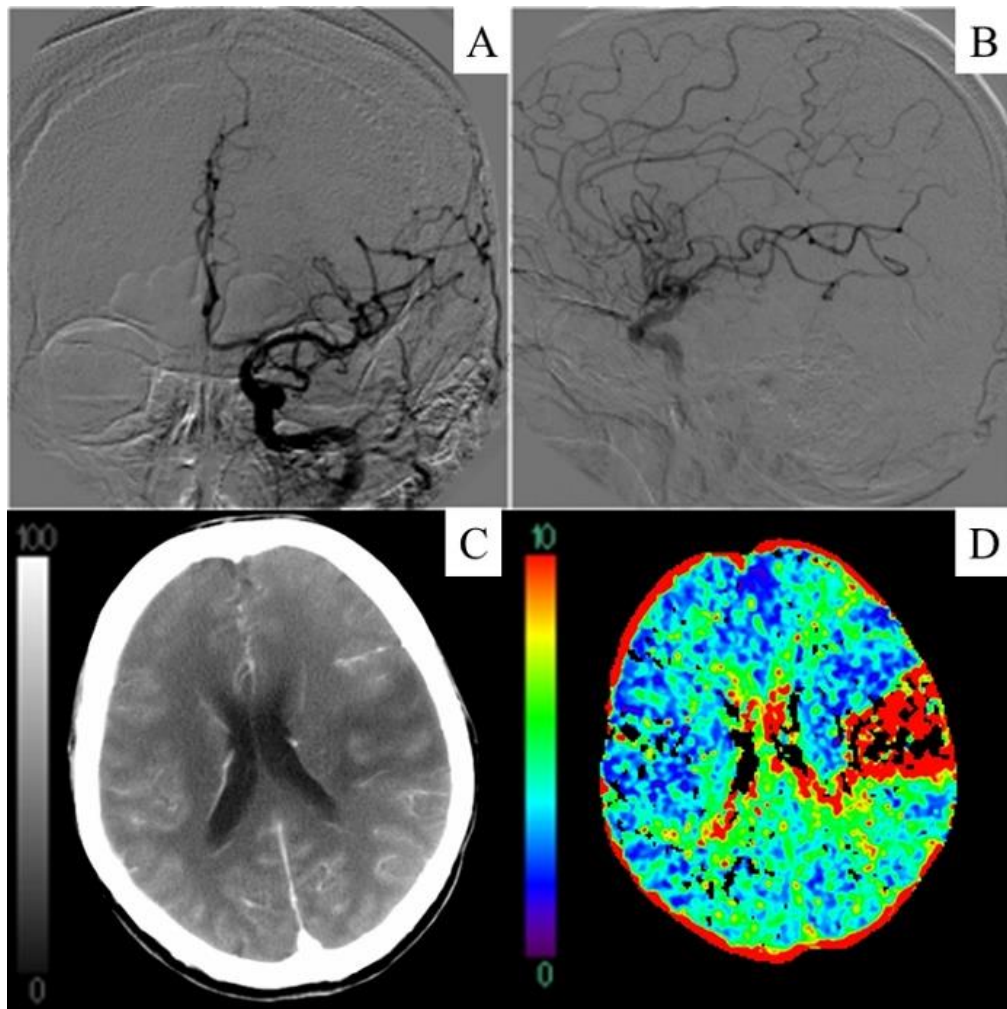


Fig. 4.3: An example of the discrepancy between modified thrombolysis in cerebral ischemia (mTICI) 3 and reperfusion score (S_{CTP}) assessed on pre-treatment and 24h follow-up CT Perfusion (CTP). A-B) Frontal (A) and sagittal (B) views from the post-procedural digital subtraction angiography (DSA) which was scored mTICI 3. C-D) Average image (C) and time-to-maximum (T_{max}) map (D) from 24h follow-up CTP showing a large ischemic ($T_{max}>10s$) lesion in the left MCA territory, S_{CTP} for this patient was 18.5%.

4.3.2 Comparison of mTICI Scores to S_{CTP} for Predicting Functional Outcome

Demographic, clinical, and imaging characteristics of the patients included in the study are summarized in Table 4.1. The median admission rLMC scores ($p<0.05$), and post-procedural mTICI scores ($p<0.05$) were higher for the good outcome group than the poor outcome group, and the median admission NIHSS score ($p<0.001$) was lower in the good outcome group than the poor outcome group. Onset to admission CT time was unknown in 21 patients, among the other 75 patients, the mean onset to CT, and onset to end IAT procedure times were not significantly different between good and poor outcome groups. Average S_{CTP} in the good and poor outcome groups were 82.3 ± 3.3 and $51.5\pm 5.8\%$ ($p<0.001$) respectively, and Average V_{24h} in good and poor outcome groups were 14.9 ± 3.2 and $37.7\pm 5.1\text{mL}$ ($p<0.001$) respectively.

Table 4.1: Demographic, clinical and imaging characteristics of the 96 patients included in the study

Variable	Good Outcome (mRS \leq 2)	Poor Outcome (mRS $>$ 2)	<i>p</i>
Number of patients [n (% of total)]	45 (47)	51 (53)	NA
Age (y) [mean (SD)]	67.8 (11)	71.2 (11)	0.133
Sex [n (% female)]	25 (55.6)	21 (41.2)	0.162
Admission NIHSS score [median (IQR)]	13* (11-18)	20* (16-24)	<0.001
Admission rLMC score [median (IQR)]	14* (10-16)	11* (7-14)	0.010
Clot burden score [median (IQR)]	6 (4-7)	6 (3-7)	0.583
Admission mTICI score [median (IQR)]	1 (0-2)	0 (0-1)	0.094
V _{adm} (mL) [mean (SE)]	84.0 (6.1)	82.2 (6.2)	0.834
V _{24h} (mL) [mean (SE)]	14.9* (3.2)	37.7* (5.1)	<0.001
S _{CTP} (%) [mean (SE)]	82.3* (3.3)	51.5* (5.8)	<0.001
Post-procedural mTICI score [median (IQR)]	4* (3-4)	3* (1-4)	0.031
IV-tPA administration [n (% receiving IV-tPA)]	18 (40.0)	13 (25.5)	0.283
Symptom onset to admission CT time (min) [mean (SE)]	155.8 \downarrow (14.4)	146.2 \downarrow (11.3)	0.647
Admission CT to end procedure time (min) [mean (SE)]	168.2 (11.2)	201.1 (12.3)	0.051
Symptom onset to end procedure time (min) [mean (SE)]	333.8 \downarrow (17.6)	347.9 \downarrow (16.5)	0.561

Table 4.1: Demographic, clinical, and imaging characteristics of the patients in the good (n=45), and poor (n=51) outcome groups. CT indicates computed tomography; IQR, interquartile range; IV-tPA, intravenous tissue plasminogen activator; min, minutes; mRS,

modified Rankin Scale; mTICI, modified thrombolysis in cerebral infarction; n, number; NIHSS, National Institute of Health Stroke Scale; p, p-value from independent samples t-test (parametric variables) or Mann-Whitney U test (non-parametric variables); rLMC, regional leptomeningeal collateral; S_{CTP}, reperfusion score; SD, standard deviation; SE, standard error; V_{24h}, 24h ischemic tissue volume; V_{adm}, admission ischemic tissue volume; y, years.

* Significant difference ($p < 0.05$) between good and poor outcome groups in an independent samples t-test (continuous variables) or Mann-Whitney U Test (ordinal/categorical variables).

‡ 10 and 11 patients in the good and poor outcome groups respectively had unknown symptom onset time and were excluded from the independent samples t-test.

Variables that were significantly different between groups were included in a logistic regression model to predict mRS outcome. In stepwise elimination, post-procedural mTICI was removed first, followed by V_{24h} , and admission rLMC score, leaving only S_{CTP} and admission NIHSS to predict outcome with significance ($p < 0.001$) (Table 4.2).

Table 4.2: Logistic regression for predicting 90-day functional outcome based on S_{CTP} and admission NIHSS

	B	SE	Wald	df	p	Odds Ratio	95% CI for Odds Ratio	
							Lower	Upper
S _{CTP}	0.030	0.009	10.705	1	0.001	1.031	1.012	1.049
Admission NIHSS	-0.137	0.043	10.825	1	0.001	0.872	0.804	0.946
Constant	0.048	0.964	0.003	1	0.960	1.049		

Table 4.2: Summary of statistics for the variables that remained in the backward-elimination multivariate logistic regression for predicting 90-day outcome. B indicates coefficients from the regression equation; CI, confidence interval; df, degrees of freedom; NIHSS, national institute of health stroke scale; p, significance of the Wald test; S_{CTP}, reperfusion score; SE, standard error associated with B; Wald, Wald statistic used to test the significance of B values.

ROC curves for predicting outcome with S_{CTP} , versus post-procedural mTICI score as predictors of good outcome are plotted in Figure 4.4. The AUC for S_{CTP} , and mTICI score were, 0.717 ± 0.053 ($p < 0.001$), and 0.618 ± 0.057 ($p < 0.05$) respectively. S_{CTP} had a significantly greater AUC than post-procedural mTICI ($p < 0.05$).

Figure 4.4: ROC curves for predicting good functional outcome based on S_{CTP} and post-procedural mTICI score

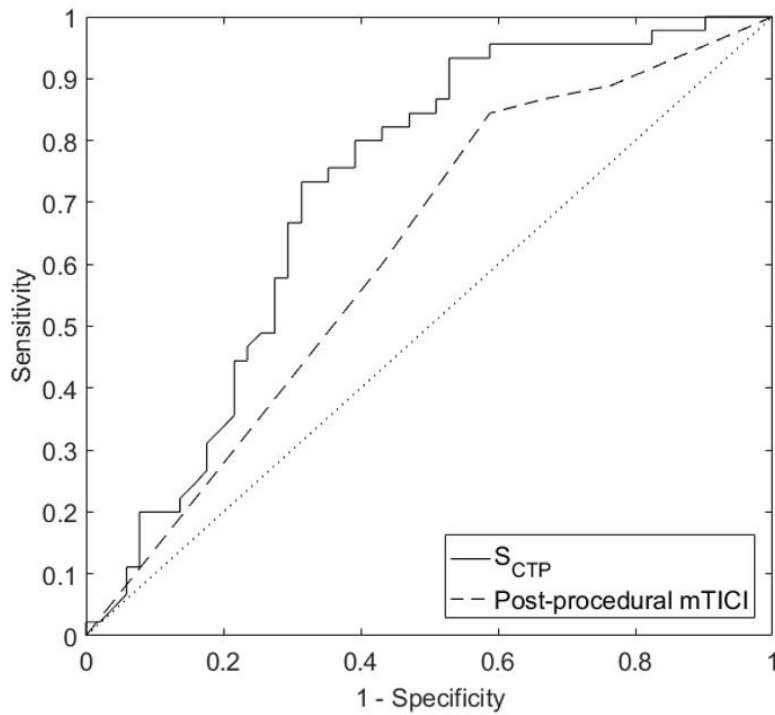


Fig. 4.4: Receiver-operator-characteristic (ROC) curves for reperfusion score (S_{CTP}) (solid), and post-procedural modified thrombolysis in cerebral ischemia (mTICI) score (dashed), with the diagonal line of no discrimination (dotted).

The optimal operating points for predicting good outcome corresponded to S_{CTP} of 81.5%, and mTICI score of 2b. $S_{CTP}>81.5\%$ had sensitivity, specificity, accuracy, PPV, and NPV of 0.73 (33/45), 0.69 (35/51), 0.71 (68/96), 0.67 (33/49), and 0.74 (35/47) respectively. The sensitivity, specificity, accuracy, PPV, and NPV of mTICI 2b/3 were 0.84 (38/45), 0.41 (21/51), 0.61 (59/96), 0.56 (38/68), and 0.75 (21/28) respectively. For the logistic regression model, the optimal threshold for predicting good outcome corresponded to: $0.03*(S_{CTP})-0.12*(\text{admission NIHSS})>0.30$. The sensitivity, specificity, accuracy, PPV, and NPV of this threshold were 0.71 (32/45), 0.82 (42/51), 0.77 (74/96), 0.78 (32/41), and 0.76 (42/55). $S_{CTP}>81.5\%$ had better specificity, accuracy, and PPV compared to mTICI 2b/3, and the regression model had better specificity, accuracy, PPV, and NPV than the S_{CTP} or mTICI threshold alone (Figure 4.5).

Figure 4.5: Sensitivity, specificity, accuracy, PPV, and NPV for regression model, $S_{CTP} > 81.5\%$ and mTICI 2b/3 for predicting functional outcome

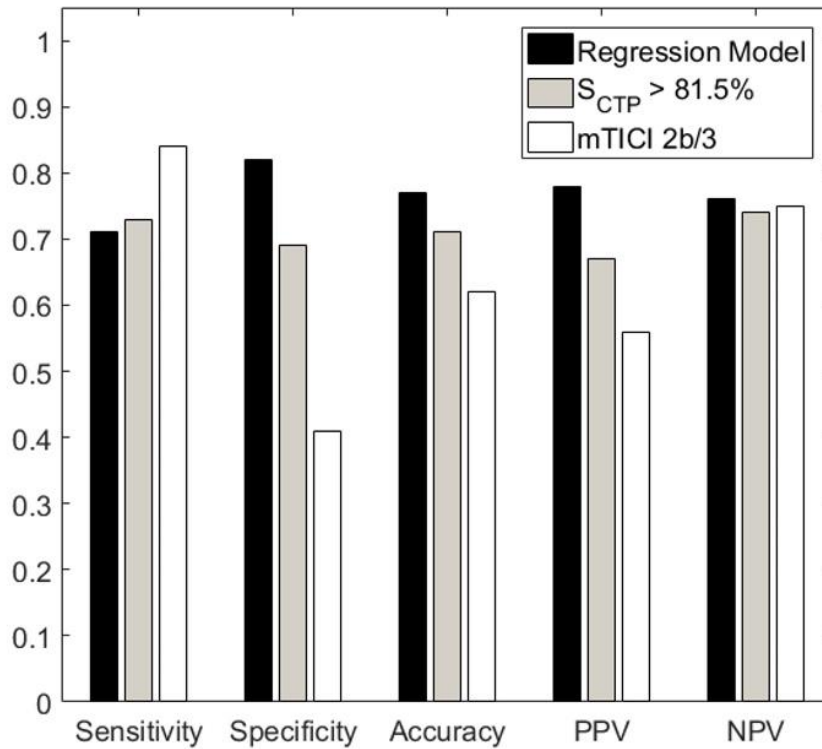


Fig. 4.5: Sensitivity, specificity, accuracy, positive predictive value (PPV), and negative predictive value (NPV) of the optimal threshold for the regression model (black), reperfusion score (S_{CTP}) $> 81.5\%$ (grey), and modified thrombolysis in cerebral infarction (mTICI) 2b/3 (white) for predicting good 90-day functional outcome.

4.4 Discussion

In clinical trials 15-35% of IAT-treated patients with mTICI 2b/3 had poor outcomes²⁻⁶. Some poor outcomes may have been due to reperfusion injury²² or lack of salvageable tissue after long onset to recanalization times²³; the discrepancy between patients with mTICI 2b/3 and those with good outcome may have also resulted from mTICI 2b/3 not accurately reflecting near-complete/complete reperfusion. Accurate prognosticators of reperfusion will be important as more patients are treated after results from DAWN and DEFUSE-3 showed the time window for IAT can be extended to 16-24h^{7,8} in neuroimaging-selected patients. This study's objectives were to compare reperfusion predicted by mTICI scores to reperfusion on admission and 24h CTP (S_{CTP}), and to compare mTICI score to S_{CTP} as prognosticators of 90-day outcome.

Regarding objective 1, S_{CTP} in patients with mTICI scores of 2b and 3 were significantly higher than in the mTICI 0 and 1 groups, but there were no significant S_{CTP} differences between patients with mTICI scores of 2a, 2b, and 3, and ~18% of mTICI 3 patients had reperfusion of less than two-thirds of the affected tissue ($S_{CTP}<67\%$). Regarding objective 2, only admission NIHSS and S_{CTP} remained significant in a stepwise logistic regression for predicting outcome. AUC was also significantly higher for S_{CTP} compared to mTICI score, and the optimal S_{CTP} threshold derived in this study ($S_{CTP}>81.5\%$) predicted good outcome with better specificity, accuracy, and PPV than mTICI 2b/3.

Prior studies found post-procedural mTICI score¹²⁻¹⁵, and >90% reperfusion on follow-up CTP were independent predictors of outcome²⁴, but few studies have directly compared prognostication of mTICI scores and follow-up CTP performed in the same

patients. These results suggest visual assessment of post-procedural DSA can distinguish patients with no reperfusion from patients with some reperfusion, but the degree of reperfusion is difficult to judge, and mTICI 3 may not accurately represent complete reperfusion on 24h CTP. As a result, low mTICI scores performed similarly to S_{CTP} for predicting poor outcome, but mTICI 2b/3 had poor specificity and PPV for predicting good outcome compared to $S_{CTP} > 81.5\%$, mostly because 18% of mTICI 3 patients were not fully reperfused, leading to poor outcome. Incomplete reperfusion following IAT in mTICI 3 patients has been reported in prior studies finding tissue classified as salvageable on admission CTP were often infarcted on follow-up, even when complete reperfusion was achieved at an early time point²⁵, and that infarct expansion between admission and 24h occurred in ~35% of mTICI 3 patients²⁶.

Perfusion on follow-up CTP may be overestimated by mTICI scores for several reasons. The mTICI score requires neuroradiologists to assess perfusion of a 3D volume based on 2D projections, potentially leading to overestimation when well perfused regions overlap non-perfused regions; this is minimized when quantifying ischemic tissue on 3D-CTP. Furthermore, reperfusion of the affected territory on DSA is assessed by presence/absence of capillary blush⁹. Degree of capillary blush constituting good perfusion, and size of the affected vascular territory may be subject to inter-rater variability; inter-rater variability is minimized by the threshold-based S_{CTP} used in this study. Lastly, capillary plugging by leukocyte adhesion²⁷, platelet accumulation²⁸, and/or lumen narrowing due to water accumulation in endothelial cells²⁹ can lead to cerebral ‘no-reflow phenomenon’, where capillary perfusion is impaired despite reperfusion of upstream arterioles. Theoretically, no-reflow phenomenon would be better visualized

using CTP than DSA, since CTP parameters are calculated directly from contrast concentration changes in capillaries of each tissue voxel, as opposed to inferring tissue perfusion based on presence/absence of capillary blush. This may explain why 9/49 mTICI 3 patients had $S_{CTP} \leq 66.7\%$ (Figure 4.3), although this could have also been caused by re-embolization between post-procedural DSA and 24h CTP³⁰⁻³².

This retrospective study had limitations. Predicting poor outcome using 24h CTP has limited clinical value, since most penumbral tissue has likely progressed to infarction by this time, limiting effectiveness of additional interventions. Furthermore, time delay between post-procedural DSA and 24h CTP introduced uncertainty, since the patients' hemodynamic status may have changed between imaging sessions. For example, mean S_{CTP} in mTICI 0 patients was $27.0 \pm 12.1\%$; 35% (6/17) of these patients had $S_{CTP} > 50\%$. In these cases, disparities between mTICI score and S_{CTP} were likely due to spontaneous clot lysis³² between post-procedural DSA and 24h CTP. Similarly, 18% of mTICI 3 patients (9/49) had $S_{CTP} < 67\%$; differences between mTICI score and S_{CTP} could have been due to re-embolization between post-procedural DSA and 24h CTP, though studies suggest re-embolization after IAT only occurs in ~10% of cases³¹⁻³³. Another study, prospectively designed to minimize time between post-procedural DSA and follow-up CTP, in a larger group of IAT-treated patients could address these limitations.

In summary, post-IAT mTICI 2b/3 did not reflect reperfusion seen on follow-up CTP, as a result, mTICI 2b/3 was not a specific marker of good outcome. S_{CTP} derived from pre- and post-procedural CTP scans was a better predictor of outcome than the commonly used mTICI score.

4.5 References

1. Campbell BCV, Mitchell PJ, Kleinig TJ, et al. Endovascular Therapy for Ischemic Stroke with Perfusion-Imaging Selection. *N Engl J Med.* 2015;372(11):1009-1018. doi:10.1056/NEJMoa1414792
2. Goyal M, Demchuk AM, Menon BK, et al. Randomized Assessment of Rapid Endovascular Treatment of Ischemic Stroke. *N Engl J Med.* 2015;372(11):1019-1030. doi:10.1056/NEJMoa1414905
3. Berkhemer OA, Fransen PSS, Beumer D, et al. A Randomized Trial of Intraarterial Treatment for Acute Ischemic Stroke. *N Engl J Med.* 2015;372(1):11-20. doi:10.1056/NEJMoa1411587
4. Saver JL, Goyal M, Bonafe A, et al. Stent-Retriever Thrombectomy after Intravenous t-PA vs. t-PA Alone in Stroke. *N Engl J Med.* 2015;372(24):2285-2295. doi:10.1056/NEJMoa1415061
5. Bracard S, Ducrocq X, Mas JL, et al. Mechanical thrombectomy after intravenous alteplase versus alteplase alone after stroke (THRACE): a randomised controlled trial. *Lancet Neurol.* 2016;15(11):1138-1147. doi:10.1016/S1474-4422(16)30177-6
6. Jovin TG, Chamorro A, Cobo E, et al. Thrombectomy within 8 Hours after Symptom Onset in Ischemic Stroke. *N Engl J Med.* 2015;372(24):2296-2306. doi:10.1056/NEJMoa1503780
7. Albers GW, Marks MP, Kemp S, et al. Thrombectomy for Stroke at 6 to 16 Hours with Selection by Perfusion Imaging. *N Engl J Med.* 2018;378(8):708-718.

doi:10.1056/NEJMoa1713973

8. Nogueira RG, Jadhav AP, Haussen DC, et al. Thrombectomy 6 to 24 Hours after Stroke with a Mismatch between Deficit and Infarct. *N Engl J Med*. 2018;378(1):11-21. doi:10.1056/NEJMoa1706442
9. Zaidat OO, Yoo AJ, Khatri P, et al. Recommendations on angiographic revascularization grading standards for acute ischemic stroke: A consensus statement. *Stroke*. 2013;44(9):2650-2663. doi:10.1161/STROKEAHA.113.001972
10. d'Esterre C, Boesen M, Hwan S, Pordeli P, Najm, M, Minhas P, et al. Time-Dependent CTP Thresholds for Patients with Acute Ischemic Stroke. *Stroke*. 2015;46(12):3390-3397. doi:10.1161/STROKEAHA.115.009250
11. Eilaghi A, Brooks J, d'Esterre C, et al. Reperfusion Is a Stronger Predictor of Good Clinical Outcome than Recanalization in Ischemic Stroke. *Radiology*. 2013;269(1):240-248. doi:10.1148/radiol.13122327
12. Soize S, Barbe C, Kadziolka K, Estrade L, Serre I, Pierot L. Predictive factors of outcome and hemorrhage after acute ischemic stroke treated by mechanical thrombectomy with a stent-retriever. *Neuroradiology*. 2013;55(8):977-987. doi:10.1007/s00234-013-1191-4
13. Yoon W, Kim SK, Park MS, Baek BH, Lee YY. Predictive Factors for Good Outcome and Mortality After Stent-Retriever Thrombectomy in Patients With Acute Anterior Circulation Stroke. *J stroke*. 2017;19(1):97-103. doi:10.5853/jos.2016.00675

14. Dekker L, Geraedts VJ, Hund H, et al. Importance of Reperfusion Status after Intra-Arterial Thrombectomy for Prediction of Outcome in Anterior Circulation Large Vessel Stroke. *Interv Neurol*. 2018;7(3-4):137-147. doi:10.1159/000486246
15. Prabhakaran S, Jovin TG, Tayal AH, et al. Posttreatment variables improve outcome prediction after intra-arterial therapy for acute ischemic stroke. *Cerebrovasc Dis*. 2014;37(5):356-363. doi:10.1159/000362591
16. Padroni M, Bernardoni A, Tamborino C, et al. Cerebral blood volume ASPECTS is the best predictor of clinical outcome in acute ischemic stroke: A retrospective, combined semi-quantitative and quantitative assessment. *PLoS One*. 2016;11(1):1-16. doi:10.1371/journal.pone.0147910
17. Menon BK, Smith EE, Modi J, et al. Regional Leptomeningeal Score on CT Angiography Predicts Clinical and Imaging Outcomes in Patients with Acute Anterior Circulation Occlusions. *AJNR Am J Neuroradiol*. 2011;32(9):1640-1645. doi:10.3174/ajnr.A2564
18. Puetz V, Dzialowski I, Hill MD, et al. Intracranial thrombus extent predicts clinical outcome, final infarct size and hemorrhagic transformation in ischemic stroke: The clot burden score. *Int J Stroke*. 2008;3(4):230-236. doi:10.1111/j.1747-4949.2008.00221.x
19. Dunn OJ. Multiple Comparisons Among Means. *J Am Stat Assoc*. 1961;56(293):52-64. doi:10.2307/2281868
20. Hanley JA, McNeil BJ. A method of comparing the areas under receiver operating

- characteristic curves derived from the same cases. *Radiology*. 1983;148(3):839-843.
doi:10.1148/radiology.148.3.6878708
21. Youden WJ. Index for rating diagnostic tests. *Cancer*. 1950;3(1):32-35.
 22. Khatri R, McKinney AM, Swenson B, Janardhan V. Blood-brain barrier, reperfusion injury, and hemorrhagic transformation in acute ischemic stroke. *Neurology*. 2012;79(Suppl 1):S52-S57. doi:10.1212/WNL.0b013e3182697e70
 23. Espinosa De Rueda M, Parrilla G, Manzano-Fernández S, et al. Combined Multimodal Computed Tomography Score Correlates with Futile Recanalization after Thrombectomy in Patients with Acute Stroke. *Stroke*. 2015;46(9):2517-2522. doi:10.1161/STROKEAHA.114.008598
 24. Albers GW, Goyal M, Jahan R, et al. Relationships between imaging assessments and outcomes in solitaire with the intention for thrombectomy as primary endovascular treatment for acute ischemic stroke. *Stroke*. 2015;46(10):2786-2794. doi:10.1161/STROKEAHA.115.010710
 25. Zhao L, Barlinn K, Bag AK, et al. Computed tomography perfusion prognostic maps do not predict reversible and irreversible neurological dysfunction following reperfusion therapies. *Int J Stroke*. 2011;6(6):544-546. doi:10.1111/j.1747-4949.2011.00681.x
 26. Haussen DC, Nogueira RG, Elhammady MS, et al. Infarct growth despite full reperfusion in endovascular therapy for acute ischemic stroke. *J Neurointerv Surg*. 2016;8(2):117-121. doi:10.1136/neurintsurg-2014-011497

27. Mori E, del Zoppo GJ, Chambers JD, Copeland BR, Arfors KE. Inhibition of polymorphonuclear leukocyte adherence suppresses no-reflow after focal cerebral ischemia in baboons. *Stroke*. 1992;23(5):712-718. doi:10.1161/01.STR.23.5.712
28. Desilles JP, Syvannarath V, Meglio L Di, et al. Downstream microvascular thrombosis in cortical venules is an early response to proximal cerebral arterial occlusion. *J Am Heart Assoc*. 2018;7(5):1-6. doi:10.1161/JAHA.117.007804
29. Ames A, Wright RL, Kowada M, Thurston JM, Majno G. Cerebral ischemia. II. The no-reflow phenomenon. *Am J Pathol*. 1968;52(2):437-453.
30. Gascou G, Lobotesis K, Machi P, et al. Stent retrievers in acute ischemic stroke: Complications and failures during the perioperative period. *Am J Neuroradiol*. 2014;35(4):734-740. doi:10.3174/ajnr.A3746
31. Kurre W, Vorlaender K, Aguilar-Perez M, Schmid E, Bätzner H, Henkes H. Frequency and relevance of anterior cerebral artery embolism caused by mechanical thrombectomy of middle cerebral artery occlusion. *Am J Neuroradiol*. 2013;34(8):1606-1611. doi:10.3174/ajnr.A3462
32. Costalat V, Lobotesis K, Machi P, et al. Prognostic factors related to clinical outcome following thrombectomy in ischemic stroke (RECOSt Study). 50 patients prospective study. *Eur J Radiol*. 2012;81(12):4075-4082. doi:10.1016/j.ejrad.2012.07.012
33. Kassem-Moussa H, Graffagnino C. Nonocclusion and Spontaneous Recanalization Rates in Acute Ischemic Stroke: A Review of Cerebral

Angiography Studies. Arch Neurol. 2002;59(12):1870-1873.

doi:10.1001/archneur.59.12.1870

Chapter 5

5 Conclusions and Future Work

The introduction to this thesis describes the pathophysiology, treatment, and medical imaging of AIS, with an emphasis placed on neuroimaging-based AIS triage and management. As stated in the introduction, the main objective of this thesis was to identify limitations and potential areas for improvement in CTP-based selection of AIS patients who could benefit from IV t-PA or IAT and CTP-based outcome prognostication following treatment. Specifically, a threshold for infarction after 3h of ischemia was developed using multimodal imaging in a porcine model of AIS, the impact of scan duration on quantitative CTP values and infarct volume derived by CBF thresholds was assessed, and the association between reperfusion on follow-up CTP and functional outcome was determined in IAT-treated AIS patients.

In this final chapter, major findings of this research and the implications for patient care will be discussed, an outline of possible future studies that should follow this work will be provided, and the major conclusions found from this work will be summarized.

5.1 Summary

5.1.1 Development of Porcine AIS Model and Derivation of 3h CBF Threshold for Infarction

Animal models of AIS are necessary to determine CTP-based CBF thresholds for different durations of ischemia because ischemia duration can be precisely controlled, a factor which is impossible to control in the clinical setting. Additionally, CBF measurement and infarct delineation with gold standard imaging techniques can be performed contemporaneously, eliminating uncertainties due to infarct expansion between

the acute phase and follow-up imaging, which is often performed 1-7 days post symptom onset in patients. As mentioned in Section 1.5, AIS models implemented in large animals, such as pigs, are a better representation of human stroke because of their gyrencephalic brain, and proportions of gray/white matter that are more similar to humans. However, the rete mirabile makes commonly used intra-luminal procedures for inducing cerebral ischemia impossible in pigs and other large mammals¹, so most models require invasive surgical procedures^{2,3} that make it difficult to maintain the animal at its basal physiological state after stroke induction.

The ET-1 based porcine model of AIS presented in Chapter 2 requires only an incision on the scalp and drilling of a small burr hole through the skull. This less invasive approach is advantageous compared to craniectomy-based approaches used in prior studies, which resulted in subarachnoid hemorrhage, ligature failure, and other technical problems in ~40% of animals⁴; similar complications did not occur in any of the 11 animals used in our study. Using this model, we were able to derive an absolute CBF threshold of $12.6 \text{ mL}\cdot\text{min}^{-1}\cdot 100\text{g}^{-1}$ for infarction after 3h of ischemia, which agreed with the 3h CBF threshold for infarction derived in the previously mentioned study using a more invasive AIS model in monkeys ($12 \text{ mL}\cdot\text{min}^{-1}\cdot 100\text{g}^{-1}$)⁴.

5.1.2 Assessment of Scan Duration Effect on Quantitative CTP Results

Despite more widespread use of CTP for AIS applications, the optimal CTP scan duration for imaging the ischemic brain has yet to be comprehensively determined. Shortening scan duration is beneficial to the patient because it decreases radiation dose. However, if the CTP scan is too short to fully capture delayed contrast washout from

ischemic tissue it can cause errors in estimated CTP parameters^{5,6}, which could cause over- or underestimated threshold-derived infarct volumes, and therefore errors in AIS patient triaging. Understanding how scan duration impacts CTP parameters and threshold-derived infarct volumes is important to ensure that CTP-based triaging of AIS patients is accurate, and reproducible between hospitals which may use different durations for brain CTP scans.

In Chapter 3 we determined the effect of scan duration on CBV, CBF, and T_{\max} values, in normal and ischemic tissue, calculated by GE Healthcare's commercially available software (CTP4D, GE Healthcare, Waukesha, WI), for durations ranging from 40s to 150s. Optimal scan durations for two time-dependent CBF thresholds for infarction previously derived by our group, which minimized radiation dose without infarct volumes being affected by truncation artifacts, were also derived. We found that CBV and T_{\max} were strongly dependent on scan duration, with median values decreasing by as much as 43% and 44% (relative to the median value from the 150s scan) respectively in ischemic tissue, and 29% and 26% respectively in contralateral normal tissue, whereas CBF was independent of scan duration, with the median value changing by only 1.4 to 6.5%. Furthermore, infarct volumes derived by both time-dependent CBF thresholds for infarction were found to be equivalent, within $\pm 2\text{mL}$, across the entire range of scan durations investigated, meaning that scan duration can be decreased to 40s to minimize the radiation dose to patients when CBF thresholds are used to estimate infarct volume. For the 2-phase CTP protocol used in this study, this would remove the entire 2nd phase and one-third of the 1st phase of the scan, decreasing radiation dose by ~48%.

5.1.3 Follow-up CTP as a Prognosticator of Functional Outcome in IAT-Treated Patients

The degree of reperfusion following IAT is commonly assessed by applying the mTICI scale to post-procedural DSA, with scores of 2b and 3 thought to represent near-complete and complete reperfusion of the previously ischemic tissue, respectively⁷. However, ~15-35% of patients in the treatment arm of clinical trials of IAT who had post-procedural mTICI scores of 2b/3 still went on to have poor functional outcomes⁸⁻¹⁴, suggesting DSA may not accurately assess reperfusion after treatment. As neuroprotection advances, accurately assessing reperfusion following IAT may become important for identifying the patients most likely to benefit from neuroprotective drugs or therapies.

In Chapter 4, the accuracy of reperfusion assessed using mTICI scores on post-procedural DSA was investigated by comparison to a reperfusion score (S_{CTP}) derived from pre- and post-treatment CTP, and the two metrics were compared as predictors of 90-day functional outcome in IAT-treated AIS patients. We found that S_{CTP} was similar between patients with post-procedural mTICI scores of 2a ($67.7 \pm 10.9\%$), 2b ($72.8 \pm .5\%$), and 3 ($82.6 \pm 2.7\%$), revealing that post-procedural mTICI scores of 3 may not necessarily reflect complete reperfusion on 24h follow-up CTP, and suggesting that although visual assessment of DSA can differentiate patients with no reperfusion from those with some reperfusion, it may not be able to accurately infer the degree of reperfusion. We also found that S_{CTP} was a significantly better predictor of functional outcome than post-procedural mTICI score; the optimal S_{CTP} threshold derived in the study ($S_{CTP} > 81.5\%$) predicted good functional outcome with better specificity (0.69 versus 0.41), accuracy (0.71 versus 0.61), and PPV (0.67 versus 0.56) compared to mTICI 2b/3.

5.2 Experimental and Clinical Impact

Patients arriving at the hospital after the population-based time windows for IV t-PA (4.5h) or IAT (6h), or those with unknown onset times were previously ineligible for treatment, but results from recent clinical trials show that eligibility for IV t-PA in patients with unknown onset time can be determined based on FLAIR-DWI mismatch¹⁵, and eligibility for IAT can be determined with infarct/penumbra¹⁴ or clinical/imaging mismatch¹³ assessed on CTP post-processed with RAPID, up to 24h post onset (detailed in Chapters 1.3 and 1.4). This represents a significant step towards more personalized care for AIS patients, but patient selection was not perfect in these trials (~50% of patients in the IAT arm of DAWN and DEFUSE 3 had poor functional outcomes^{13,14}); incorporating time-dependent CBF thresholds for infarction could potentially improve patient selection by providing more precise definition of the infarct core at different times since symptom onset. Besides estimating admission infarct volume, applying multiple thresholds for different ischemia durations from admission CTP-CBF maps could be used to predict the increase in infarct volume over time. This could inform decisions regarding inter-hospital transfer of patients being considered for IAT, by using the estimated increase in infarct volume to predict whether the patient would still be eligible for IAT based on infarct/penumbra or clinical/imaging mismatch criteria upon arrival. The animal study described in Chapter 2 derived a CBF threshold for infarction after 3 hours of ischemia, if similar thresholds were derived for a range of ischemia durations then this type of analysis could become feasible. The findings of Chapter 2 are complemented by the findings of Chapter 3, that quantitative CBF values from CTP are independent of scan duration, for scans 40s or longer, and that infarct volumes derived by CBF thresholds are equivalent,

within $\pm 2\text{mL}$, across scan durations ranging from 40s to 150s. Therefore, CTP scan duration can be shortened to 40s to decrease radiation dose to patients by $\sim 48\%$, without truncation artifacts affecting AIS patient triaging decisions made based on infarct volumes derived by time-dependent CBF thresholds.

Another important finding from this thesis is that reperfusion assessed on follow-up CTP is a more accurate indicator of 90-day functional outcome than mTICI scores assessed on post-procedural DSA. Post-treatment reperfusion estimated by mTICI score is commonly used to compare different revascularization therapies or IAT devices. Our findings suggest that follow-up CTP should be used for these comparisons instead, since follow-up CTP provides more accurate quantification of post-treatment reperfusion and is more strongly associated with outcome than the commonly used mTICI score. As neuroprotective drugs and therapies continue to improve, these findings could take on even greater importance as a method of identifying patients with incomplete reperfusion who would most likely benefit from additional therapies.

5.3 Future Work

This thesis suggests several directions of further investigations into the applications of perfusion imaging in AIS, some of these directions are discussed in this section.

5.3.1 Deriving CBF Thresholds for a Greater Range of Ischemia Durations

The main limitation of the ET-1 porcine AIS model used in Chapter 2 was that the cerebral ischemia in the distal MCA territory was not highly reproducible between animals and did not mimic LVO in patients, this was likely because ET-1 was not injected in the

immediate vicinity of the proximal MCA in all cases. With improved localization of the MCA using TDCs from dynamic CTP images (Figure 5.1), it should be possible to inject ET-1 close to the origin of the MCA, thus producing a proximal constriction more similar to LVO. Furthermore, the ischemic territory will be more reproducible, and we will be able to extend the ischemia duration well beyond 3h with repeated ET-1 injections at the same site. This would allow absolute CBF thresholds for infarction to be derived for a greater range of ischemia durations using a similar procedure to what was used in Chapter 2 but changing the duration between the ET-1 injection and the start of ^{18}F -FFMZ PET imaging. This could be performed in several groups of animals, each with a different time interval between ET-1 injection and infarct imaging, or alternatively, FMZ labelled with ^{11}C (half-life ~20 minutes) could be used, since the shorter half-life could allow the infarct to be delineated at multiple time points in the same animals.

Figure 5.1: Localization of MCA in porcine AIS model with dynamic images from CTP

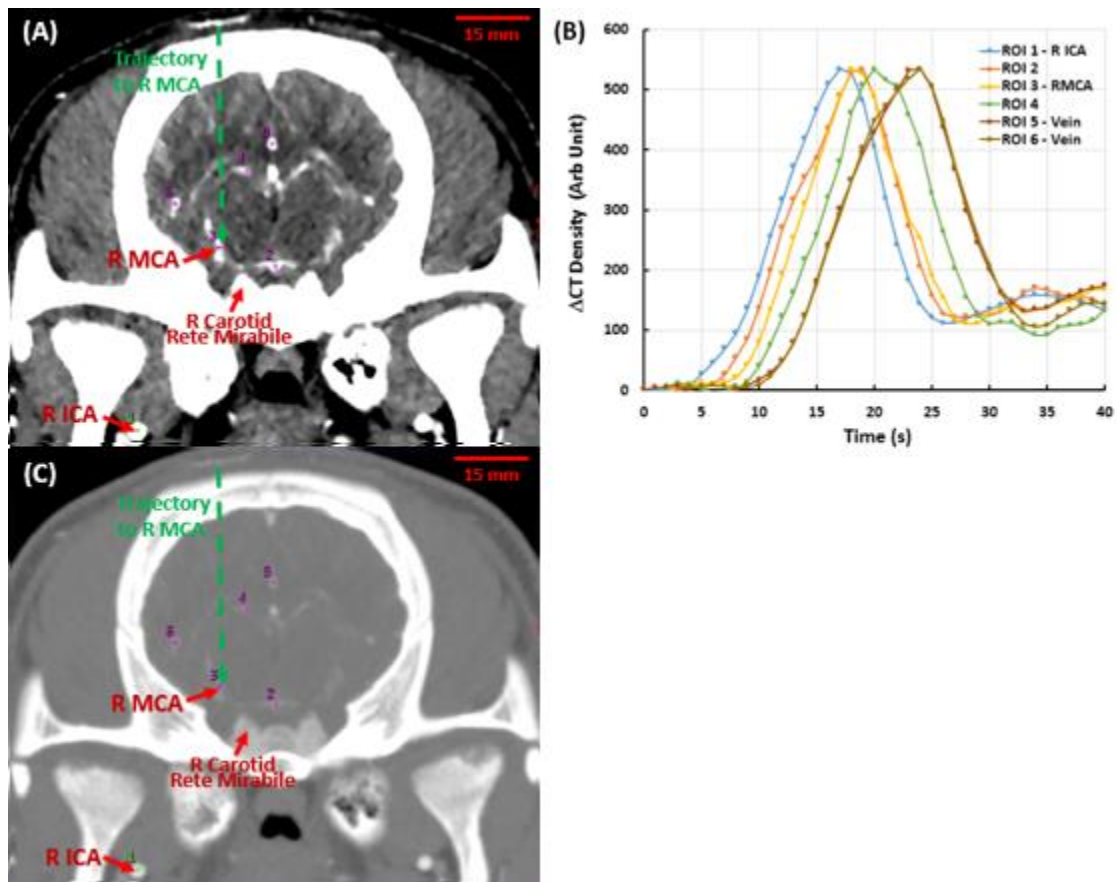


Fig. 5.1: Targeting the right MCA for ET-1 injection to induce stroke. (A) CTP image at time of maximal contrast enhancement in arteries and proximal veins; (C) same image as (A) but in bone window to show the anatomical landmarks of the skull and carotid rete mirabile; (B) TDCs from ROI 1-6 including the R ICA, MCA and proximal veins.

5.3.2 Using PS to Identify Patients at Increased Risk of Hemorrhagic Transformation

To further improve CTP-based patient selection for IV t-PA or IAT, methods for identifying patients at increased risk of hemorrhagic transformation could be developed based on assessing BBB permeability using PS maps from admission CTP. PS thresholds could be established based on the average PS within the infarct, or the volume of tissue within the infarct with elevated PS (relative to the contralateral side).

Figure 5.2: Elevated PS in patient with hemorrhagic transformation after IAT

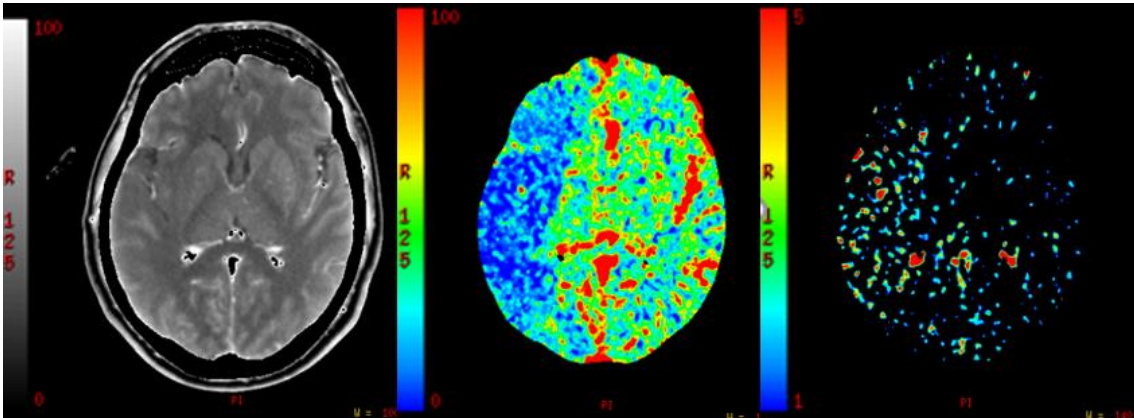


Fig. 5.2: Average image (left), CBF map (middle), and PS map (right) from admission CTP of a 46-year-old, male patient with occlusion of the M1 segment of the right MCA, who was treated with IAT but had grade 2 parenchymal hematoma on 7-day follow-up imaging. Elevated PS is seen throughout the ischemic tissue in the right MCA territory on admission CTP.

5.3.3 Assessment of Post-IAT Reperfusion using ‘DSA Perfusion’ Maps

In Chapter 4 we found that follow-up CTP provides more accurate assessment of post-thrombectomy reperfusion compared to post-procedural mTICI scores assessed on DSA and was a more accurate predictor of functional outcome. However, performing follow-up CTP requires transferring the patient from the angiography suite to a CT scanner, it would be more advantageous if there was a similar method of assessing reperfusion which could be performed in the angiography suite. Our group has recently created software capable of producing perfusion maps from dynamic DSA acquisitions (Figure 5.3). This would provide a more quantitative, less subjective alternative to the mTICI score for assessing reperfusion on post-procedural DSA. If the accuracy for predicting functional outcomes using this new technique is similar to what was observed using follow-up CTP in Chapter 4, then ‘DSA perfusion’ maps could improve outcome prediction after IAT without the need for additional follow-up CTP to be performed.

Figure 5.3: Blood flow maps derived from DSA (anterior-posterior view)

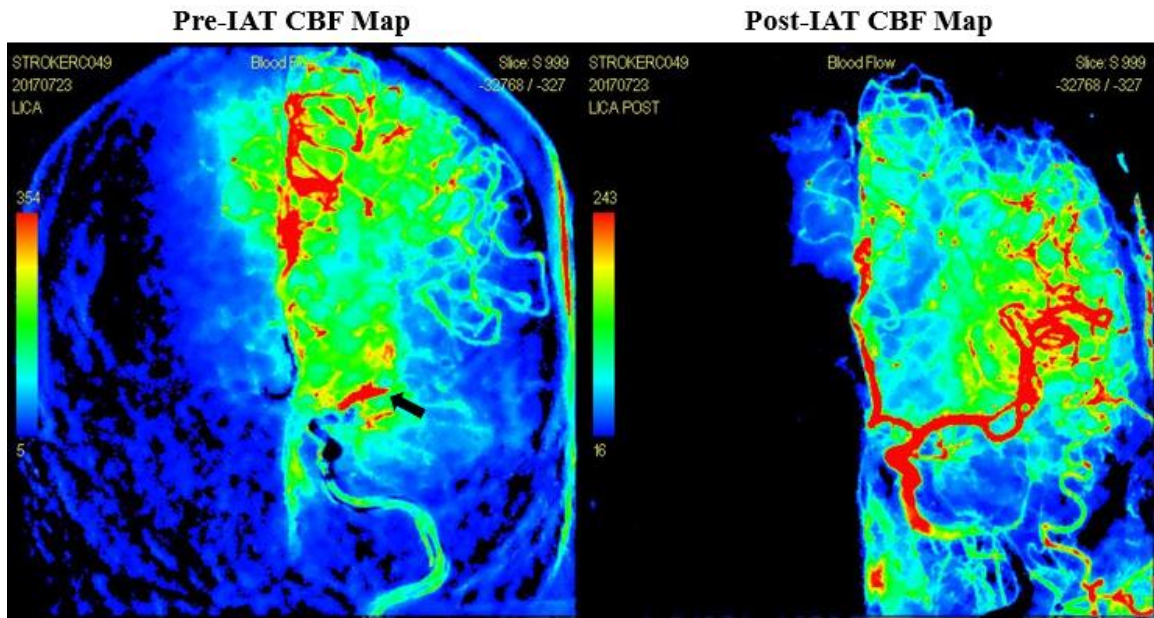


Fig. 5.3: Blood flow maps derived from DSA before (left) and after thrombectomy (right), shown in the anterior-posterior view. Black arrow in pre-IAT CBF map shows occlusion of MCA resulting in ischemic downstream tissue. After IAT, flow in the MCA and downstream tissue was been restored.

5.4 Conclusion

In summary, the significant findings of this thesis include:

1. As shown in a porcine model of AIS, tissue with $\text{CBF} < 12.6 \text{ mL}\cdot\text{min}^{-1}\cdot 100\text{g}^{-1}$ will progress to infarction after 3h of ischemia.
2. CBV and T_{max} values computed with commercially available CTP software depend on the duration of the CTP scan, whereas CBF is independent of the scan duration. By extension, infarct volumes derived by time-dependent CBF thresholds are equivalent, within $\pm 2\text{mL}$, over a range of scan durations from 40s to 150s.
3. Reperfusion assessed on follow-up CTP is a more accurate predictor of 90-day functional outcome in IAT-treated AIS patients than mTICI scores from post-procedural DSA.

5.5 References

1. Burbridge B, Matte G, Remedios A. Complex intracranial arterial anatomy in swine is unsuitable for cerebral infarction projects. *Can Assoc Radiol J.* 2004;55(5):326-329.
2. Imai H, Konno K, Nakamura M, et al. A new model of focal cerebral ischemia in the miniature pig. *J Neurosurg.* 2006;104(2 Suppl):123-132. doi:10.3171/ped.2006.104.2.123
3. O'Brien MD, Waltz AG. Transorbital approach for occluding the middle cerebral artery without craniectomy. *Stroke.* 1973;4(2):201-206. doi:10.1161/01.STR.4.2.201
4. Jones T, Morawetz R, Crowell R, et al. Thresholds of focal cerebral ischemia in

awake monkeys. *J Neurosurg.* 1981;54(6):773-782.
doi:10.3171/jns.1981.54.6.0773

5. Borst J, Marquering HA, Beenen LFM, et al. Effect of extended CT perfusion acquisition time on ischemic core and penumbra volume estimation in patients with acute ischemic stroke due to a large vessel occlusion. *PLoS One.* 2015;10(3):e0119409. doi:10.1371/journal.pone.0119409
6. d'Esterre CD, Aviv RI, Lee T-Y. The evolution of the cerebral blood volume abnormality in patients with ischemic stroke: A CT perfusion study. *Acta radiol.* 2012;53(4):461-467. doi:10.1258/ar.2012.110582
7. Zaidat OO, Yoo AJ, Khatri P, et al. Recommendations on angiographic revascularization grading standards for acute ischemic stroke: A consensus statement. *Stroke.* 2013;44(9):2650-2663. doi:10.1161/STROKEAHA.113.001972
8. Saver JL, Goyal M, Bonafe A, et al. Stent-Retriever Thrombectomy after Intravenous t-PA vs. t-PA Alone in Stroke. *N Engl J Med.* 2015;372(24):2285-2295. doi:10.1056/NEJMoa1415061
9. Goyal M, Demchuk AM, Menon BK, et al. Randomized Assessment of Rapid Endovascular Treatment of Ischemic Stroke. *N Engl J Med.* 2015;372(11):1019-1030. doi:10.1056/NEJMoa1414905
10. Berkhemer OA, Fransen PSS, Beumer D, et al. A Randomized Trial of Intraarterial Treatment for Acute Ischemic Stroke. *N Engl J Med.* 2015;372(1):11-20. doi:10.1056/NEJMoa1411587

11. Jovin TG, Chamorro A, Cobo E, et al. Thrombectomy within 8 Hours after Symptom Onset in Ischemic Stroke. *N Engl J Med.* 2015;372(24):2296-2306. doi:10.1056/NEJMoa1503780
12. Bracard S, Ducrocq X, Mas JL, et al. Mechanical thrombectomy after intravenous alteplase versus alteplase alone after stroke (THRACE): a randomised controlled trial. *Lancet Neurol.* 2016;15(11):1138-1147. doi:10.1016/S1474-4422(16)30177-6
13. Nogueira RG, Jadhav AP, Haussen DC, et al. Thrombectomy 6 to 24 Hours after Stroke with a Mismatch between Deficit and Infarct. *N Engl J Med.* 2018;378(1):11-21. doi:10.1056/NEJMoa1706442
14. Albers GW, Marks MP, Kemp S, et al. Thrombectomy for Stroke at 6 to 16 Hours with Selection by Perfusion Imaging. *N Engl J Med.* 2018;378(8):708-718. doi:10.1056/NEJMoa1713973
15. Thomalla G, Simonsen CZ, Boutitie F, et al. MRI-Guided Thrombolysis for Stroke with Unknown Time of Onset. *N Engl J Med.* 2018;379(7):611-622. doi:10.1056/NEJMoa1804355

Appendices

Appendix A: Supplementary Figures for Chapter 2

Figure A.1: CBF Histograms for each Animal

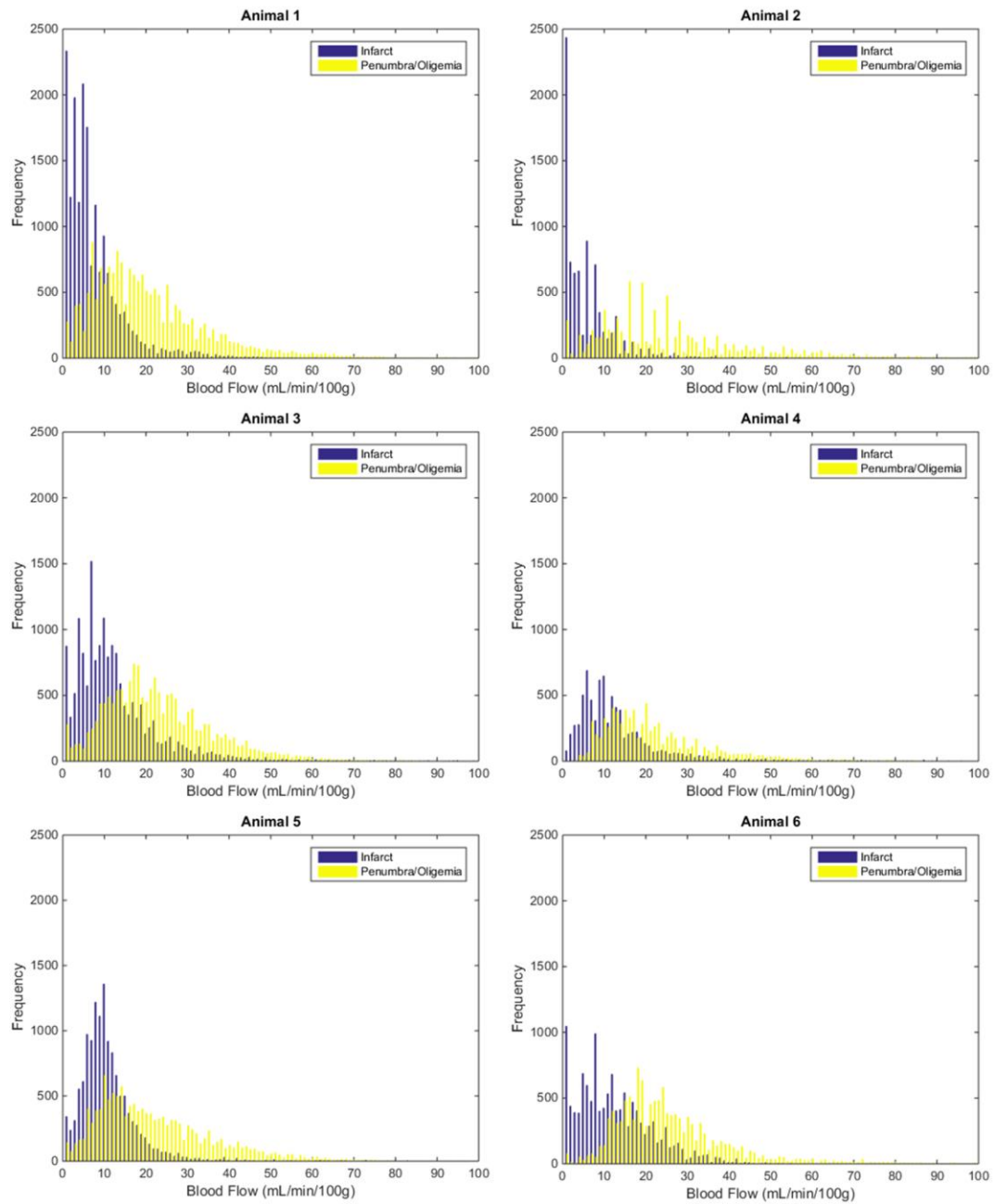


Fig. A.1: Frequency distributions of CBF values from infarct (blue) and penumbra/oligemia tissue (yellow) for each of the 6 animals from Chapter 2.

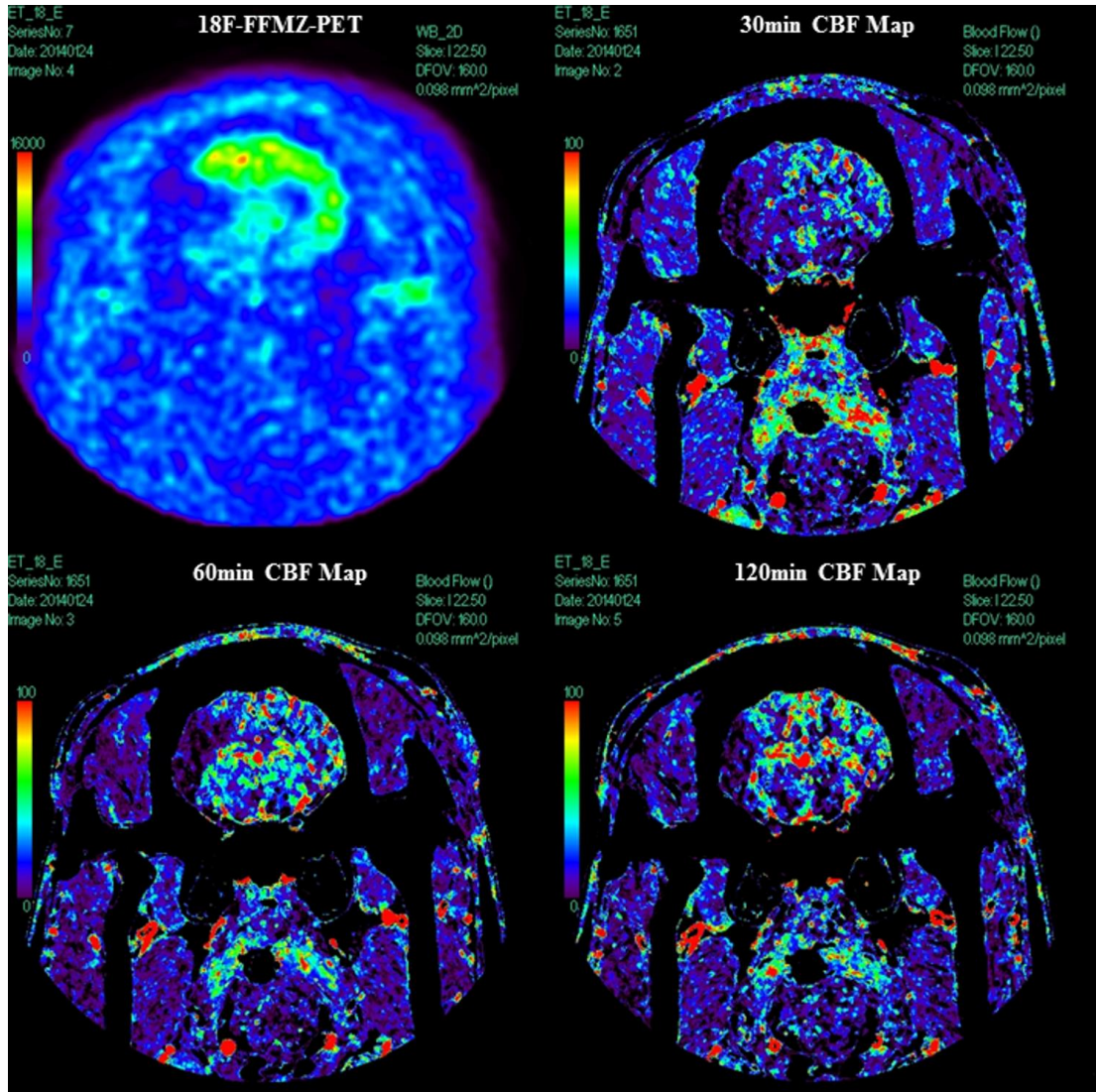
Figure A.2: ^{18}F -FFMZ PET and CBF maps from Animal 1**Fig A.2:** ^{18}F -FFMZ PET and CBF maps from 30, 60, and 120min post ET-1 injection in slice with the largest extent of infarct in Animal 1.

Figure A.3: ^{18}F -FFMZ PET and CBF maps from Animal 2

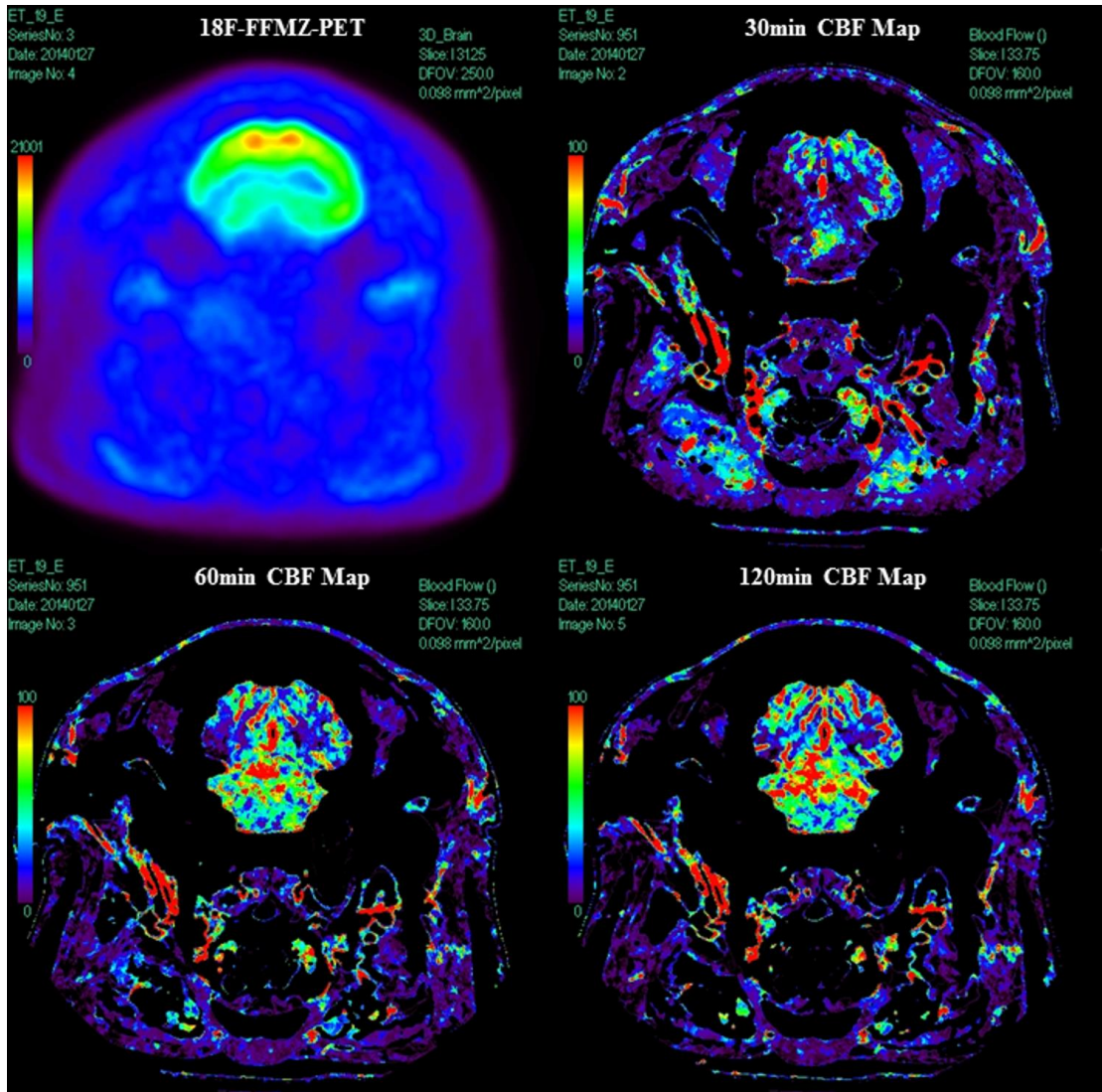


Fig A.3: ^{18}F -FFMZ PET and CBF maps from 30, 60, and 120min post ET-1 injection in slice with the largest extent of infarct in Animal 2.

Figure A.4: ^{18}F -FFMZ PET and CBF maps from Animal 3

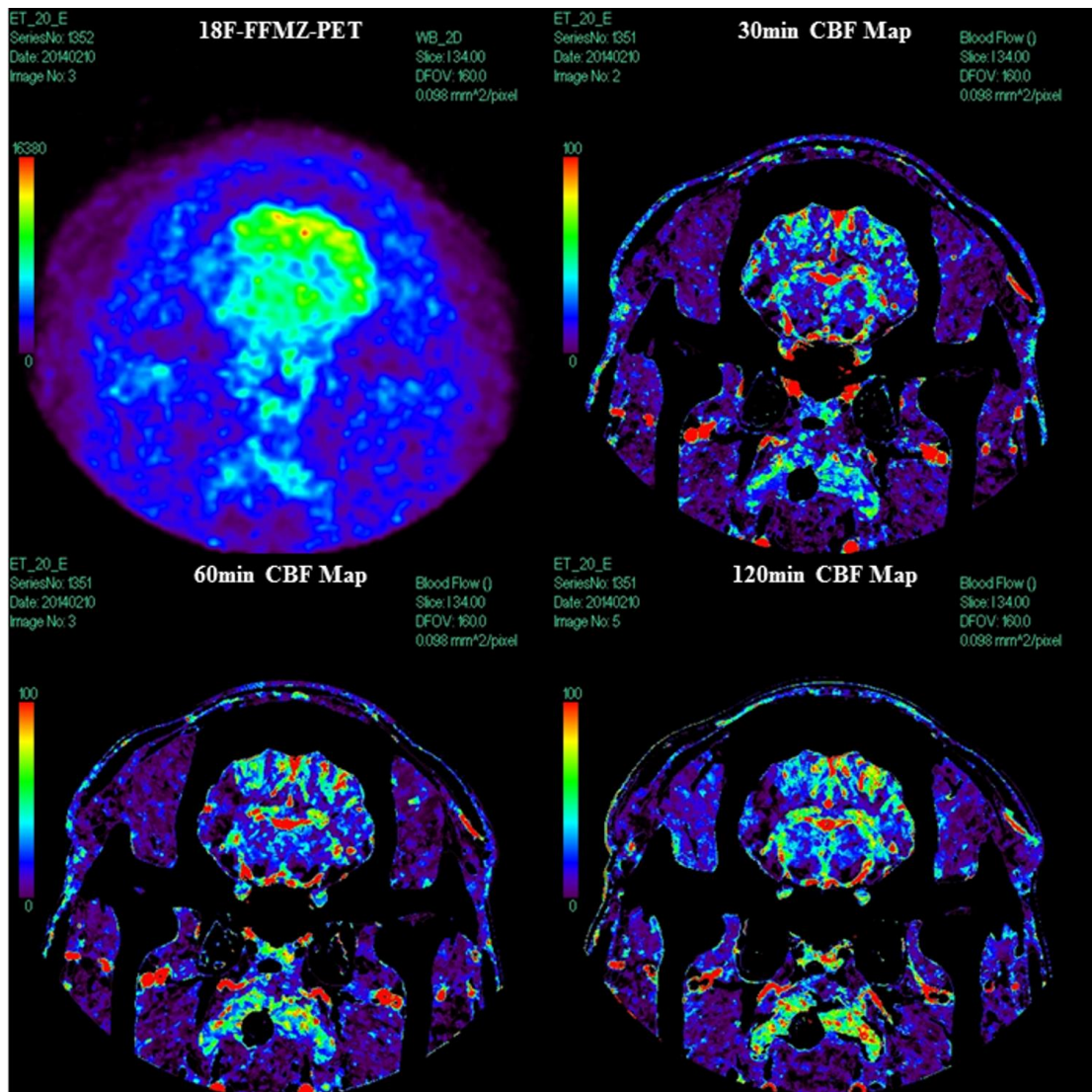


Fig A.4: ^{18}F -FFMZ PET and CBF maps from 30, 60, and 120min post ET-1 injection in slice with the largest extent of infarct in Animal 3.

Figure A.5: ^{18}F -FFMZ PET and CBF maps from Animal 4

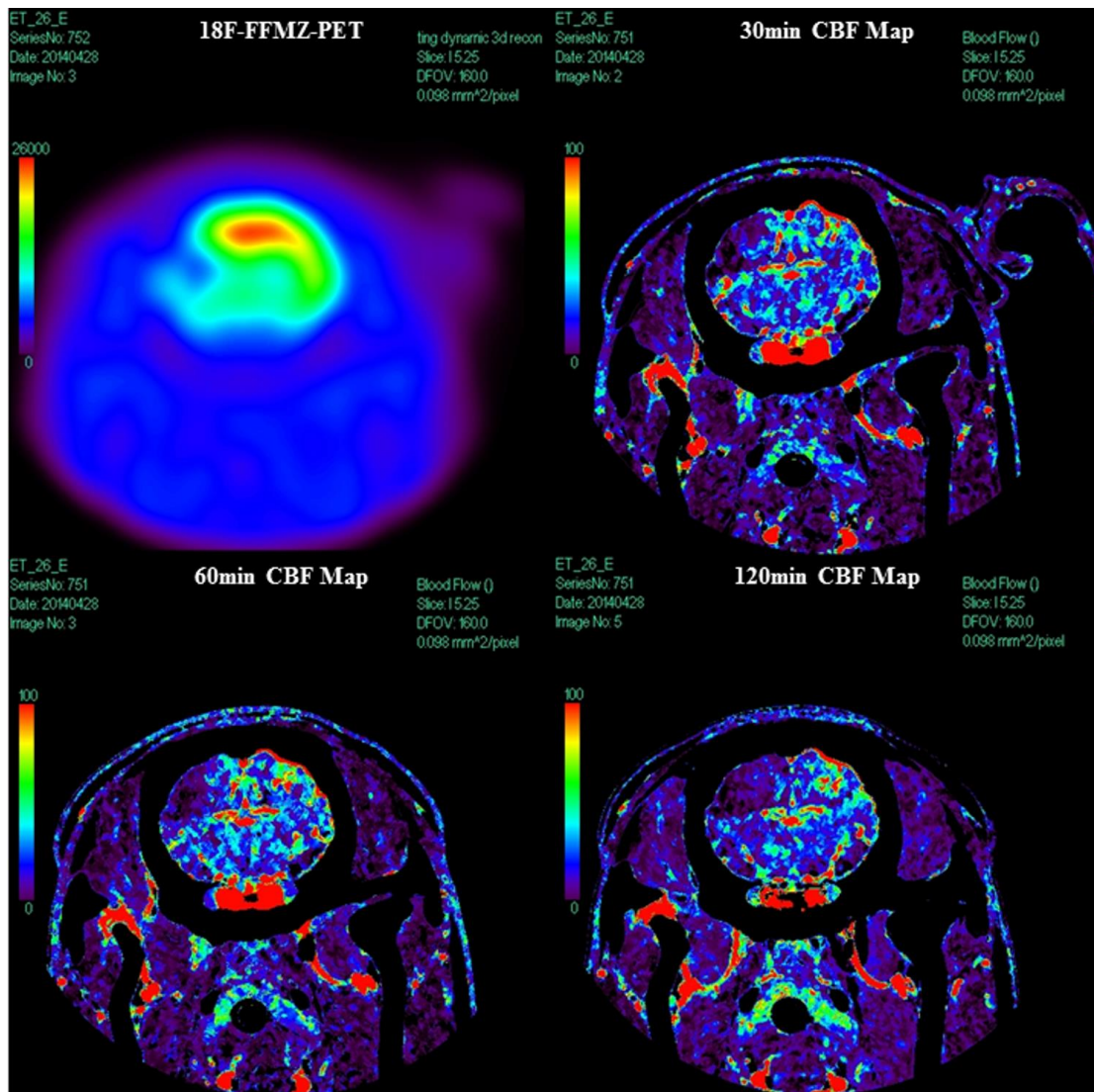


Fig A.5: ^{18}F -FFMZ PET and CBF maps from 30, 60, and 120min post ET-1 injection in slice with the largest extent of infarct in Animal 4.

Figure A.6: ^{18}F -FFMZ PET and CBF maps from Animal 5

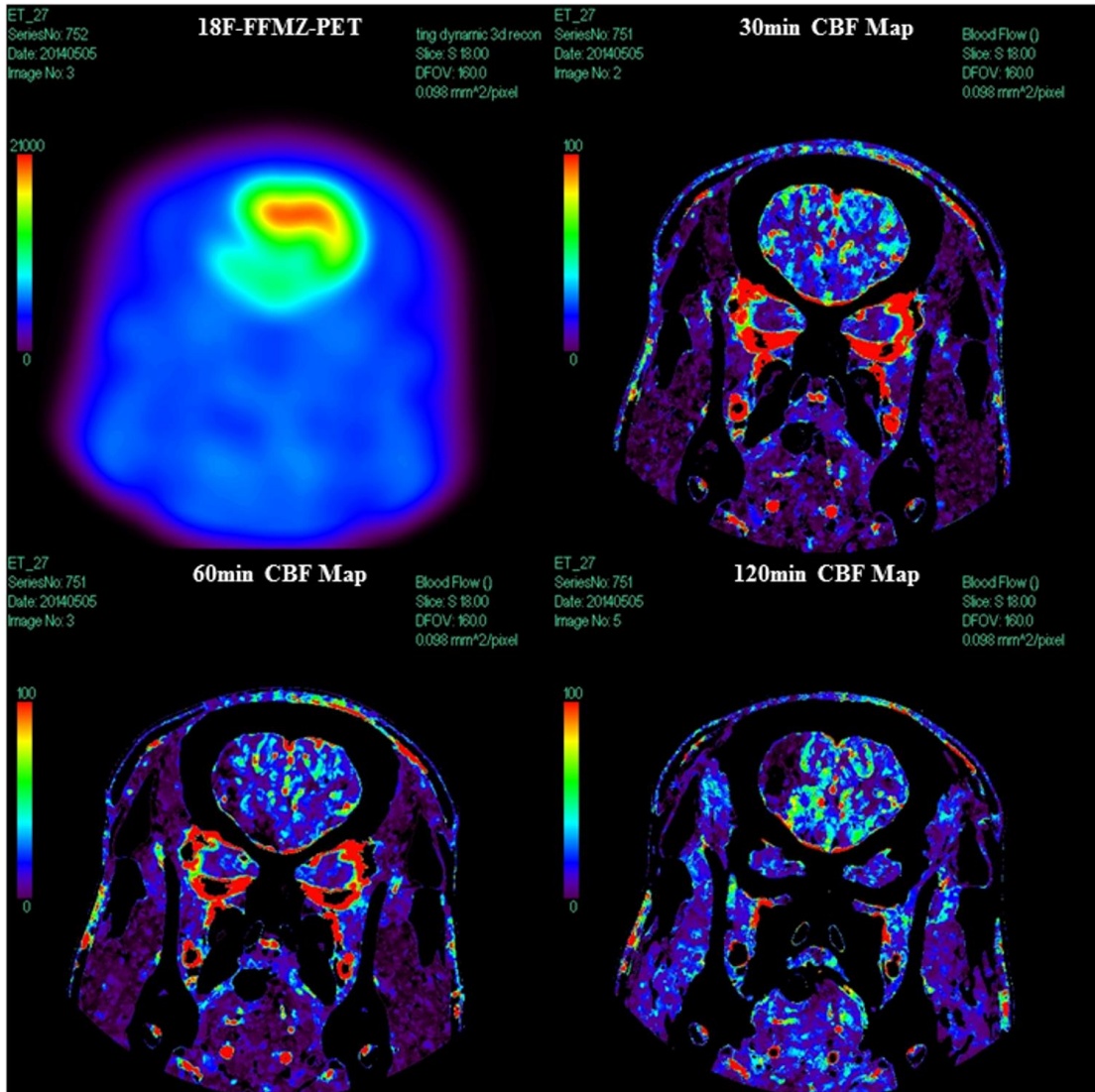


Fig A.6: ^{18}F -FFMZ PET and CBF maps from 30, 60, and 120min post ET-1 injection in slice with the largest extent of infarct in Animal 5.

Figure A.7: ^{18}F -FFMZ PET and CBF maps from Animal 6

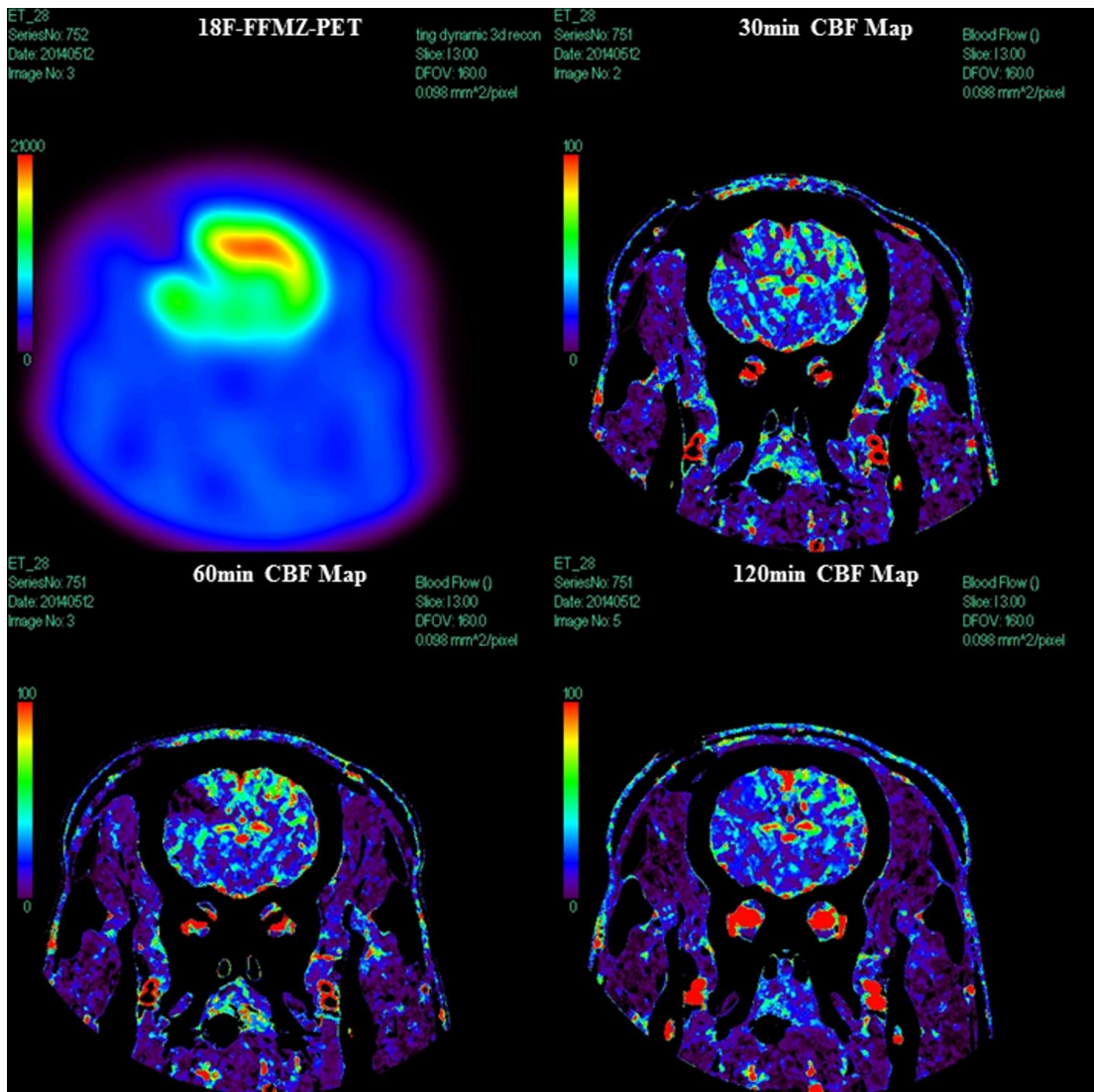
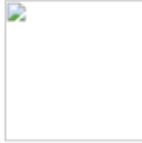


Fig A.7: ^{18}F -FFMZ PET and CBF maps from 30, 60, and 120min post ET-1 injection in slice with the largest extent of infarct in Animal 6.

Appendix B: Animal Ethics Approval for the work contained in Chapter 2

From: [REDACTED]
Sent: Friday, October 07, 2011 3:14 PM
To: [REDACTED]
Cc: [REDACTED]
Subject: eSirius Notification - New Animal Use Protocol is APPROVED2007-050-06::5



AUP Number: 2007-050-06
PI Name: St. Lawrence, Keith
AUP Title: Using Near-infrared Spectroscopy To Measure Cerebral Blood Flow In The Neurointensive Care Unit

Official Notice of Animal Use Subcommittee (AUS) Approval: Your new Animal Use Protocol (AUP) entitled "Using Near-infrared Spectroscopy To Measure Cerebral Blood Flow In The Neurointensive Care Unit

" has been APPROVED by the Animal Use Subcommittee of the University Council on Animal Care. This approval, although valid for four years, and is subject to annual Protocol Renewal.2007-050-06::5

1. This AUP number must be indicated when ordering animals for this project.
2. Animals for other projects may not be ordered under this AUP number.
3. Purchases of animals other than through this system must be cleared through the ACVS office. Health certificates will be required.

The holder of this Animal Use Protocol is responsible to ensure that all associated safety components (biosafety, radiation safety, general laboratory safety) comply with institutional safety standards and have received all necessary approvals. Please consult directly with your institutional safety officers.

Submitted by: Copeman, Laura
on behalf of the Animal Use Subcommittee
University Council on Animal Care



Appendix C: Ethics Approval for the work contained in Chapter 3



Conjoint Health Research Ethics Board
 Research Services Office
 2500 University Drive, NW
 Calgary
 Telephone: [REDACTED]

CERTIFICATION OF INSTITUTIONAL ETHICS APPROVAL

Ethics approval for the following research has been renewed by the Conjoint Health Research Ethics Board (CHREB) at the University of Calgary. The CHREB is constituted and operates in compliance with the *Tri-Council Policy Statement: Ethical Conduct for Research Involving Humans* (TCPS 2); Health Canada Food and Drug Regulations Division 5; Part C; ICH Guidance E6: Good Clinical Practice and the provisions and regulations of the Health Information Act, RSA 2000 c H-5.

Ethics ID: REB14-2012_REN4
 Principal Investigator: Bijoy Menon
 Co-Investigator(s): Shelagh Coutts
 Andrew Demchuk
 Michael Hill
 Eric Smith
 Peter Stys
 Student Co-Investigator(s): There are no items to display
 Study Title: A prospective cohort study assessing leptomeningeal Collateral status and variability in patients with acute ischemic stroke using CT
 Sponsor: Heart and Stroke Foundation of Alberta
 Canadian Institutes of Health Research

Effective: Friday, February 23, 2018

Expires: Saturday, February 23, 2019

Restrictions:

This Certification is subject to the following conditions:

1. Approval is granted only for the research and purposes described in the application.

2. Any modification to the approved research must be submitted to the CHREB for approval.
3. An annual application for renewal of ethics certification must be submitted and approved by the above expiry date.
4. A closure request must be sent to the CHREB when the research is complete or terminated.

Approved By:

Kathleen Oberle, PhD, Vice-Chair , CHREB

Date:

Thursday, February 01, 2018

Note: This correspondence includes an electronic signature (validation and approval via an online system).

Appendix D: Copyright Agreement

Copyright agreement for Figure 1.1:

ELSEVIER LICENSE TERMS AND CONDITIONS

Oct 17, 2018

This Agreement between University of Western Ontario -- Eric Wright ("You") and Elsevier ("Elsevier") consists of your license details and the terms and conditions provided by Elsevier and Copyright Clearance Center.

License Number 4451460588891
 License date Oct 17, 2018
 Licensed Content Publisher Elsevier
 Licensed Content Publication Trends in Biotechnology
 Licensed Content Title Functional CT: physiological models
 Licensed Content Author Ting-Yim Lee
 Licensed Content Date Aug 1, 2002
 Licensed Content Volume 20
 Licensed Content Issue 8
 Licensed Content Pages 8
 Start Page S3
 End Page S10
 Type of Use reuse in a thesis/dissertation
 Portion figures/tables/illustrations
 Number of figures/tables/illustrations
 1
 Format electronic
 Are you the author of this Elsevier article?
 No
 Will you be translating? No
 Original figure numbers Figure 2
 Title of your thesis/dissertation
 Applications of CT Perfusion-based triaging and prognostication in acute ischemic stroke
 Expected completion date Dec 2018
 Estimated size (number of pages)
 200
 Requestor Location University of Western Ontario
 1151 Richmond Street
 London, ON
 Canada
 Attn: University of Western Ontario
 Publisher Tax ID GB 494 6272 12
 Total 0.00 CAD
 Terms and Conditions

Curriculum Vitae

Eric Wright, M.Sc.
Western University
Department of Medical Biophysics
1151 Richmond Street North
London, Ontario

EDUCATION

Ph.D. Medical Biophysics Sept. 2013
 Western University | London, ON
 Department of Medical Biophysics to Dec. 2018
 Dissertation: Applications of CT Perfusion-based triaging and
 prognostication in acute ischemic stroke
 Supervisor: Dr. Ting-Yim Lee

M.Sc. Clinical Medical Biophysics May 2016
 Western University | London, ON
 Department of Medical Biophysics to Aug. 2018

B.M.Sc. Medical Biophysics Sept. 2009
 Western University | London, ON
 Department of Medical Biophysics to Apr. 2013

EMPLOYMENT

Teaching Assistant Jan. 2017
 Department of Medical Biophysics
 Western University | London, ON to Apr. 2017
 Course Title/Code: Practical Medical Imaging / MEDBIO 9520B

Quality Assurance Apprenticeship Sept. 2016
 London Regional Cancer Program | London, ON to Dec. 2016

Undergraduate Research Assistant May 2012
 Lawson Imaging
 Lawson Health Research Institute | London, ON to Aug. 2012

MEMBERSHIP

Student Membership | American Association of Physicists in Medicine

SCHOLARSHIPS

Ontario Graduate Scholarship Department of Medical Biophysics Western University London ON Value: \$15,000	May 2016 to May 2017
Ontario Graduate Scholarship Department of Medical Biophysics Western University London ON Value: \$15,000	May 2014 to May 2015
CIHR Strategic Training Program in Vascular Research Department of Medical Biophysics Western University London ON Value: \$24,000	Sept. 2013 to Sept. 2015
Dr. G.E. Hall Scholarship Department of Medical Biophysics Western University London ON Value: \$500	2012

AWARDS

1st Place Oral Presentation <i>Afternoon Session</i> London Imaging Discovery Day 2018 London, ON	2018
1st Place Poster Presentation <i>Stroke Category</i> Robarts Research Retreat 2017 London, ON	2017
1st Place Oral Presentation <i>Salon E Afternoon Session</i> London Health Research Day 2017 London, ON	2017
1st Place Poster Presentation <i>Medical Imaging Trials Network of Canada (MITNEC) Consortium</i> 14th Annual Imaging Network Ontario Symposium Toronto, ON	2016

2nd Place Poster Presentation | *Canadian Atherosclerosis Imaging Network (CAIN) / MITNEC Consortium*
13th Annual Imaging Network Ontario Symposium
London, ON

2015

SUBMITTED MANUSCRIPTS

1. **Wright EA**, Fainardi E, Bernardoni A, d'Esterre CD, Goyal M, Menon BK, Lee TY. Reperfusion assessed on admission and follow-up CT Perfusion is a more accurate predictor of 90-day functional outcome than modified thrombolysis in cerebral ischemia 2b/3. *Radiology*. Submitted October 12th, 2018.
 2. **Wright EA**, d'Esterre CD, Hur L, McDougall C, Horn M, Najm M, Goyal M, Menon BK, Lee TY. Impact of truncation artifacts on CT Perfusion-derived CBV, CBF, and T_{max} Measurements. *American Journal of Neuroradiology*. Submitted October 22nd, 2018.
-

PEER REVIEWED PUBLICATIONS

1. **Wright EA**, d'Esterre CD, Morrison L, Cockburn N, Kovacs M, Lee TY. Absolute Cerebral Blood Flow Infarction Threshold for 3-hour ischemia time determined with CT Perfusion and 18F-FFMZ-PET Imaging in a Porcine Model of Cerebral Ischemia. *PLoS One*. 2016; 11(6): e0158157.
 2. Diop M, **Wright EA**, Toronov V, Lee TY, St. Lawrence K. Improved light collection and wavelet de-noising enable quantification of cerebral blood flow and oxygen metabolism by an off-the-shelf spectrometer. *Journal of Biomedical Optics*. 2014; 19(5): 057007
 3. Elliott JT, **Wright EA**, Tichauer KM, Diop M, Morrison L, Pogue BW, Lee TY, St. Lawrence K. Arterial input function of an optical tracer for dynamic contrast enhanced imaging can be determined from pulse oximetry saturation measurement. *Physics in Medicine and Biology*. 2012; 57(24): 8285-8295.
-

CONFERENCE PUBLICATIONS

1. **Wright EA**, St. Lawrence K, Diop M. Conversion of a low cost off-the-shelf spectrometer into a suitable instrument for deep tissue spectroscopy. *Proceedings of SPIE Volume 8573. Design and Quality for Biomedical Technologies VI*. 2013.
-

CONFERENCE PRESENTATIONS

ORAL PRESENTATIONS

1. **Wright EA**, d'Esterre CD, Hur L, McDougall C, Horn M, Goyal M, Demchuk A, Menon BK, Lee TY. Effect of scan duration on CT Perfusion-derived hemodynamic parameters and infarct volume. 16th Annual Imaging Network Ontario Symposium (2018), Toronto ON
2. **Wright EA**, Hur L, Goyal M, Demchuk A, Menon BK, Lee TY. Effect of scan duration on infarct volumes from CT Perfusion-derived T_{max} and CBF maps. 13th Annual London Imaging Discovery Day (2018), London ON

3. **Wright EA**, d'Esterre CD, Fainardi E, Lee TY. Assessing Reperfusion in Ischemic Stroke Patients using CT Perfusion after Successful Intra-Arterial Therapy. 15th Annual Imaging Network Ontario Symposium (2017), London ON
4. **Wright EA**, d'Esterre CD, Fainardi E, Lee TY. Prognostic Value of CT Perfusion for Predicting Good Functional Outcome in Ischemic Stroke Patients After Successful Intra-Arterial Therapy. London Health Research Day 2017, London ON
5. **Wright EA**, d'Esterre CD, Morrison L, Cockburn N, Kovacs M, Lee TY. Ischemia-time dependent CBF threshold for infarction determined in a porcine model of stroke using CT Perfusion and F-18 FFMZ PET imaging. IUPESM World Congress on Medical Physics and Biomedical Engineering (2015), Toronto ON
6. **Wright EA**, d'Esterre CD, Morrison L, Cockburn N, Kovacs M, Lee TY. Ischemia time dependent absolute cerebral blood flow threshold for infarction found using CT Perfusion and F-18 FFMZ PET Imaging. 2014 Canadian Stroke Congress, Vancouver, BC

POSTER PRESENTATIONS

1. **Wright EA**, d'Esterre CD, Hur L, Goyal M, Demchuk A, Menon BK, Lee TY. Scan duration effect on CT Perfusion parameter calculations and infarct volumes. Robarts Research Retreat 2018, London ON
2. **Wright EA**, d'Esterre CD, McDougall C, Horn M, Goyal M, Demchuk A, Menon BK, Lee TY. Investigating the impact of scan duration on CT Perfusion-derived hemodynamic parameters and infarct or penumbra volumes. London Health Research Day 2018, London ON
3. **Wright EA**, Hur L, Goyal M, Demchuk A, Menon BK, Lee TY. CT Perfusion-derived tissue volumes in acute stroke patients are affected by scan duration. American Association of Physics in Medicine Annual Meeting 2018, Nashville, USA
4. **Wright EA**, d'Esterre CD, Fainardi E, Lee TY. Prognostic Value of CT Perfusion for Predicting Good Functional Outcome in Ischemic Stroke Patients After Successful Intra-Arterial Therapy. 30th Annual Canadian Student Health Research Forum (2017), Winnipeg MB
5. **Wright EA**, d'Esterre CD, Fainardi E, Lee TY. Assessing Reperfusion in Recanalized Ischemic Stroke Patients treated with Intra-Arterial Therapy using CT Perfusion. International Stroke Conference 2017, Houston, USA
6. **Wright EA**, d'Esterre CD, Fainardi E, Lee TY. Reperfusion on follow-up CT Perfusion as a prognosticator of outcome in recanalized stroke patients treated with intra-arterial therapy. Robarts Research Retreat 2017, London ON
7. **Wright EA**, Keenlside L, Lee TY. A Perfusion Phantom for Validating CT Perfusion Cerebral Blood Flow Measurements made by Different Calculation Algorithms. London Imaging Discovery Day 2016, London ON
8. **Wright EA**, Keenlside L, Lee TY. Designing and Testing a Perfusion Phantom for Validation of Deconvolution-based Cerebral Blood Flow Measurements. London Health Research Day 2016, London ON
9. **Wright EA**, Keenlside L, Lee TY. Designing and testing a perfusion phantom for validating cerebral blood flow measurements made with deconvolution techniques. 14th Annual Imaging Network Ontario Symposium (2016), Toronto ON
10. **Wright EA**, d'Esterre CD, Morrison L, Cockburn N, Kovacs M, Lee TY. Cerebral Blood Flow Threshold for Infarction after 3 Hours of Ischemia Determined in a Porcine Model of Stroke. International Stroke Conference 2016, Los Angeles, USA
11. **Wright EA**, d'Esterre CD, Morrison L, Cockburn N, Kovacs M, Lee TY. Determination of ischemia-time dependent CBF threshold for infarction using CT

Perfusion and F18-FFMZ PET imaging. London Health Research Day 2015, London ON

12. **Wright EA**, d'Esterre CD, Morrison L, Cockburn N, Kovacs M, Lee TY Ischemia-time dependent absolute CBF threshold for infarction determined in a porcine model of acute stroke. 13th Annual Imaging Network Ontario Symposium (2015), London ON
13. **Wright EA**, d'Esterre CD, Morrison L, Cockburn N, Kovacs M, Lee TY. CBF threshold for infarction after 3hrs of ischemia determined in a porcine model of acute stroke: A multi-modality study using CT Perfusion and 18F-FFMZ PET. Roberts Research Retreat 2015, London ON

STUDENT MENTORSHIP

Mentee: Daniel Mendes – Faculty of Science, Undergraduate Research Assistant

May to
Aug. 2018

OTHER CREDENTIALS

Anatomy and Radiology Contouring Bootcamp for Radiation Oncology Residents
London, ON

Nov. 2017

Canada Good Clinical Practice, Collaborative Institutional Training Initiative
London, ON

Dec. 2016

Teaching Assistant Training Program | Teaching Support Centre
Western University | London ON

Jan. 2017